

METHODS OF EXTRAPOLATING LOW CYCLE FATIGUE DATA TO HIGH  
STRESS AMPLITUDES

by

DAVID C. RADONOVICH

A thesis submitted in partial fulfillment of the requirements  
for the degree of Master of Science  
in the Department of Mechanical, Materials, and Aerospace Engineering  
in the College of Engineering and Computer Science  
at the University of Central Florida  
Orlando, Florida

Fall Term

2007

## ABSTRACT

Modern gas turbine component design applies much effort into prediction and avoidance of fatigue. Advances in the prediction of low-cycle fatigue (LCF) cracks will reduce repair and replacement costs of turbine components. These cracks have the potential to cause component failure. Regression modeling of low-cycle fatigue (LCF) test data is typically restricted for use over the range of the test data. It is often difficult to characterize the plastic strain curve fit constants when the plastic strain is a small fraction of the total strain acquired. This is often the case with high strength, moderate ductility Ni-base superalloys.

The intent of this project is to identify the optimal technique for extrapolating LCF test results into stress amplitudes approaching the ultimate strength. The proposed method to accomplish this is by finding an appropriate upper and lower bounds for the cyclic stress-strain and strain-life equations. Techniques investigated include: monotonic test data anchor points, strain-compatibility, and temperature independence of the Coffin-Manson relation.

A Ni-base superalloy (IN738 LC) data set with fully reversed fatigue tests at several elevated temperatures with minimal plastic strain relative to the total strain range was used to model several options to represent the upper and lower bounds of material behavior. Several high strain LCF tests were performed with stress amplitudes approaching the ultimate strength. An augmented data set was developed by combining the high strain data with the original data set. The effectiveness of the bounding equations is judged by comparing the bounding equation results with the base data set to a linear regression model using the augmented data set.

For Caroline and Joshua

## ACKNOWLEDGMENTS

Several people and organizations deserve recognition for contributing to this project. Dr. Ali Gordon of the University of Central Florida deserves credit for much technical support and encouragement. Thanks to Mr. Phillip Gravett, Dr. Harald Harders, Dr. Sachin Shinde, Mr. Allister James, Mr. Stefan Mazzola, and Mr. David Kosich of Siemens Power Generation for their efforts to support this project. Support provided by the United States Department of Energy was also very much appreciated.

## TABLE OF CONTENTS

LIST OF FIGURES .....	vii
LIST OF TABLES .....	x
NOMENCLATURE .....	xii
1. INTRODUCTION .....	13
2. BACKGROUND .....	16
2.1. Low Cycle Fatigue.....	16
2.2. Reference Methods .....	32
2.3. Existing Experimental Results.....	41
2.4. Thesis Objective.....	45
3. METHOD .....	48
3.1. Normalization of Test Data.....	48
3.2. Lower Bounds.....	49
3.3. Upper Bounds .....	50
3.4. Comparison Method.....	58
3.5. Test Equipment .....	59
3.6. Testing Procedure .....	63
3.7. Test Post-Processing.....	67
4. RESULTS .....	68
4.1. Base Data Set .....	68
4.2. Fatigue Test Results.....	71
4.3. Comparison.....	80

5.	DISCUSSION.....	94
5.1.	Augmented Data Model.....	94
5.2.	Base Data Model.....	96
5.3.	Lower Bound Model.....	99
5.4.	Upper Bounds 1 Model.....	102
5.5.	Upper Bounds 2 Model.....	105
5.6.	Upper Bounds 3 Model.....	107
6.	CONCLUSIONS.....	111
7.	RECOMMENDATIONS.....	113
	APPENDIX A – EXPERIMENTAL HYSTERESIS LOOPS AND STRESS HISTORIES .....	115
	APPENDIX B – SPECIMEN PHOTOGRAPHS .....	127
	REFERENCES .....	133

## LIST OF FIGURES

Figure 1.1. Longitudinal section of SGT6-5000F industrial gas turbine.....	14
Figure 2.1. Graphical depiction of the three types of fatigue. ....	17
Figure 2.2. LCF test with stable hysteresis loops. ....	18
Figure 2.3. Depiction of strain hardening. ....	20
Figure 2.4. Depiction of strain softening. ....	21
Figure 2.5. Cyclic stress-strain and strain-life curves.....	22
Figure 2.6. Depiction of sufficient data to characterize elastic and plastic strain. ....	28
Figure 2.7. LCF data set with insufficient plastic strain data for definition of plastic strain terms.....	29
Figure 2.8. Linear-elastic FE model stress results. ....	30
Figure 2.9. Process of LCF life determination.....	31
Figure 2.10. Approximation methods to curve fit from LCF test data for IN738 LC at 750°C. ....	36
Figure 2.11. Depiction of monotonic test. ....	40
Figure 2.12. Depiction of anchor point.....	41
Figure 2.13. IN713LC monotonic and cyclic stress-strain curve. ....	44
Figure 2.14. Strain-life curve for IN713 LC at room temperature.....	45
Figure 2.15. Bounding estimates for the stress-strain and strain-life equations. ....	46
Figure 3.1. Depiction of method for protection of proprietary test data.....	49
Figure 3.2. Effect of strain hardening on initial versus stable mid-life hysteresis loops. ....	51

Figure 3.3. Plots of (a) initial and stabilized stress range, and (b) initial and mid-life plastic strain used for UB1.....	54
Figure 3.4. Scatter in strain-life equation with temperature. ....	57
Figure 3.5. LCF test equipment. ....	60
Figure 3.6. Photograph and Depiction of load frame component details. ....	61
Figure 3.7. ASTM uniform gage specimen design [19]. ....	63
Figure 4.1. Experimental and modeled cyclic stress-strain and strain life behavior of IN738 LC using base data set. ....	70
Figure 4.2. Cyclic (a) stress and (b) strain history for test D912-1 for IN738 LC at 400°C. ....	72
Figure 4.3. Stress versus time output for 1.4% strain range at 24°C, 750°C, and 850°C.	76
Figure 4.4. Strain versus cycle plot comparison at 750°C. ....	77
Figure 4.5. (a) Hysteresis loop and (b) stress history plot for specimen D912-14 at 1.4% strain range and 750°C. ....	79
Figure 4.6. Comparison of calculated cyclic yield strengths using various methods. ....	81
Figure 4.7. Comparison of (a) cyclic stress-strain models and (b) strain-life models for IN738 LC at 24°C. ....	83
Figure 4.8. Comparison of (a) cyclic stress-strain models and (b) strain-life models for IN738 LC at 400°C. ....	85
Figure 4.9. Comparison of (a) cyclic stress-strain models and (b) strain-life models for IN738 LC at 750°C. ....	87
Figure 4.10. Comparison of (a) cyclic stress-strain models and (b) strain-life models for IN738 LC at 850°C. ....	89

Figure 4.11. Comparison of (a) cyclic stress-strain models and (b) strain-life models for IN738 LC at 900°C.....	91
Figure 5.1. Comparison of (a) cyclic stress-strain curve and (b) strain-life curves using the augmented data model and data for IN738 LC at various temperatures.....	95
Figure 5.2. Comparison of (a) cyclic stress-strain curve and (b) strain-life curves using the base model and base data for IN738 LC at various temperatures.....	98
Figure 5.3. Comparison of (a) cyclic stress-strain curve and (b) strain-life curves using the LB model and base data for IN738 LC at various temperatures.....	101
Figure 5.4. Comparison of (a) cyclic stress-strain curve and (b) strain-life curves using the UB1 model and base data for IN738 LC at various temperatures. ....	104
Figure 5.5. Comparison of (a) cyclic stress-strain curve and (b) strain-life curves using the UB2 model and base data for IN738 LC at various temperatures. ....	106
Figure 5.6. Comparison of (a) cyclic stress-strain curve and (b) strain-life curves using the UB3 model and base data for IN738 LC at various temperatures. ....	108

## LIST OF TABLES

Table 2.1. Linear regressions required to find curve fit constants.....	27
Table 2.2. Strain-life fatigue constant comparison.....	36
Table 2.3. Comparison of basic properties of IN713LC and IN738 LC.....	43
Table 3.1. Constants $C_1$ and $C_2$ from linear regression using base data set.....	53
Table 3.2. Planned Test Matrix.....	64
Table 4.1. Quantity, normalized strain range, and temperature of LCF data points in base data set for IN738 LC.....	68
Table 4.2. Values of $R^2$ from regression analysis using base data set.....	69
Table 4.3. Modified test matrix.....	74
Table 4.4. High strain range test results.....	75
Table 4.5. Values of $R^2$ from various extrapolation methods at 24°C.....	82
Table 4.6. Values of $R^2$ for various methods at 400°C.....	84
Table 4.7. Values of $R^2$ for various methods at 750°C.....	86
Table 4.8. Values of $R^2$ for various methods at 850°C.....	88
Table 4.9. Values of $R^2$ for various methods at 900°C.....	90
Table 4.10. Temperature average values of $R^2$ for extrapolation methods.....	92
Table 4.11. Temperature average values of R-squared error for best fit over all test data. .....	93
Table 5.1. Comparison of Constants $C_1$ and $C_2$ from linear regression with base data set and augmented data set.....	103
Table 5.2. Temperature average values of $R^2$ for extrapolation methods.....	109

Table 5.3. Temperature average values of  $R^2$  error for best over all test data..... 110

## NOMENCLATURE

$\Delta\varepsilon_{el}$	Elastic strain range
$\Delta\varepsilon_{el}/2$	Elastic strain amplitude
$\Delta\varepsilon_i$	Initial strain range
$\Delta\varepsilon_s$	Stabilized strain range
$\Delta\varepsilon_{pl}$	Plastic strain range
$\Delta\varepsilon_t$	Total strain range
$\Delta\varepsilon_t/2$	Total strain amplitude
$\Delta\sigma$	Stress range
$\dot{\varepsilon}$	Strain rate
$\varepsilon_a$	Strain amplitude
$\varepsilon_{el}$	Elastic strain
$\varepsilon_f$	Failure strain
$\varepsilon_f'$	Fatigue ductility coefficient
$\varepsilon_{pl}$	Plastic strain
$\varepsilon_t$	Total strain
$\sigma$	Stress
$\sigma_a$	Stress amplitude
$\sigma_f'$	Fatigue strength coefficient
$\sigma_f$	Failure stress
$\sigma_m$	Mean stress
$\sigma_{max}$	Maximum stress
$\sigma_{min}$	Minimum stress
$\sigma_{ULT}$	Ultimate tensile strength
$b$	Fatigue strength exponent
$c$	Fatigue ductility exponent
$e$	Elongation
$K'$	Cyclic strength coefficient
$n'$	Cyclic strain hardening exponent
$N_i$	Cycles to failure
$N_f$	Cycles to initiation
$R_\varepsilon$	Strain ratio
$FE$	Finite element
$LCF$	Low-cycle fatigue
$TMF$	Thermal-mechanical fatigue

## 1. INTRODUCTION

Modern F-class industrial gas turbine engines operate at high firing temperatures of 1260 °C (2300 °F), and are often used for peaking duty operation, which accumulates numerous cycles due to frequent starting and stopping of the engine [23]. These conditions cause high cyclic stress on gas turbine components, which can result in thermal-mechanical fatigue (TMF). This phenomenon is caused by cyclic strains induced by superimposed thermal and mechanical loading.

Many TMF cracks on gas turbine components are dominated by thermal stress. Often, these cracks propagate until they reach a region where the thermal stress has diminished, and crack growth is arrested. Occasionally, TMF cracks propagate into a region where non-remitting loads dominate, and result in component failure. To avoid undue risk, TMF cracks are repaired or replaced at considerable expense and increase of component life cycle costs.

The cost of a typical set of F-class turbine components is \$12 Million [1], which depending on operation will require replacement every three to six years. A longitudinal section of an SGT6-5000F, F-class industrial gas turbine is shown in Figure 1.1. It is estimated that there are at least 1,000 F-class turbines in the United States alone. This represents a component replacement cost of \$2.6 Billion / year to U.S. power producers. Considering that F-class turbines represents only a fraction of total number of industrial gas turbines, and that many thousands of air-craft engines are also affected by TMF, it is a very costly damage mode indeed.

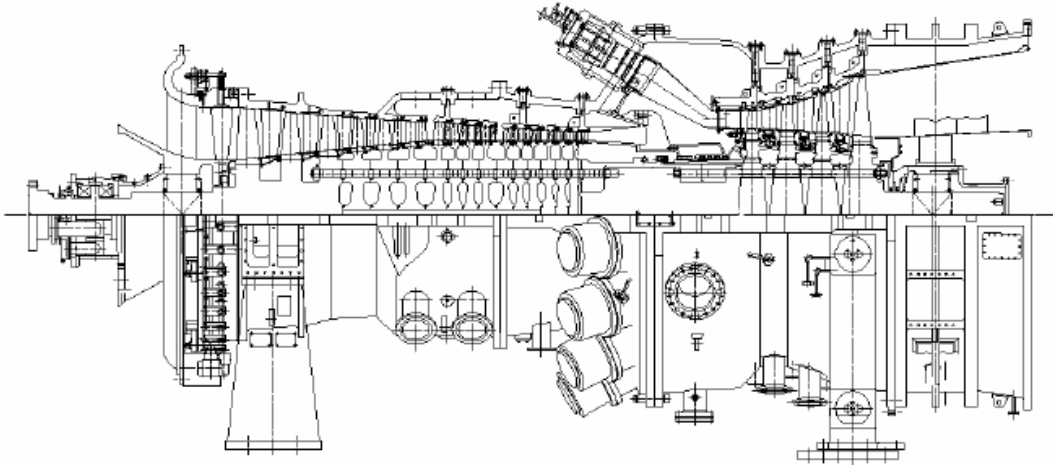


**Figure 1.1. Longitudinal section of SGT6-5000F industrial gas turbine.**

In practice, the phenomenon of TMF is quite complex. Most laboratory studies have focused on isothermal low-cycle fatigue (LCF) testing, assuming that tests conducted at the maximum temperature will show the worst behavior for the material [2]. Typically, a material is characterized by developing LCF characteristic curves at several temperatures of interest in the design. The effect of creep-fatigue interaction may be included by considering “hold-time” effects, or holding the specimen in tension or compression during isothermal fatigue testing. The low cycle fatigue range is typically considered less than 10,000 cycles in the gas turbine industry.

Many different alloys are used for their unique properties in a gas turbine, and properly characterizing the LCF life of each alloy is expensive and time consuming. Currently, the most widely used curve fitting method for LCF data discourages approximation and extrapolation outside of the data set. Most approximation methods that do exist have been calibrated to steel.

There is financial incentive to fully utilize conventionally cast (CC) Ni-base superalloys rather than upgrading to more costly directionally solidified (DS) or single crystal (SC) alloys. Any methods which can be applied to reduce scatter in a data set will effectively increase the minimum material allowable limits used for component design.

The focus of this project is examination of an existing data set of IN738 LC, which has limited plastic strain data and shows some unexpected behavior. It is not initially known whether the cause of the apparent anomalies is due to normal experimental or modeling error. Resolving the unexpected behavior will reduce scatter and allow the fully capability of the material behavior to be utilized.

Several methods are employed to find the optimal technique for extrapolating LCF data into stress amplitudes approaching the ultimate strength. Predictions are made by utilizing a base data set with limited plastic strain data, which are compared to an accepted model of high strain behavior including high strain range data. The merit of the extrapolation techniques as a tool to determine whether data is anomalous is also investigated.

## 2. BACKGROUND

### 2.1. Low Cycle Fatigue

The current methodology for low cycle fatigue is discussed in this section. Topics include: standard definitions in low cycle fatigue, the procedure used for linear regression curve fitting of test data, issues with the current methodology, and a procedure for component lifing.

Fatigue is the process of progressive localized permanent structural change occurring in a material subjected to conditions that produce fluctuating stresses and strains at some point or points, and that may culminate in cracks or complete fracture after a sufficient number of fluctuations [24]. Fatigue has been divided into three regimes, which depend on the number of cycles to failure as shown in Figure 2.1. The number of cycles where transition from HCF to LCF behavior occurs varies by material. One source suggests that high cycle fatigue is for cycles to failure greater than  $10^5$ , and low-cycle fatigue is for cycles between  $10^2$  and  $10^4$  [4]. This source also advises that the phenomena of low-cycle fatigue changes below 20 cycles, and has termed this range very low-cycle fatigue (VLCF).

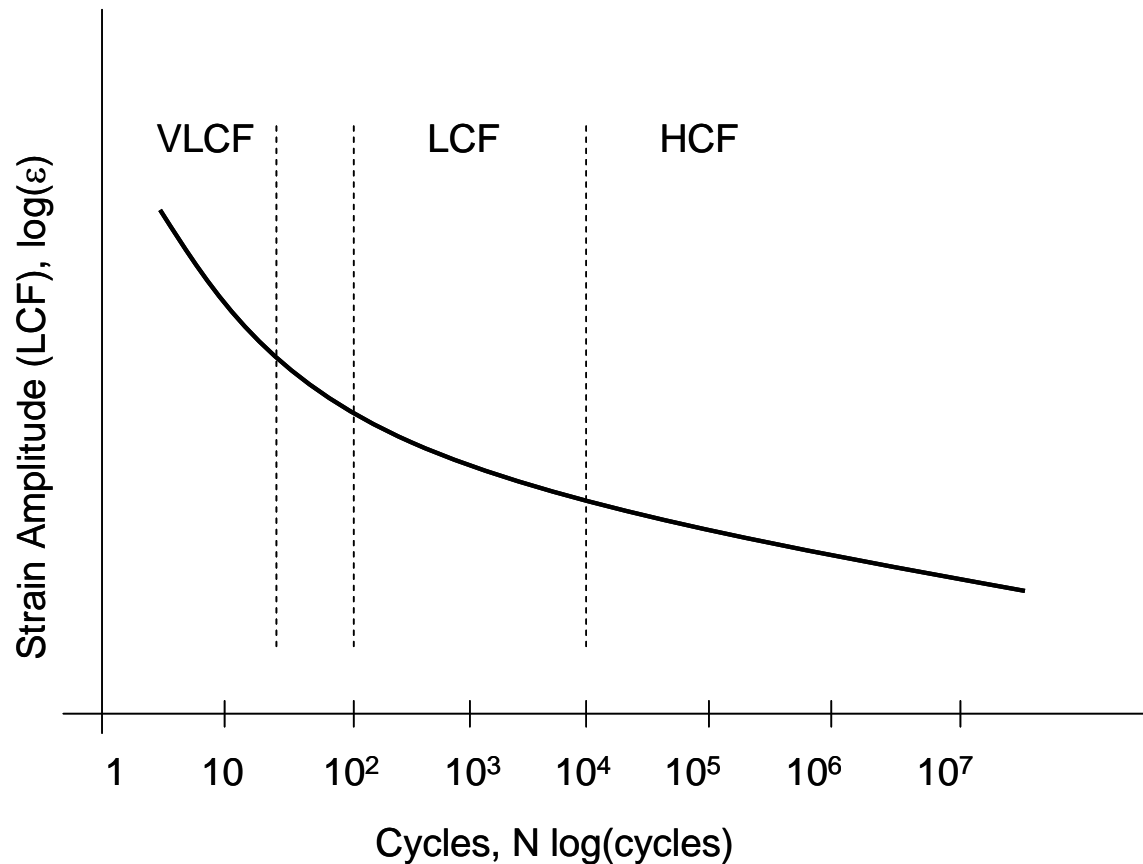


**Figure 2.1. Graphical depiction of the three types of fatigue.**

High cycle fatigue is defined by elastic stress governing the life, and low-cycle fatigue is defined where yielding effects (plasticity) govern the behavior [3]. Lemaitre describes high cycle fatigue having stress amplitudes less than yield, and low cycle fatigue as having stress amplitudes between yield and ultimate strength [4]. Stress-controlled experiments are used to characterize HCF life, whereas strain-controlled testing is used to characterize LCF life. The key output of either type of test is a hysteresis loop. The shapes of the cyclic stress versus strain curves typically change from initial loading until it achieves a stabilized shape as shown in Figure 2.2.

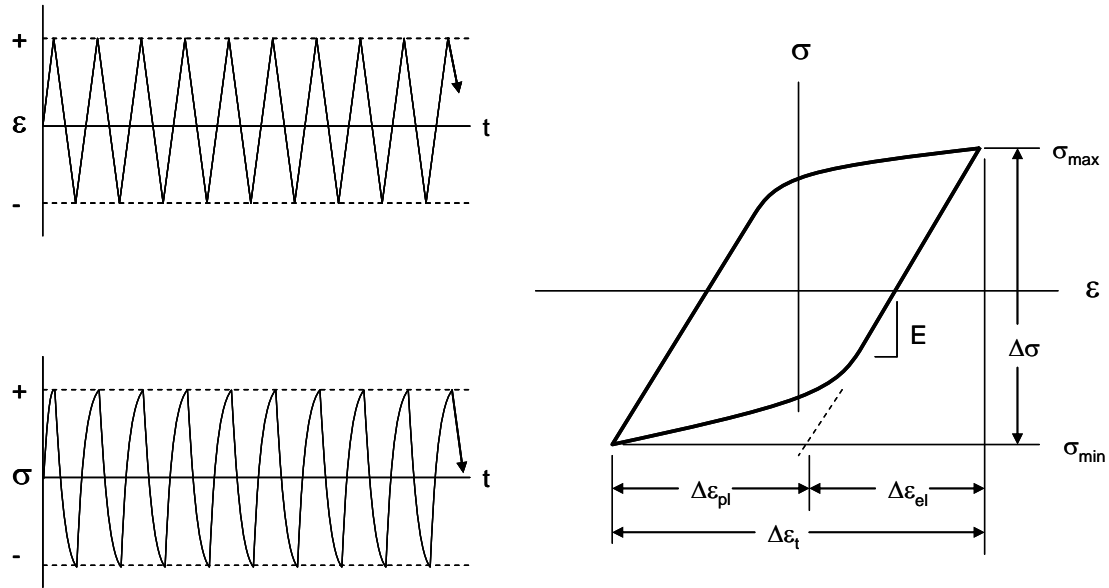


**Figure 2.2. LCF test with stable hysteresis loops.**

A collection of variables used to describe the cyclic stress versus strain curve are shown in the following. The stress range ( $\Delta\sigma$ ) is given by the maximum and minimum stress where  $\sigma_{\max}$  is the maximum stress and  $\sigma_{\min}$  is the minimum stress in the hysteresis loop, i.e.

$$\Delta\sigma = \sigma_{\max} - \sigma_{\min} \quad (2.1)$$

Mean stress ( $\sigma_m$ ) is the average of the maximum and minimum stress in the hysteresis loop, i.e.

$$\sigma_m = \frac{\sigma_{\max} + \sigma_{\min}}{2} \quad (2.2)$$

Equation 2.3 defines the total strain range ( $\Delta\varepsilon_t$ ) as the sum of the elastic ( $\Delta\varepsilon_{el}$ ) and plastic ( $\Delta\varepsilon_{pl}$ ) strain ranges, i.e.

$$\Delta\varepsilon_t = \Delta\varepsilon_{el} + \Delta\varepsilon_{pl} \quad (2.3)$$

The stress amplitude ( $\sigma_a$ ) and strain amplitude ( $\varepsilon_a$ ) is half of the stress range ( $\Delta\sigma$ ) and strain range ( $\Delta\varepsilon$ ) are respectively defined as

$$\varepsilon_a = \frac{\Delta\varepsilon}{2} \quad (2.4)$$

$$\sigma_a = \frac{\Delta\sigma}{2} \quad (2.5)$$

The test conditions are also described by the strain ratio ( $R_\varepsilon$ ). The strain ratio is the ratio of the minimum to maximum strain, i.e.

$$R_\varepsilon = \frac{\varepsilon_{\min}}{\varepsilon_{\max}} \quad (2.6)$$

The data in this thesis corresponds to fully reversed fatigue testing with an  $R_\varepsilon = -1$ .

Nickel-base superalloys have been shown to exhibit strain hardening, strain softening, and strain rate dependence depending on LCF conditions [6,7,8]. Typically, the test conditions are specified by  $\Delta\varepsilon$ ,  $R_\varepsilon$ , temperature, and strain rate ( $\dot{\varepsilon}$ ). Strain-

hardening is the increase in stress over time during constant strain-controlled testing as depicted in Figure 2.3. Strain hardening increases the magnitude of the maximum and minimum stress in a hysteresis loop over time. Strain softening is the reduction in stress over time during constant strain testing as depicted in Figure 2.4. The magnitude of the maximum and minimum stress in the hysteresis loop is reduced over time.

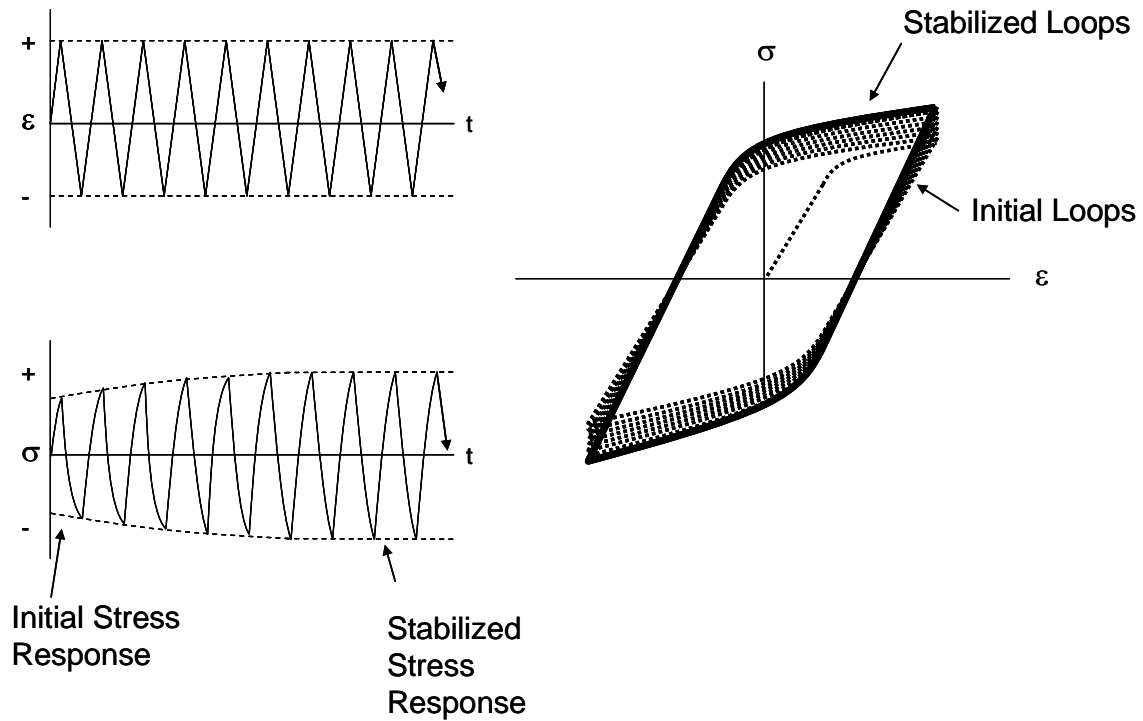
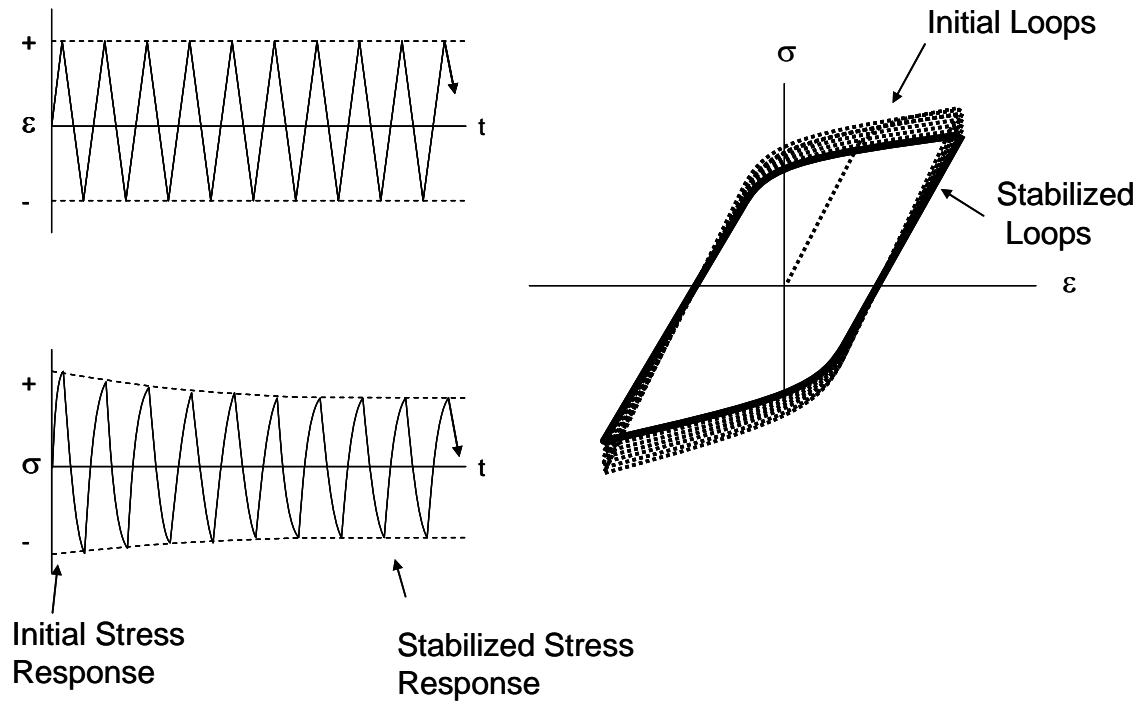


Figure 2.3. Depiction of strain hardening.



**Figure 2.4. Depiction of strain softening.**

Another important aspect of LCF data is strain rate dependence. Yield strength and ultimate strength have displayed strain rate dependence for IN738 LC [7, 22]. It is important to compare like similar strain rates when evaluating the differences between materials. All IN738 LC LCF test data used in this project was tested at a strain rate of 6.0%/min.

Linear regression analysis is used to interpolate the cyclic stress-strain and strain-life data at each temperature, as shown in Figure 2.5.

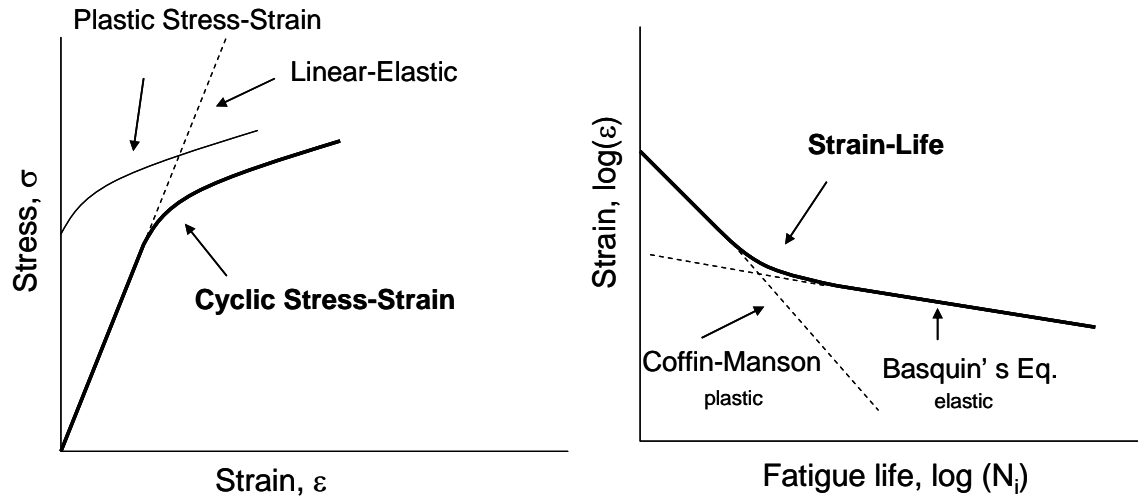


Figure 2.5. Cyclic stress-strain and strain-life curves.

There are two strain components that make up the cyclic stress-strain curve, which are the linear-elastic portion ( $\epsilon_{el}$ ) and the plastic stress-strain ( $\epsilon_{pl}$ ). The linear-elastic strain is given by Eq. 2.7 for a uni-axial stress state as a function of the elastic modulus ( $E$ ),

$$\epsilon_{el} = \frac{\sigma}{E} \quad (2.7)$$

The plastic strain ( $\epsilon_{pl}$ ), given by Eq.2.8, is a function of the strain hardening coefficient ( $K'$ ), and the strain hardening exponent ( $n'$ ),

$$\epsilon_{pl} = \left( \frac{\sigma}{K'} \right)^{1/n'} \quad (2.8)$$

The combined elastic and plastic strains constitute the total strain that is known as the cyclic stress-strain equation,

$$\varepsilon_t = \frac{\sigma}{E} + \left( \frac{\sigma}{K'} \right)^{1/n'} \quad (2.9)$$

Likewise, the strain-life equation is made up of an elastic and plastic term. The elastic strain-life term is known as Basquin's Equation [5],

$$\frac{\Delta \varepsilon_{el}}{2} = \frac{\sigma_f'}{E} (N_i)^b \quad (2.10)$$

where  $\sigma_f'$  is the fatigue strength coefficient, b is the fatigue strength exponent, E is the elastic modulus.

The plastic strain-life term is known as the Coffin-Manson Equation [5],

$$\frac{\Delta \varepsilon_{pl}}{2} = \varepsilon_f' (N_i)^c \quad (2.11)$$

where  $\varepsilon_f'$  is the strain ductility coefficient, c is the strain ductility exponent.

The combined total strain equation is known as the strain-life equation,

$$\frac{\Delta \varepsilon_t}{2} = \frac{\sigma_f'}{E} (N_i)^b + \varepsilon_f' (N_i)^c \quad (2.12)$$

Note that the strain-life equation is defined in terms of cycles (N). However, most published texts [3,5] show the strain-life equation as a function of reversals to failure ( $2N_f$ ), where two reversals equals one cycle. However, the published texts also show graphs of strain-life as a function of strain amplitude versus cycles (N). This is a source of confusion since the same symbol (N) is used interchangeably to denote cycles or reversals based on the context of the discussion. To avoid confusion, all equations and graphs will define N as cycles, and reversals will not be referred to in this text.

Cycles may be more precisely specified as cycles to failure ( $N_f$ ) or cycles to initiation ( $N_i$ ). Cycles to initiation is the number of cycles until initiation of a crack is determined by a certain percentage load drop during strain-controlled testing. Cycles to failure is defined as the number of cycles until specimen failure occurs. Basquin's equation and the Coffin-Manson equation were originally published in terms of cycles to failure ( $N_f$ ). However, the more modern practice is to divide fatigue into crack initiation and crack growth after a crack has reached a minimum detectable size [16]. As such, Basquin's equation and the Coffin-Manson equation, which together form the strain-life equation will be defined in terms of cycles to initiation ( $N_i$ ). It is recognized that older reference data may use the convention of cycles to failure ( $N_f$ ).

Although all of the data used within this thesis was intended to be fully-reversed data with zero mean stress, a small mean stress occurred due to normal material behavior. The method to account for the mean stress was by using the Modified Morrow [5] form of Basquin's equation,

$$\frac{\Delta \varepsilon_e}{2} = \frac{\sigma_f' - \sigma_m}{E} (N_i)^b \quad (2.13)$$

where the  $\sigma_m$  term represents the mean stress for each data point.

The Modified Morrow [5] strain-life equation is given by

$$\frac{\Delta \varepsilon_t}{2} = \frac{\sigma_f' - \sigma_m}{E} (N_i)^b + \varepsilon_f' (N_i)^c \quad (2.14)$$

Linear regression is used to determine the seven constants ( $E, K', n', \sigma_f', b, \varepsilon_f', c$ ), which define the cyclic stress-strain, and strain-life equations. The procedure for linear regression curve fitting is defined by the ASTM standard practice [9]. Six constants are found from log-log relationships ( $\varepsilon$  versus  $N$  and  $\sigma$  versus  $\varepsilon$ ), and one constant is from a linear relationship ( $\sigma$  versus  $\varepsilon$ ). Linear regression is given by standard least squared curve fitting procedure for the linear function. The SLOPE and INTERCEPT functions built into MS Excel can be used for linear regression. These functions readily provide the slope and intercept for two given arrays of dependent and independent variables.

The standard least squares fitting procedure is slightly modified for a log-log fit. The data is input into the form shown in the following equation

$$\log(y) = m \log(x) + b \quad (2.15)$$

where  $\log(x)$  is the independent variable,  $\log(y)$  is the dependent variable,  $m$  is the slope, and  $b$  is the intercept.

To provide Eq. 2.15 in the power law form, the base 10 is taken of both sides, and rearranged to form Eq. 2.16

$$y = 10^b x^m \quad (2.16)$$

This shows that the standard linear regression procedure can be used for log-log data to define the constant and exponent of a power law function, where  $10^b$  is the constant, and  $m$  is the exponent.

The standard procedure requires a separate linear regression be performed using data at each temperature level. Table 2.1 lists the required linear regressions to find the seven constants to determine the stress-strain and strain-life equations.

**Table 2.1. Linear regressions required to find curve fit constants.**

Constant Name	Dependent Variable	Independent Variable	MS Excel Function Used	Constant Value
$\sigma_f/E$	$\log(\varepsilon_{el, \text{Modified Morrow}})$	$\log(N_i)$	INTERCEPT	$10^0$
b	$\log(\varepsilon_{el, \text{Modified Morrow}})$	$\log(N_i)$	SLOPE	m
$\varepsilon_f'$	$\log(\varepsilon_{pl})$	$\log(N_i)$	INTERCEPT	$10^0$
c	$\log(\varepsilon_{pl})$	$\log(N_i)$	SLOPE	m
E	$\sigma_a$	$\varepsilon_{el}$	SLOPE	m
K'	$\log(\sigma_a)$	$\log(\varepsilon_{pl})$	INTERCEPT	$10^0$
n'	$\log(\sigma_a)$	$\log(\varepsilon_{pl})$	SLOPE	m

One issue arises that limits the allowable data for use in the regression analysis. In very high cycle fatigue (VHCF) testing, the plastic strain is approximately zero, and is too small for detection. Data points with negligible plastic strain must be neglected from regression analysis to find the constants involving plastic strain ( $\varepsilon_f', c, K', n'$ ).

The ASTM standard practice [9] provides a recommended number of data points to find curve fits at two quality levels: preliminary and design. A preliminary curve fit is provided by 6 to 12 tests, and 12 to 24 data points is necessary to provide curve fits acceptable for design. The quantity of data points at 24°C, 750°C, and 900°C are considered preliminary quality levels, and the 400°C and 850°C are considered design quality levels.

If the test matrix is chosen carefully, the test data points will include sufficient data to characterize both the elastic and plastic strains as depicted in Figure 2.6. This will provide curve fit constants, which are valid over the entire range of stress amplitude and cycles that are classified as low-cycle fatigue. Recall that LCF is typically defined by stress amplitudes between yield strength and ultimate strength, and cyclic lives between  $10^2$  to  $10^4$  cycles [4].

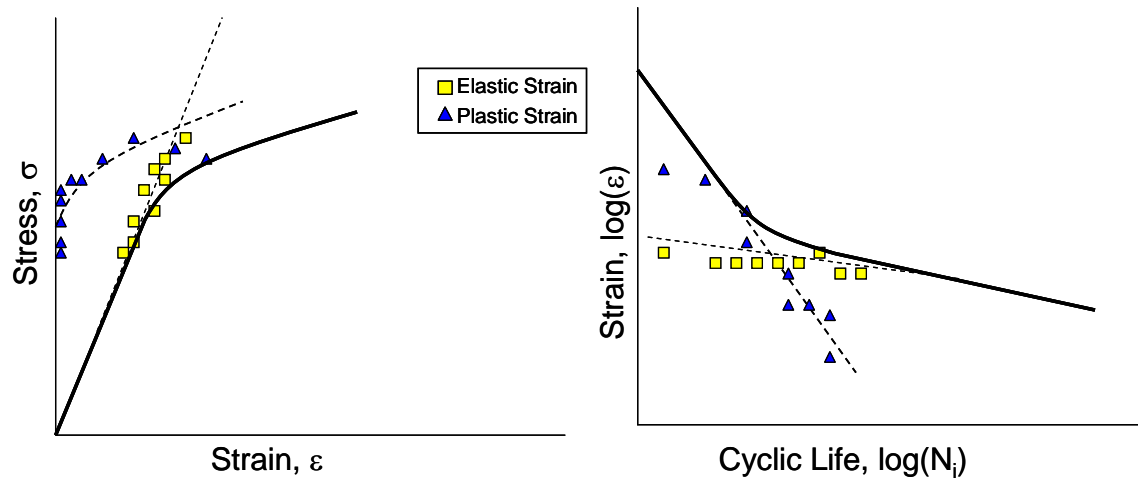


Figure 2.6. Depiction of sufficient data to characterize elastic and plastic strain.

Issues often arise when attempting to curve fit the stress-strain, and strain-life equation. One reference offers the following guidelines when attempting to fit the strain-life equation to test data [5]:

- 1) Not all materials may be represented by the total strain-life equation (Eq. 2.12).
- 2) The four fatigue constants ( $\sigma'_f, b, \epsilon'_f, c$ ) may represent a curve fit to a limited number of data points. The values of these constants may be changed if more data points are included in the curve fit.
- 3) The fatigue constants are determined from a set of data points over a given range. Gross errors may occur when extrapolating fatigue life estimates outside this range.
- 4) The use of the strain-life equation is strictly a matter of mathematical convenience and is not based on a physical phenomenon.

Fatigue data that comprise of experiments where the  $\Delta\varepsilon_{pl} \ll \Delta\varepsilon_t$  are very useful for characterizing the fatigue constants for Basquin's equation. However, when the plastic strain data is negligible the plastic strain constants ( $\varepsilon'_f, c, K', n'$ ) are known to very limited accuracies. Figure 2.7 represents the condition where there is limited plastic strain data. In this case, many potential curve fits (shown as curves A, B, or C) could pass through the limited plastic strain data points.

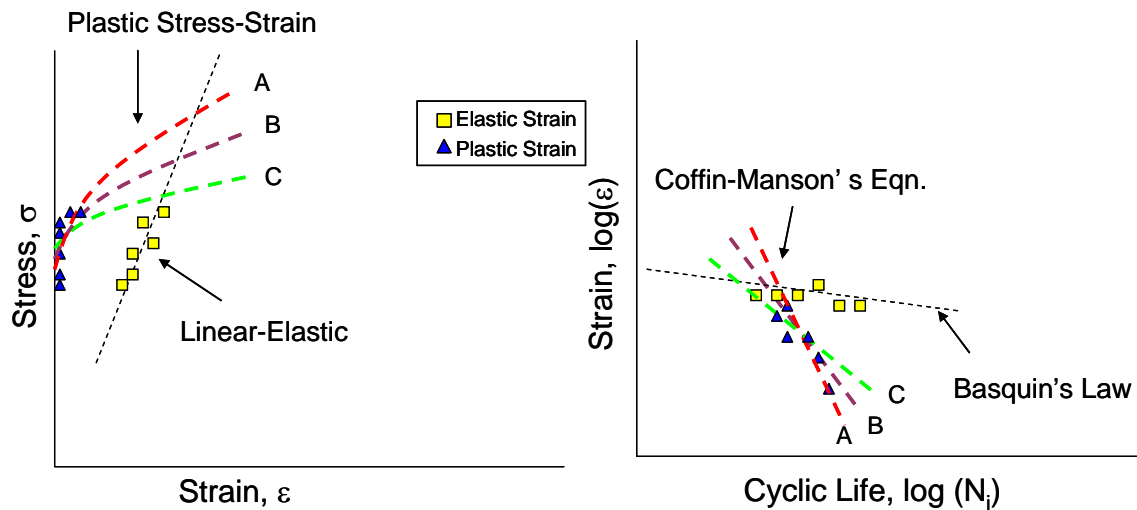
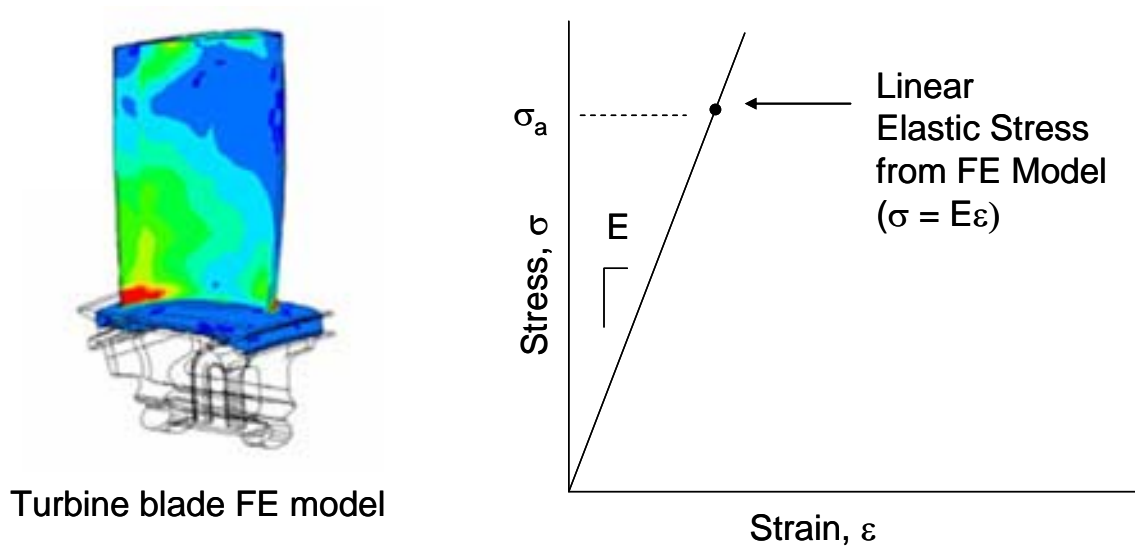


Figure 2.7. LCF data set with insufficient plastic strain data for definition of plastic strain terms.

Several other short-comings in the accepted methodology are noted. The current methodology is simply a curve fit through the acquired test data, and does not provide any guidance for determining whether the resulting model fits the anticipated behavior. Also, no published methods exist to estimate the fatigue properties of a Ni-base superalloy. This information would be very helpful for initial set up of an LCF test matrix.

The following is a presentation of one approach to estimating the LCF life of a gas turbine component. Steady-state component stress can be predicted by the use of a

linear-elastic FE model as shown in Figure 2.8. The model shown in this figure is of a rotating turbine blade, which must sustain significant thermal and mechanical loading. The first step in calculating LCF life is recording the stress and temperature ( $\sigma_a$  and  $T_a$ ) in the region of concern in the FE model.



**Figure 2.8. Linear-elastic FE model stress results.**

A stress shake-down must be performed to capture the effects of initial yielding. This initial yielding shake-down is used to find the stress ( $\sigma_A$ ) and strain ( $\epsilon_A$ ) on the monotonic stress-strain curve, which corresponds to the elastic stress ( $\sigma_a$ ) and strain ( $\epsilon_a$ ) from the FE model as shown in Figure 2.9. The monotonic stress-strain curve is of the same form as the cyclic stress-strain curve (Eq. 2.9), except that the constants ( $K'$  and  $n'$ ) are from tensile test data. The cyclic stress-strain curve is used at the peak temperature of interest ( $T_a$ ). A common method for shake-down uses Neuber's rule [3],

$$\sigma_A \varepsilon_A = \frac{(K_t \sigma_a)^2}{E} \quad (2.17)$$

where  $K_t$  a stress concentration factor applied to the linear elastic stress, and  $E$  is the elastic modulus. The stress ( $\sigma_A$ ) and strain ( $\varepsilon_A$ ) are found by iteratively solving with the monotonic stress-strain equation (similar to Eq. 2.9).

The Bauschinger effect is commonly used to describe unloading, which is the observation that yielding upon unloading often occurs prior to the stress reaching the yield strength for monotonic compression. Kinematic hardening assumes that yielding occurs upon unloading at  $2\sigma_y$ , and is in agreement with the Bauschinger effect [3].

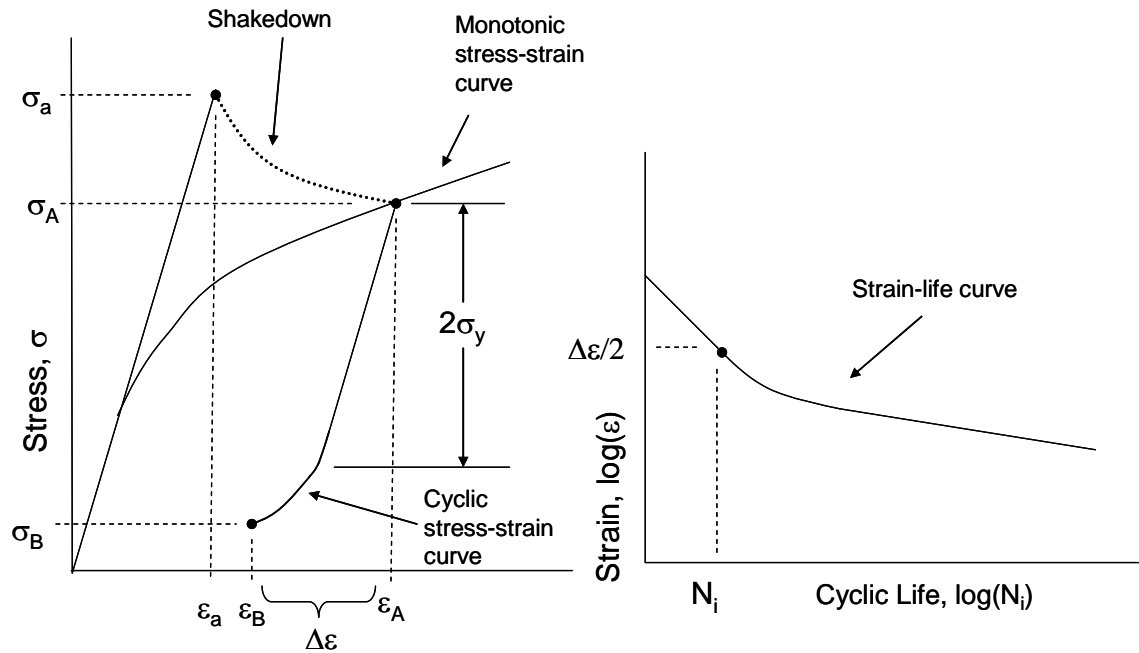


**Figure 2.9. Process of LCF life determination.**

If the stress ( $\sigma_B$ ) and temperature ( $T_b$ ) upon shut-down are known, then kinematic hardening and the cyclic stress-strain curve can be used to solve for the strain ( $\varepsilon_B$ ) upon

unloading. This information can be used to estimate the strain range ( $\Delta\varepsilon$ ) that the component will experience during cyclic operation. This strain range can be compared to data from a strain-life curve to estimate the component cyclic life. The strain-life data is typically from tests corresponding to the steady-state operating temperature of the component ( $T_a$ ).

## 2.2. Reference Methods

Historically, there have been several methods used to estimate the low-cycle fatigue behavior of materials. These classes of methods include: equations of approximation, strain compatibility, and anchor points. In the following, each of these methods is discussed, and the limitations of each are discussed.

Many approximations exist for estimating the four fatigue constants ( $\sigma_f', b, \varepsilon_f', c$ ) in the strain-life curve (Eq. 2.12) [10, 11, 12, 13, 14]. Some of the most well known approximation methods include: Manson's Universal Slopes, Manson's Four Point, and the Modified Four Point by Ong. Each of these methods approximates fatigue data in terms of monotonic tensile test data. If monotonic tests at elevated temperatures are available, the temperature dependence effect can be estimated with these equations.

Manson proposed the Four-Point Correlation Method, which provides an approximation for the strain-life constants [11],

$$\sigma_f' = \frac{E}{2} \times 10^{b \log(2) + \log\left[\frac{2.5\sigma_{ULT}(1+e)}{E}\right]} \quad (2.18a)$$

$$b = \frac{\log\left[\frac{2.5(1+e)}{0.9}\right]}{\log\left[\frac{1}{4 \times 10^5}\right]} \quad (2.18b)$$

$$\varepsilon_f' = \frac{1}{2} \times 10^{c \log\left(\frac{1}{20}\right) + \log\left(\frac{1}{4}e^{3/4}\right)} \quad (2.18c)$$

$$c = \frac{1}{3} \log\left[\frac{0.0132 - \Delta\varepsilon^*}{1.91}\right] - \frac{1}{3} \log\left(\frac{1}{4}e^{3/4}\right) \quad (2.18d)$$

$$\Delta\varepsilon^* = 10^{b \log(4 \times 10^4) + \log\left[\frac{2.5\sigma_{ULT}(1+e)}{E}\right]} \quad (2.18e)$$

This method used knowledge of typical points on the strain-life curve for the elastic and plastic components to estimate the constants [10]. These equations are a function of the elongation to failure ( $e$ ), and the ultimate tensile strength ( $\sigma_{ULT}$ ). A new variable is defined in this equation ( $\Delta\varepsilon^*$ ), which is the elastic strain range at  $10^4$  cycles.

The equations for Manson's Universal Slopes approximation method are as follows [10]:

$$\sigma_f' = 3.5\sigma_{ULT} \quad (2.19a)$$

$$b = -0.12 \quad (2.19b)$$

$$\varepsilon_f' = \left\{ \ln\left[\frac{1}{1-RA}\right] \right\}^{0.6} \quad (2.19c)$$

$$c = -0.6 \quad (2.19d)$$

This method is a function of the ultimate tensile strength ( $\sigma_{ULT}$ ), and the reduction in area (RA). These equations assume that the slopes of the elastic and plastic strain terms in the strain-life equation are constant for all materials.

The constants for Ong's Modified Four-Point Correlation method [11] is given by:

$$\sigma_f' = \sigma_{ULT}(1 + e) \quad (2.20a)$$

$$b = \frac{1}{6} \left\{ \log \left[ 0.16 \left( \frac{\sigma_{ULT}}{E} \right)^{0.81} \right] \right\} - \log \left( \frac{\sigma_{ULT}}{E} \right) \quad (2.20b)$$

$$\varepsilon_f' = e \quad (2.20c)$$

$$c = \frac{1}{4} \log \left( \frac{0.00737 - \Delta \varepsilon_e^*}{2.074} \right) - \log(e) \quad (2.20d)$$

$$\frac{\Delta \varepsilon_e^*}{2} = \left( \frac{\sigma}{E} \right) 10^{\frac{2}{3} \left\{ \log \left[ 0.16 \left( \frac{\sigma_{ULT}}{E} \right)^{0.81} \right] - \log \left( \frac{\sigma_f'}{E} \right) \right\}} \quad (2.20e)$$

$$\sigma_f \cong \sigma_f' \quad (2.20f)$$

This approximation uses the same procedure as Manson's Four-Point Method except that the author adjusted some terms to improve the curve fit to tensile data [13]. These equations are a function of the ultimate strength ( $\sigma_{ULT}$ ), the elongation to failure ( $e$ ), and the elastic modulus ( $E$ ). The term variable  $\frac{\Delta \varepsilon_e^*}{2}$  is the elastic strain at  $10^4$  cycles.

There are limitations to the approximation models. Of the 29 materials evaluated in Manson's paper which proposes his two methods, only one is a Ni-base superalloy (Inconel-X). Most of the tests used in deriving these relations were with steel. Also,

most of the LCF tests used to examine the correlation are at room temperature. Several investigators [11,12, and 14] compare the approximation methods to test data, most of which is at room temperature. Meggiolaro and Castro [14] compare the strain-life curve in the low-cycle range for steel at various temperatures between room temperature to 800°C, and come to the unlikely conclusion that the temperature effects do not generally affect the results.

The method used to evaluate the three approximation methods is by comparing the resulting approximation models to the standard methodology model and strain-controlled test data at the test temperature of 750°C. Comparison of the results show that the approximation methods are non-conservative, and use of these equations is expected to over-estimate life as shown in Figure 2.10. Manson's Four Point correlation and Ong are very similar, but over estimate life by an order of magnitude. Manson's Universal Slopes over-estimates life by two orders of magnitude.

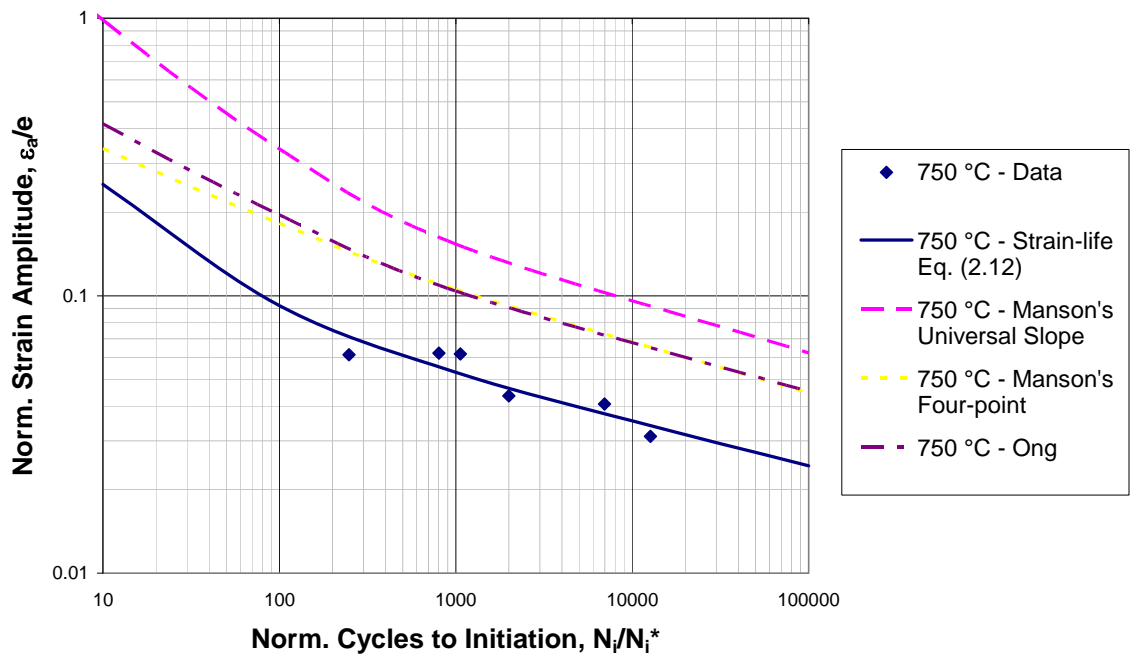


Figure 2.10. Approximation methods to curve fit from LCF test data for IN738 LC at 750°C.

The  $R^2$  errors listed in Table 2.2 confirm that the standard method provides the best fit through the test data. See section 3.4 for a thorough description of  $R^2$ . As such, it was concluded that most approximation methods do not work well for predicting the behavior of this alloy at elevated temperatures.

Table 2.2. Strain-life fatigue constant comparison.

Method	Curve Fit from LCF Test Data	Manson's Universals Slopes (1965)	Manson's four point (1965)	Ong (1993)
$R^2$ Error	0.914	0.661	0.738	0.708

Burke and Beck [8] offer a unique proposal by offering a modified-strain life equation (Eq. 2.12). This paper involved LCF test data of Ni-base superalloy IN617 at 760 and 871°C. The proposed approximation method is to combine the plastic strain data for both temperatures in determining the slope of the Coffin-Manson (Eq. 2.10) or fatigue ductility exponent (c). Recall that the present methodology groups data into like temperatures for regression analysis. This proposed equation is shown in Eq. 2.21, with the constants defined the same as Eq. 2.12. Note that the temperature dependence is demonstrated by showing the constants as a function of T.

$$\frac{\Delta \varepsilon_i}{2} = \varepsilon'_f(T)(N_i)^{-c} + \frac{\sigma'_f(T)}{E(T)}(N_i)^{-b(T)} \quad (2.21)$$

A method exists for approximating the constants in the stress-strain equation ( $K', n'$ , Eq. 2.9) from known constants in the strain-life equation ( $\sigma'_f, b, \varepsilon'_f, c$ , Eq. 2.12). This method is provided by an assumption of strain equality between the elastic and plastic strains from the stress-strain relation (Eq. 2.9) and the elastic and plastic terms from the strain-life relation (Eq. 2.12). Equality of the elastic terms yields Eq. 2.22., and equality of the plastic terms yields Eq. 2.23.

$$\frac{\Delta \varepsilon_e}{2} = \frac{\sigma}{E} = \frac{\sigma'_f}{E}(N_i)^b \quad (2.22)$$

$$\frac{\Delta \varepsilon_p}{2} = \left( \frac{\sigma}{E} \right)^{1/n'} = \varepsilon_f' (N_i)^c \quad (2.23)$$

Equation 2.24 results if Eqns. 2.22 and 2.23 are solved for stress, and set equal to each other. This equation represents the strain compatibility relation in terms of cycles to initiation.

$$\sigma_f' (N_i)^b = K' \varepsilon_f'^{n'} (N_i)^{cn'} \quad (2.24)$$

Since the reversals to failure must be equal to each other, the intercept and slope of the two power law fits must be equal. This equality results in the two well known compatibility relations solved for  $K'$  and  $n'$  as shown in Eqns. 2.25 [5].

$$K' = \frac{\sigma_f'}{\varepsilon_f'^{n'}} \quad (2.25a)$$

$$n' = \frac{b}{c} \quad (2.25b)$$

The recently published reference texts [3,5, and 16] agree that the preferred method to calculate  $K'$  and  $n'$  is by linear regression from stress and strain test data rather than Eqns. 2.25. Stephens, Fatemi, Stephens, and Fuchs [16] offers some insight into why linear regression should be used. This text states that the resulting values of  $K'$  and  $n'$  could be similar or different depending on whether Eqns. 2.25 are used instead of

linear regression. A large difference can indicate that the elastic and plastic strain-life equation (Eq. 2.12) is not well represented by log-log linearized fits.

Most approximation methods estimate fatigue constants from monotonic test data. A common approximation [6,10] used to estimate the failure stress ( $\sigma_f$ ) by including the increase in stress in a monotonic test after necking, or reduction in the cross-sectional area of the specimen has begun is given by:

$$\sigma_f = \sigma_{ULT}(1 + e) \quad (2.26)$$

which is a function of the ultimate strength ( $\sigma_{ULT}$ ) and elongation ( $e$ ). This estimate of the failure stress is depicted in Figure 2.11.

Likewise, the failure strain ( $\varepsilon_f$ ) is often estimated by the failure elongation ( $e$ ) or plastic deformation measured from a failure specimen.

$$\varepsilon_f = e \quad (2.27)$$

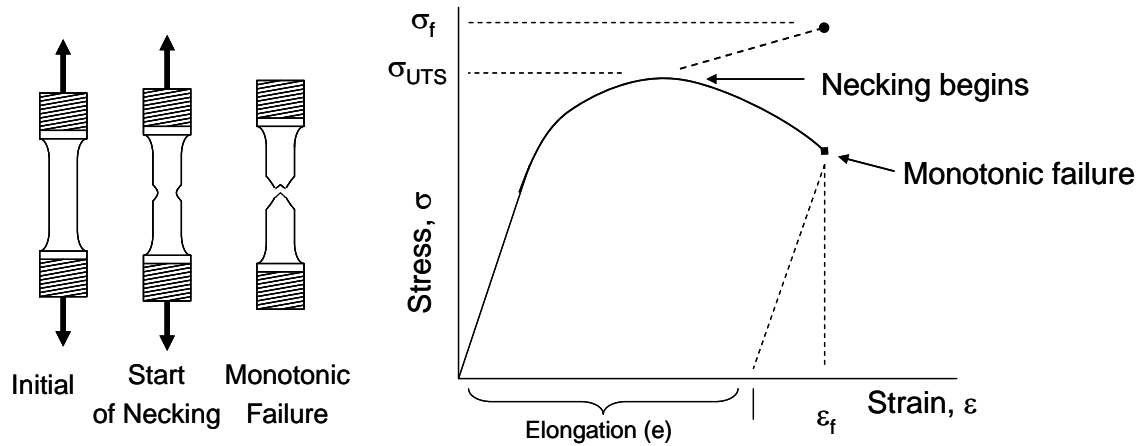


**Figure 2.11. Depiction of monotonic test.**

Another approximation technique is to include a monotonic test data point in with an existing LCF data set, which has been termed an anchor point. The purpose of the anchor point is to provide an improved qualitative fit of the stress-strain and strain-life curves outside of the LCF data points. A well chosen anchor point must not affect the curve fit over the range where actual LCF test data exists. The method of including the anchor point is to treat it as a fatigue data point during the linear regression modeling process. An anchor point is included with a typical LCF data set in Figure 2.12. The anchor point is included at  $\frac{1}{2}$  cycle, where the stress amplitude is the failure stress and the elongation is the failure strain.

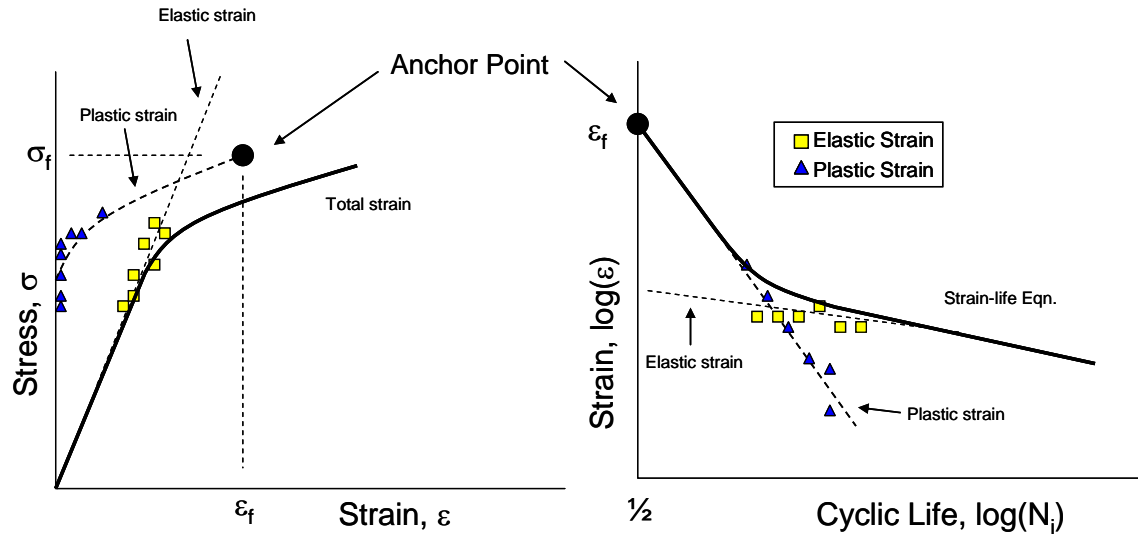


Figure 2.12. Depiction of anchor point.

### 2.3. Existing Experimental Results

Several references include IN738 LC strain-life data in the open literature. Note that IN738 LC is a cast, Ni-base superalloy typically used for turbine components, where the LC stands for low carbon. Viswanathan [2] compares IN738 LCF and TMF strain-life data at 427 °C and 871 °C at several strain rates. The Aerospace Structural Metals Handbook [17] contains strain-life data points for IN738 and IN738 LC, which includes critical information such as temperature, heat treatment, and strain rate. However, none of this data is of the same heat treatment, strain rate, and temperature as the data used for this thesis. Also, none of the stress amplitude information is available in this data.

Another interesting data set was available in the master's thesis by Yandt [18]. This data is from IN738 LC at 950°C with a similar heat treatment, and used a standard ASTM specimen design. However, these tests were at a lower strain rate of 0.1% /minute, which is much lower than 6.0%/minute as used in this data.

Danzer and Bressers [25] have published work using IN738 LC to consider the creep-fatigue interaction effects, rather than extrapolation of LCF test data to high stress amplitudes as with this project. Their work involves testing creep rupture and LCF tests independently, and are combining the effects with a linear time dependent damage accumulation rule.

Another source for data is provided by Marchionni [22]. This source includes LCF test data at 850°C at the same strain rate as this project (6.0%/min). However, the cyclic lives are a fraction of the measured values using data from this project for an unknown reason. The strain range is very high in this data upto 2.5%. The specimen design is tubular for induction heating, and it is possible that the difference in life is due to the specimen design. This data also shows the effect of testing in air rather than inert gas reduces the cyclic life at 850°C for IN738 LC.

Data from Morrow and Tuler [6] proved valuable by providing a reference data set with some very high strain LCF tests using Ni-base alloy IN713 LC. This data set is unique because it includes a broad range of test data into the very low cycle regime (0.67% to 4.1% strain and 5390 to 3 cycles). This data is from fully reversed tests at room temperature. One difference is that the specimens were from cast cylinders, whereas the IN738 LC data in the project was from a cast slab, and machined into specimens.

The base material of IN713 LC is somewhat similar to IN738 LC. IN738 LC is typically used for turbine blades, and IN713 LC is a disk material. Both materials are cast, and have similar basic mechanical properties at room temperature as shown in Table 2.3.

Table 2.3. Comparison of basic properties of IN713LC and IN738 LC.

Material	IN 713 LC	IN 738 LC
Reference	[6]	[17]
<b>Main Constituents (Weight %)</b>		
Nickel	73.5	61.5
Chromium	13.0	16.1
Cobalt	2.3	8.4
Titanium	0.6	3.6
Aluminum	6.0	3.3
Tungsten		2.6
Molybdenum	4.5	1.7
Tantalum		1.7
Niobium		0.9
Carbon	0.1	0.2
Silicon	0.4	
Iron	1.0	
Manganese	0.2	
<b>Basic Properties</b>		
Ultimate Tensile Strength (MPa)	1069	1062
0.2% Yield Strength (MPa)	831	883
Elongation %, min	10	8
Reduction in Area %, min	10	11

The data set for IN713 LC shows some interesting trends at high strain ranges. A plot of the stress-strain curve is shown in Figure 2.13. It is seen that the data tends to follow a consistent power law fit, but above about 1.45% strain, the data shows a decrease towards the monotonic curve. Since the data points above 1.45% strain show a steep drop off in stress amplitude, only the data points below 1.45% strain were used to create the cyclic stress-strain curve fit.

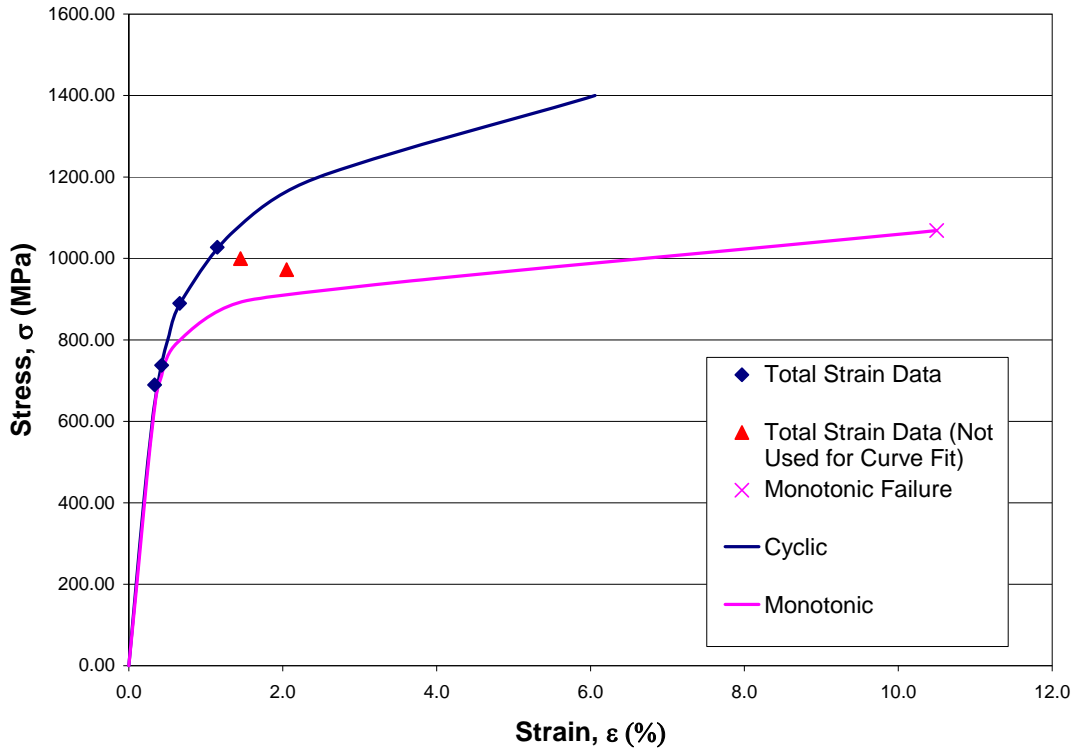


**Figure 2.13. IN713LC monotonic and cyclic stress-strain curve.**

The data reveals that significant strain hardening has occurred below 1.45% strain. Recall that Figure 2.3 shows the effect of strain hardening, which results in a cyclic stress-strain curve above the monotonic stress-strain curve. An interesting feature of this data is that it appears to reveal an upper limit provided by the cyclic stress-strain curve, and a lower limit provided by the monotonic stress-strain curve.

A similar plot of the strain-life data for IN713 LC at room temperature is shown in Figure 2.14. Lemaitre and Dufailly [4] report that the Coffin-Manson relationship over-predicts the reversals to failure at very low cycles. It is possible that this data shows a similar trend since the 4.1% strain data shows a drop from the strain-life equation.

However, the strain-life equation is typically determined from data from stable hysteresis loops, and it is doubtful whether these could be achieved at only 3 cycles.

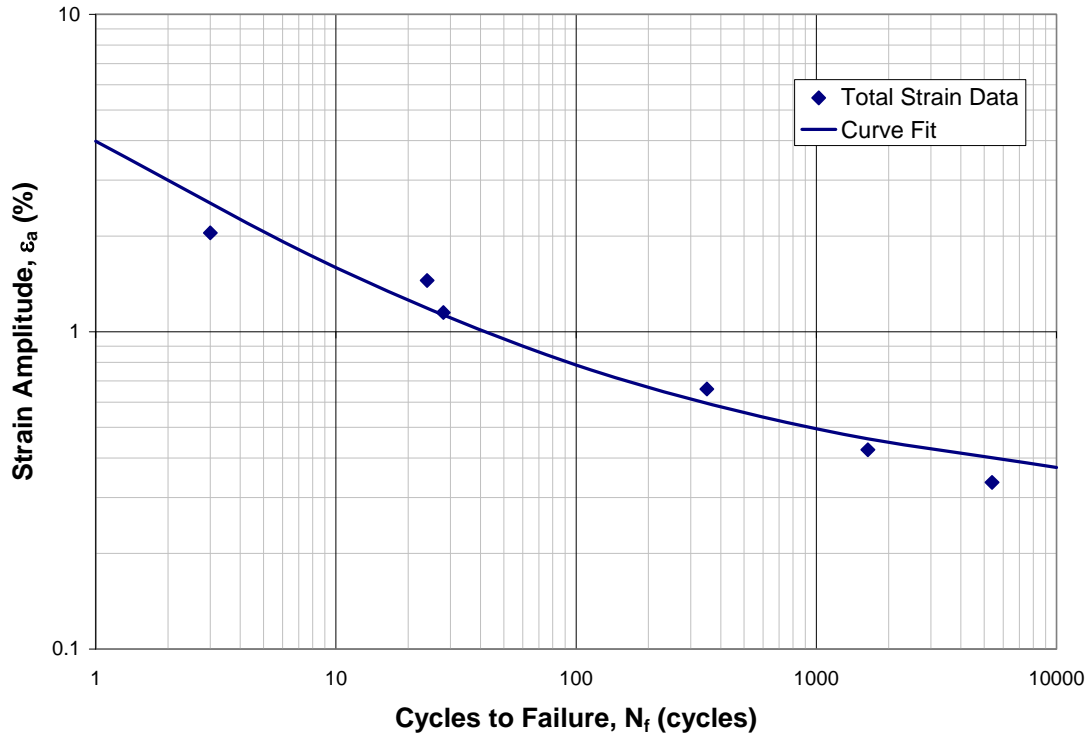


Figure 2.14. Strain-life curve for IN713 LC at room temperature.

#### 2.4. Thesis Objective

Section 2.1 highlighted several of the issues have been discussed with the current LCF methodology. This methodology stipulates that the stress-strain (Eq. 2.9) and strain-life (Eq. 2.12) equations are only valid over the range of the available data. There are few publications showing efforts to extrapolate from moderate strain-range data sets into high strain-range and high stress amplitudes. It was demonstrated that several published extrapolation methods did not work well at approximating the high temperature strain-life behavior of a Ni-base superalloy.

An investigation will be used to prove or disprove the following:

- 1) Low cycle fatigue behavior is described by an “upper bounds” when strain hardening or softening affects the stress-strain and strain-life equation, and a “lower bounds” when strain hardening or softening effects are negligible or at very high strain ranges where strain hardening or softening does not have sufficient cycles to occur. This hypothesis is shown graphically in Figure 2.15.

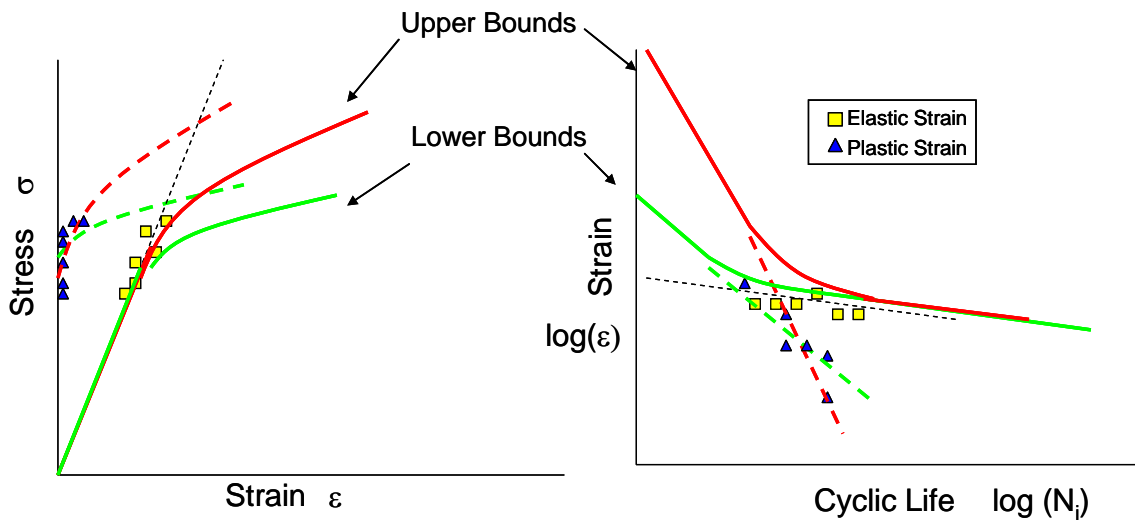


Figure 2.15. Bounding estimates for the stress-strain and strain-life equations.

- 2) The anchor point approach of including monotonic test data with fatigue test data is an accurate method for extrapolating high strain low cycle fatigue behavior when strain hardening or softening is negligible or at very high strain ranges where strain hardening or softening does not have sufficient cycles to occur.
- 3) An anchor point can be an accurate representation of the upper bounds of material behavior, when it is scaled by estimated changes in the shape of the hysteresis loop

- between initial and mid-life cycles for to account for strain hardening or softening.
- 4) If the constants describing the elastic strains are known, then an effective anchor point failure stress can be calculated from monotonic test data at  $\frac{1}{2}$  cycle, and making an assumption that the failure strain is equal to the elongation at failure. This effective anchor point will describe an upper bounds of material behavior including strain hardening or softening effects as necessary.
  - 5) If significant scatter exists in the plastic strain-life data used for the Coffin-Manson (Eq. 2.11), and data exists for several different temperatures, then it is more accurate to group together all strain-life data, and assume temperature independence of the Coffin-Manson equation for all temperature data.

If these goals are achieved, the results will be a more accurate understanding of the behavior of IN738 LC at high stress amplitudes and high strain ranges.

### 3. METHOD

The following section presents several options, which allow improved ability to extrapolate from an existing test data set to predict high strain behavior of a Ni-base superalloy. The procedures for obtaining and handling the experimental fatigue data are discussed in the following sections.

#### 3.1. Normalization of Test Data

The objective of this document is to show trends from a test data set, but the actual values of the data cannot be disclosed to the reader. Therefore, the value of each test data point has been normalized. The LCF test data used in this thesis is defined in terms of both the stress-strain curve and strain-life curves. Each stress ( $\sigma$ ) has been divided by the ultimate strength ( $\sigma_{ULT}$ ). Each strain ( $\epsilon$ ) has been divided by the failure elongation ( $e$ ). The measured cyclic lives to crack initiation ( $N_i$ ) have been divided by an arbitrary constant ( $N_i^*$ ) as shown in Figure 3.1. A similar process has been utilized as necessary to avoid disclosing the values of other test data throughout this document.

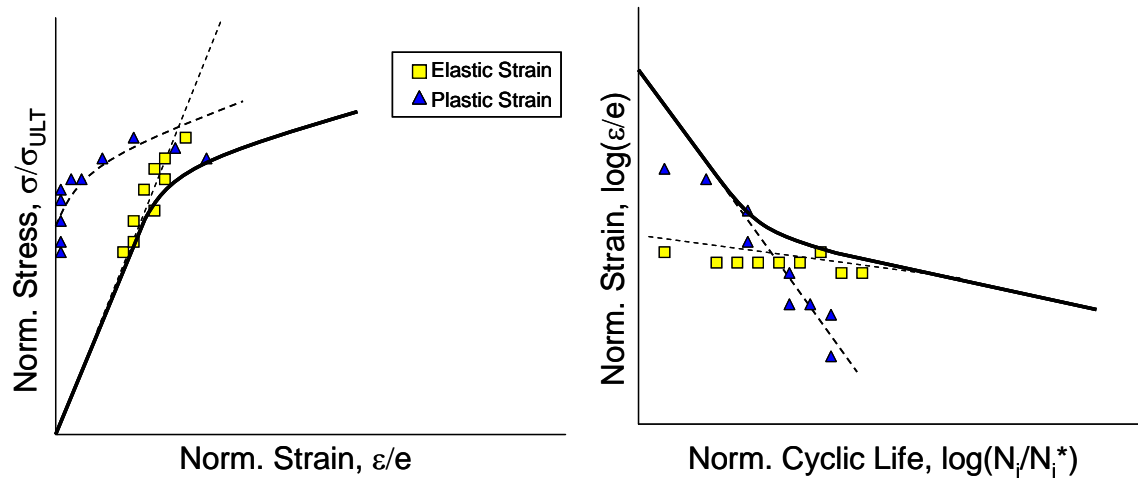


Figure 3.1. Depiction of method for protection of proprietary test data.

### 3.2. Lower Bounds

Recall that Section 2.3 included a reference data set with high strain test data for IN713 LC at room temperature, which showed significant strain hardening. Recall that the base anchor point is considered a method for providing a qualitative improvement in the cyclic stress-strain and strain-life curves at strain ranges outside of LCF test data. However, this method assumes that the base anchor point will provide an accurate estimate of behavior under certain circumstances. It is believed that the base anchor point will be accurate when very little strain hardening or softening occurs, or at very high strain ranges where failure occurs when insufficient cycles for strain hardening or softening effects have occurred.

The proposed method for predicting the lower bounds (LB) behavior to achieve is to include an anchor point representing monotonic failure into the base data set. This is equivalent to the reference anchor point as described in Section 2.2, and depicted in Figure 2.12.

### 3.3. Upper Bounds

The first option will be denoted as upper bounds, Option 1 (UB1). This option recognizes that the anchor point method described in Section 2.2 does not account for strain hardening or softening, and the intention of option 1 is to modify the base anchor point to account for these effects. The reference test data shown in Section 2.3 demonstrates that strain hardening effects are significant in a similar Ni-base superalloy.

The proposed methodology uses changes in the hysteresis loop between the first cycle and the mid-life stabilized cycle to extrapolate the monotonic anchor point to include strain hardening or softening effects as necessary. Figure 2.3 shows the typical changes in the hysteresis loops between the initial and stabilized mid-life cycles that occur during strain hardening.

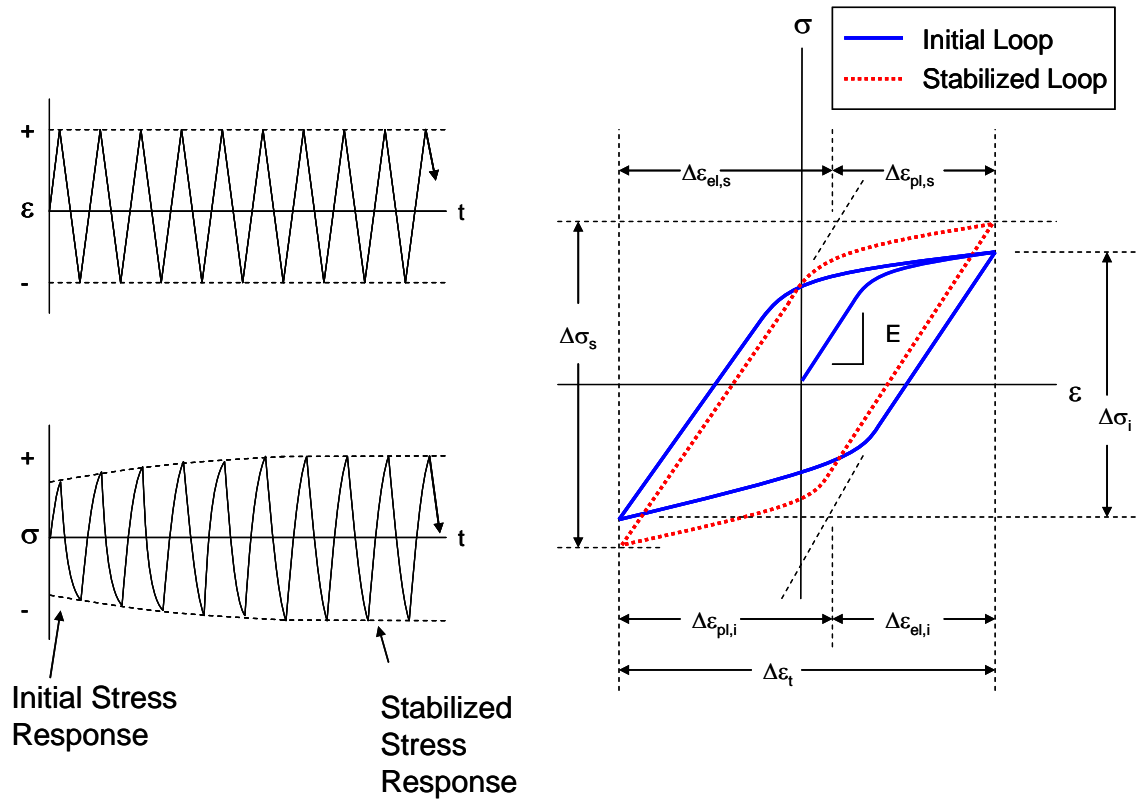


**Figure 3.2. Effect of strain hardening on initial versus stable mid-life hysteresis loops.**

Strain hardening is known to increase the stress amplitude until it achieves a stabilized value, and the initial stress range ( $\Delta\sigma_i$ ) will increase to the stabilized stress range ( $\Delta\sigma_s$ ). However, strain hardening may also change the amount of the plastic strain ( $\Delta\varepsilon_{pl}$ ), even if the total strain must remain constant during testing as depicted in Figure 3.2. Here, the initial plastic strain is termed  $\Delta\varepsilon_{pl,i}$ , and the stabilized plastic strain is termed  $\Delta\varepsilon_{pl,s}$ .

The changes in the initial stress range compared to the mid-life stress range for each data point for each temperature are graphed in Figure 3.3a. Likewise, the changes in the initial plastic strain range as compared to the stable mid-life plastic strain range for

each data point at each temperature is shown in Figure 3.3b. Here, the normalized initial

and stabilized stress range are termed  $\frac{\Delta\sigma_i}{\sigma_{ULT}}$  and  $\frac{\Delta\sigma_s}{\sigma_{ULT}}$ , and the normalized initial and

stabilized strain range are  $\frac{\Delta\varepsilon_i}{\Delta\varepsilon_i^*}$  and  $\frac{\Delta\varepsilon_s}{\Delta\varepsilon_s^*}$  respectively.

Assuming linear interpolation, a conversion factor can be applied to the monotonic test data anchor point to account for strain hardening effects. Note that it is assumed that the intercept is negligible and is zero. The new anchor point defined for the failure stress is given by Eq. 3.1:

$$\sigma_f = C_1\sigma_{ULT}(1 + e) \quad (3.1)$$

Here,  $C_1$  is the correction factor from linear regression as described,  $\sigma_{ULT}$  is the ultimate strength, and  $e$  is the failure elongation. Again, the intercept is assumed to be negligible and zero.

Similarly, the failure strain is written with a correction factor  $C_2$  from linear regression as described, which is scaled by the failure elongation ( $e$ ) as given in Eq. 3.2:

$$\varepsilon_f = C_2e \quad (3.2)$$

The constants  $C_1$  and  $C_2$  have been found using the process described as shown in Table 3.1.

**Table 3.1. Constants  $C_1$  and  $C_2$  from linear regression using base data set.**

Temperature (°C)	$C_1$ - Base Data Model	$C_2$ - Base Data Model
24	1.090	0.694
400	1.437	0.543
750	1.049	0.632
850	0.876	1.105

The resulting anchor point is the same as that depicted in Figure 2.12. One may note that negligible strain hardening may actually occur at a cyclic fatigue anchor point at few cycles. If very high strain cycles are expected, then the lower bounds (LB) life estimate equations should be used instead. The purpose of this correction factor, rather, is to capture the effect of strain hardening on the stress-strain and strain-life curve that moderate strain range LCF data points may experience.

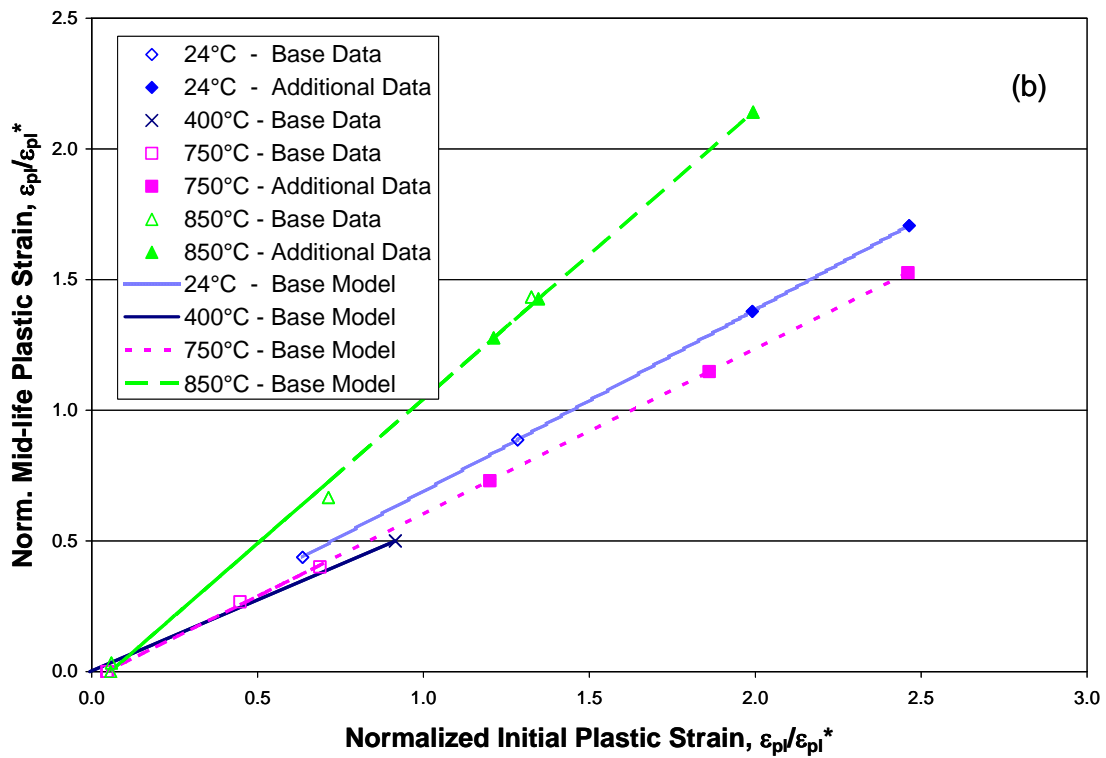
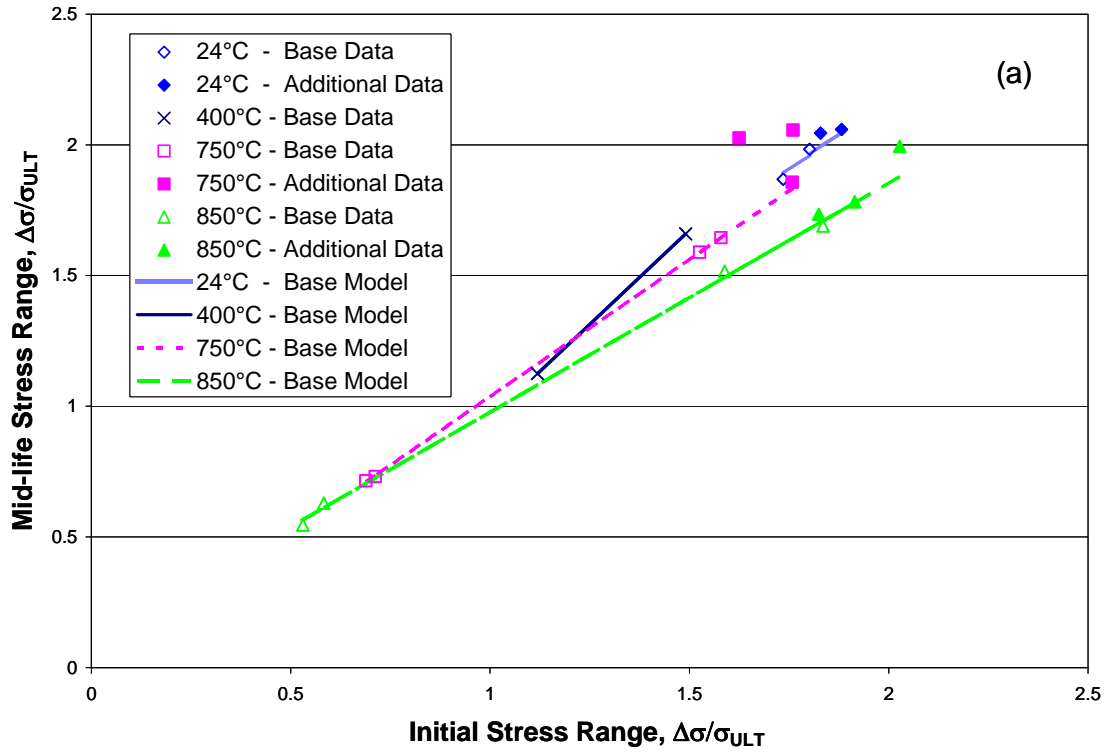


Figure 3.3. Plots of (a) initial and stabilized stress range, and (b) initial and mid-life plastic strain used for UB1.

The second option is denoted as upper bounds, Option 2 (UB2). This option utilizes an anchor point calculated by assuming strain compatibility to provide an estimate of upper bounding behavior. Recall that Section 2.2 described strain compatibility for the stress-strain and strain-life equation.

Recall, the condition of the base data set is that insufficient plastic strain data exists to characterize plastic strain terms in the stress-strain and strain-life equations as depicted in Figure 2.6. However, sufficient data does exist to characterize the elastic strain terms in the stress-strain and strain-life equations. As such, the constants describing the elastic strain terms are known  $(\sigma'_f, E, b)$ . Strain compatibility applied to the elastic strain terms resulted in Eq. 2.22. Equation 3.3 results if the elastic modulus is cancelled from each side of the equation, where  $\sigma'_f$  is the fatigue strength coefficient,  $b$  is the fatigue strength exponent, and  $N_i$  is the number of cycles to initiation.

$$\sigma = \sigma'_f (N_i)^b \quad (3.3)$$

Since the anchor point of choice corresponds to 1/2 cycle, and strain compatibility has been assumed, the failure stress can be calculated in terms of the fatigue strength coefficient ( $\sigma'_f$ ) and fatigue strength exponent ( $b$ ) as shown in Eq. 3.4.

$$\sigma_f = \sigma'_f \left[ \frac{1}{2} \right]^b \quad (3.4)$$

The failure strain is assumed to be equal to the elongation as shown in Eq. 3.5, which is identical to the original reference anchor point described in Section 2.2.

$$\varepsilon_f = e \tag{3.5}$$

A depiction of anchor point 2 is the same as shown for the base anchor point in Figure 2.12. The proposed method is to treat this anchor point as an LCF data point, and include it in the normal linear regression process.

The third option for the upper bounds is denoted as upper bounds, Option 3 (UB3). This hypothesis resulted from an observation that much scatter exists in the plastic strain-life data for IN738 LC as shown in Figure 3.4. The resulting strain-life curves show a similar slope at 400°C, 750°C, and 850°C, a shallow slope at 24°C, and a steep change in slope at 900°C. The shallow slope at 24°C is most likely due to a lack of test data at this temperature. The combined slope and intercept is very similar to the 400°C data, which appears to be along a median of the cluster of data.

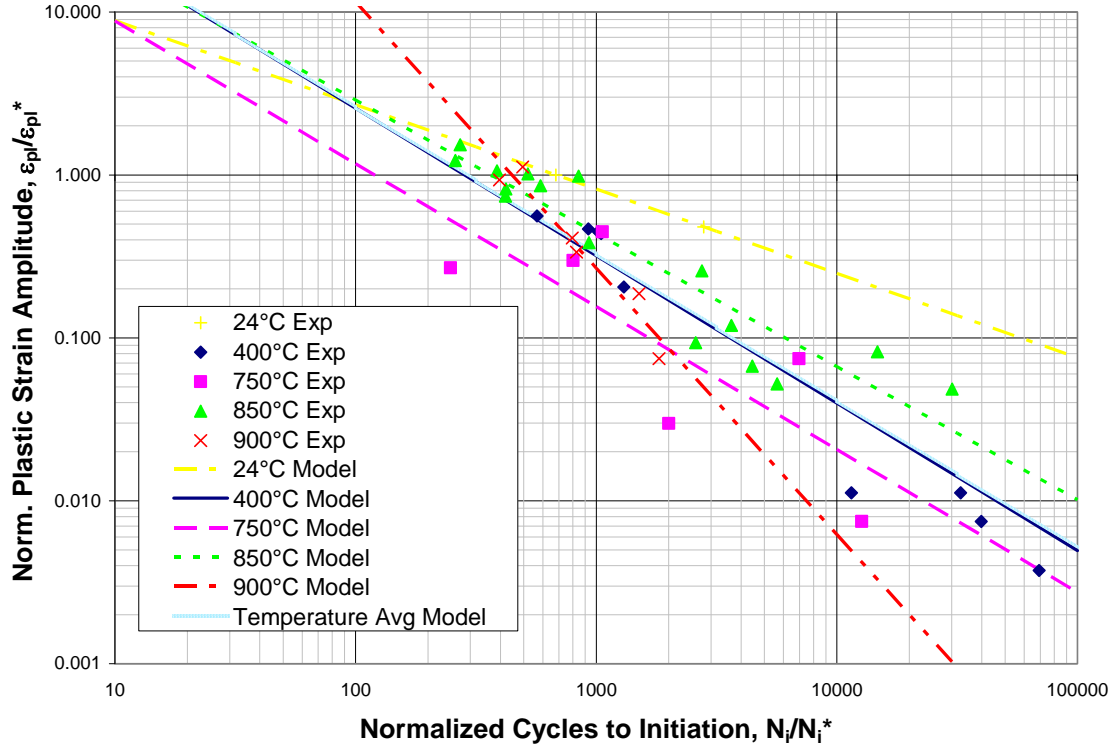


**Figure 3.4. Scatter in strain-life equation with temperature.**

Option UB3 is provided by grouping together all of the strain-life data, and treating it as temperature independent. The underlying assumption for using this method is that the error due to treating the plastic strain life data as temperature independent is smaller than the error due to scatter in the data. This is similar to the method proposed by Burke and Beck [8] for IN 617, except that both the strain hardening coefficient ( $\epsilon'_f$ ) and the strain hardening exponent ( $c$ ) are assumed to be temperature independent. The revised strain-life equation is shown in Eq. 3.6:

$$\frac{\Delta \epsilon_t}{2} = \epsilon'_f (2N_f)^{-c} + \frac{\sigma'_f(T)}{E(T)} (2N_f)^{-b(T)} \quad (3.6)$$

where  $\frac{\Delta \varepsilon_t}{2}$  is the total strain amplitude,  $\varepsilon_f'$  is the fatigue ductility coefficient,  $c$  is the fatigue ductility exponent,  $\sigma_f'$  is the fatigue strength coefficient, and  $b$  is the fatigue strength exponent. Note that constants which remain temperature dependent are shown as a function of  $T$ . Finally, the strain compatibility equations solved for  $K'$  and  $n'$  (Eqs. 2.25) are employed to find the cyclic strength coefficient ( $K'$ ) and the strain hardening exponent ( $n'$ ).

### 3.4. Comparison Method

The tool used for curve fit comparison is calculation of  $R^2$ , or coefficient of determination. This is one commonly used measure of the degree of linear association between an independent and dependent variable [20]. The equation for  $R^2$  is given by Eq. 3.7:

$$R^2 = \frac{[\sum (x - \bar{x}) \sum (y - \bar{y})]^2}{\sum (x - \bar{x})^2 \sum (y - \bar{y})^2} \quad (3.7)$$

where  $x$  is the independent variable, and  $\bar{x}$  is the mean independent variable,  $y$  is the dependent variable, and  $\bar{y}$  is the mean dependent variable. The calculation tool is MS Excel using the RSQ command. The output from the  $R^2$  calculation is a value between one and zero, where zero shows no linear correlation between the two variables, and one

shows a perfect linear correlation. This command has two arrays as inputs, which include a list of independent variables, and dependent variables.

The input to  $R^2$  is two arrays of strain, one being calculated and the other measured. After all seven of the curve fit constants ( $\sigma'_f, b, \varepsilon'_f, E, K', n'$ ) have been determined by linear regression using a particular method, the strain amplitudes may be calculated by either the stress-strain equation (Eq. 2.9) or the Modified Morrow strain-life equation (Eq. 2.14) as a function of the stress amplitude or cycles and mean stress. The  $R^2$  function is used to compare the calculated strains versus the measured strains. Specifically, the calculated strains from the stress-strain equation are compared to the strain amplitudes, and the Morrow-adjusted strains from the Modified Morrow strain-life equation are compared to the Modified Morrow strains.

### 3.5. Test Equipment

All mechanical tests were carried out at Siemens test lab in Casselberry, FL. The system is an MTS TestStar system. The main components of the system includes: a computer, a digital controller, a manual load control unit, a load frame, and a hydraulic pump as shown in Figure 3.5.

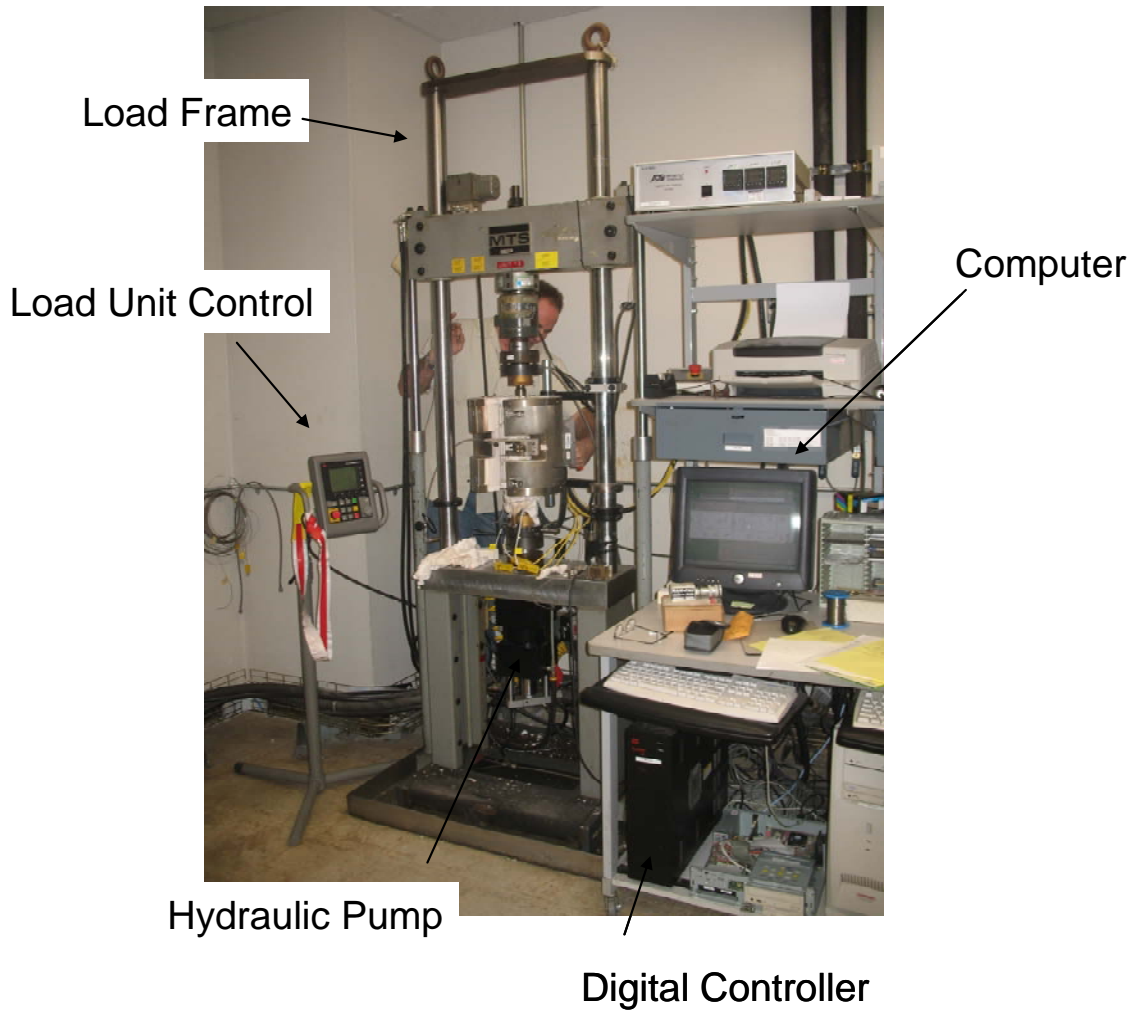


**Figure 3.5. LCF test equipment.**

The load frame contains all of the active equipment for loading and testing the specimen. The load control unit provides a local input device for manual operation of the hydraulics, and input of test parameters. The hydraulic pump provides the force for loading the specimens.

The digital controller and computer control the test during operation. The TestStar software is the main user interface, which allows the operator to control the test parameters, and post-process the results. Some test parameters that can be controlled

include: test temperature, strain rate, strain range, waveform shape, and testing control settings. The resulting plots include: cycle count, deflection, and load fluctuations over time.

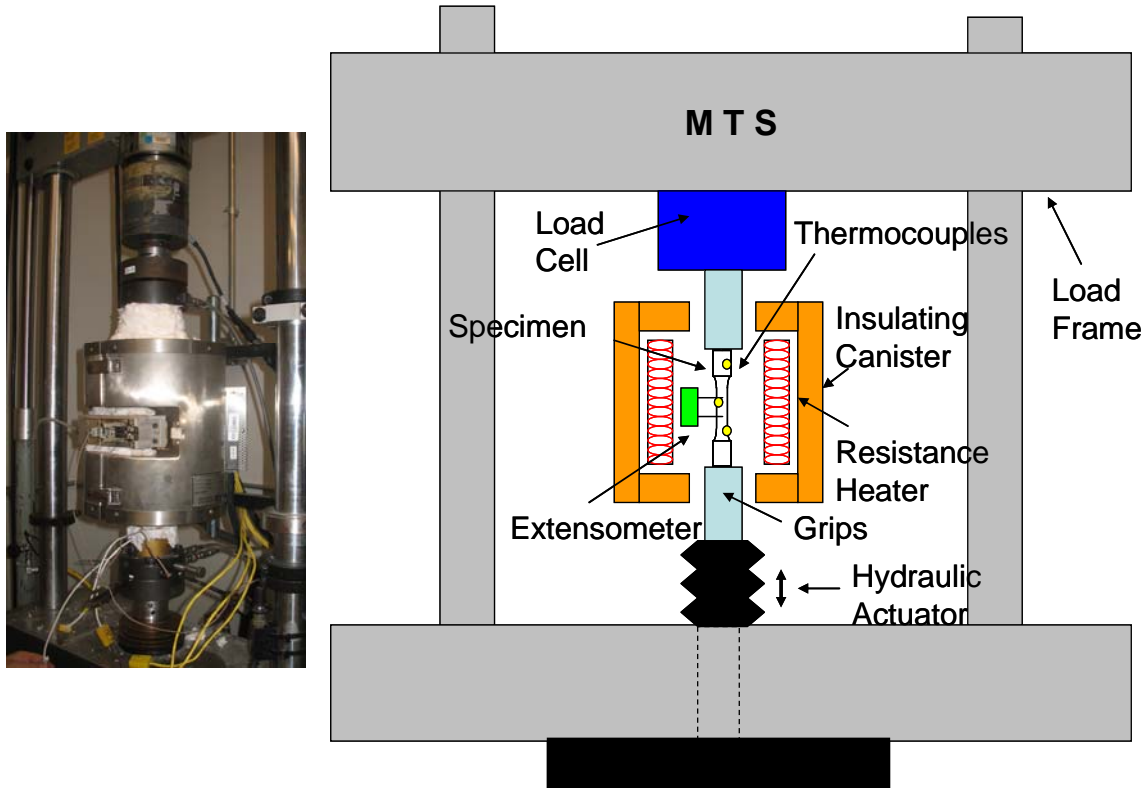


**Figure 3.6. Photograph and Depiction of load frame component details.**

Many critical components are located within the load frame. The specimen is mounted in the grips as depicted in Figure 3.6. The grips must often be water cooled due to the high temperatures in elevated temperature testing. The specimen is loaded by the hydraulic actuator as directed by the controller. The load cell measures the loading applied to the specimen.

The extensometer is the strain measurement device, and it measures the strain within the gage length (see Figure 3.7 for location). The type of extensometer used for this testing is spring loaded against the specimen, with the contact rods made of a high

temperature ceramic. The contact rods have a notch to match the diameter of the specimen to maximize the contact area between the specimen and extensometer to avoid slipping during testing.

The heating is provided by resistance heating. Resistance heating is fairly inefficient, and efforts are made to reduce heat loss to the environment during testing by encasing the coils in an insulated canister. The insulating canister is hard mounted to the load frame, and split into two halves which pivot about a bar to allow opening and closing. Latches are on the canister for securing closed during testing. Additional insulating felt material is placed about the inner and outer holes of the canister to avoid heat loss.

Low-cycle fatigue life is strongly affected by temperature, and temperature measurement is provided by thermocouples. Three thermocouple leads are wire tied to the specimen along the specimen to capture temperature distribution in the specimen. The control unit uses feedback from the thermocouples to maintain constant temperature during testing.

The specimens were made from a cast slab of IN738 LC, which was HIP'd, heat treated, and solution aged. The slab was blanked into rectangular blocks, and the blocks were machined into specimens. About 30 specimens were machined from the slab, of which 20 are available for testing.

A specimen design in conformance with the ASTM standard uniform-gage test section specimen was used for testing. The ends are threaded, and neck down in the center in an area known as the gage section, which is where specimen failure is intended to occur. The gage length was 3X to diameter, and the surface finish of the specimen is

polished to  $0.2 \mu\text{m}$  surface finish to minimize the surface effects on the measured life of the specimen.

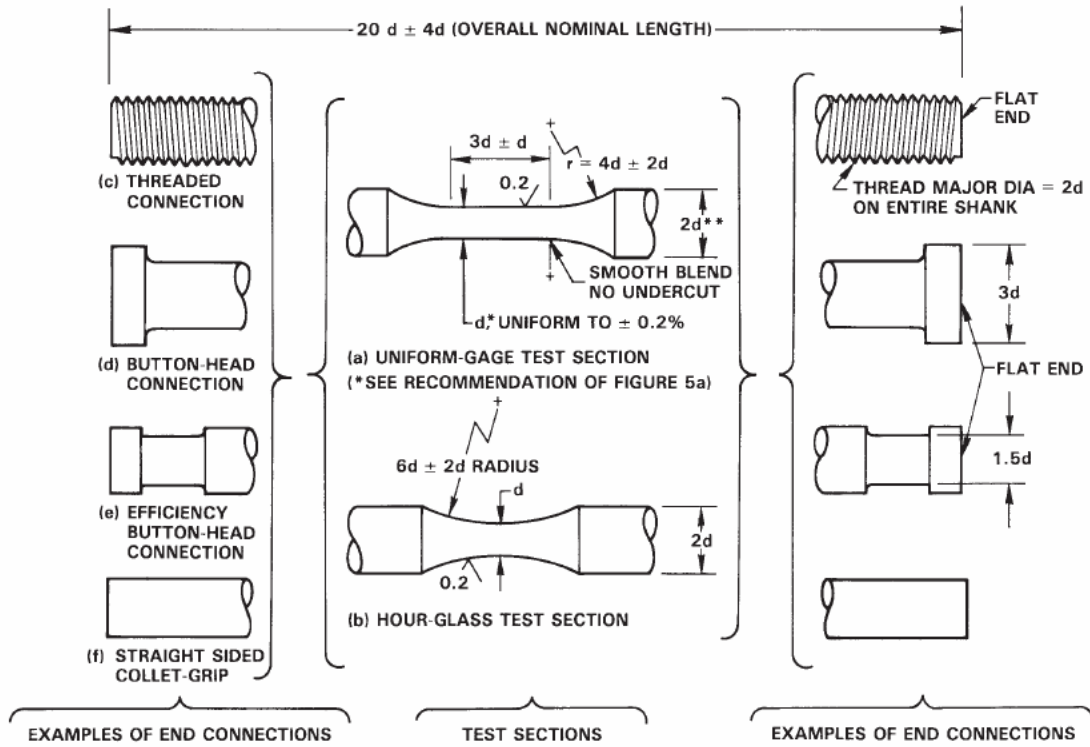


Figure 3.7. ASTM uniform gage specimen design [19].

### 3.6. Testing Procedure

The planned test matrix was established to provide test data characterizing the high stress amplitude, and high strain range behavior of IN738 LC, a Ni-base superalloy. High stress amplitudes are defined as approaching the ultimate strength, and are defined by  $\sigma_a/\sigma_{ULT}$  near unity as shown in Table 3.2. The normalized strain amplitudes ( $\Delta\epsilon/\epsilon$ ) were estimated from the existing data set to provide stress amplitudes approaching the ultimate strength. The plan was to gather additional high strain test data to supplement

the existing data set at four temperatures of interest (400°C, 750°C, 850°C, and 900°C).

Each test would be done in duplicate to include a statistical distribution in the study.

**Table 3.2. Planned Test Matrix.**

Test Temp (°C)	Norm. Stress Amplitude ( $\sigma_a/\sigma_{ULT}$ )	Norm. Strain Range ( $\Delta\varepsilon/e$ )	Test Quantity
400	0.876	0.222	2
400	0.919	0.295	2
750	1.006	0.187	2
750	1.111	0.249	2
850	0.934	0.145	2
850	1.036	0.194	2
900	0.743	0.114	2
900	0.772	0.153	2
TOTAL			16

The tests shall be performed per the standard strain-controlled LCF testing procedure per the ASTM standard [19]. The planned normalized strain range is within the maximum allowable strain range per the ASTM standard for a standard uniform gage section specimen which is being used. The ASTM standard suggests an hour-glass specimen design for tests above 2.0% strain range. There is no other known reason to deviate from standard testing practice procedure.

The ASTM standard stipulates several requirements for a test to be valid. The metal temperature in the gage section must be uniform over the duration of the test, which is defined by Eq. 3.8:

$$T_n = \Delta T \tag{3.8}$$

where  $T_n$  is the nominal test temperature in °C, and  $\Delta T$  is 2°C or 1%, whichever is greater. A test should be kept in strain control during the duration of the test. If material behavior permits, the strain range should be constant to within a few percent of the applied strain value.

Specimens made from coupons will have a surface finish history due to manufacturing process. Unless the test is meant to characterize the surface finish effect on LCF life, the effect of the surface finish should be minimized. This is accomplished by polishing the specimens and testing in an inert gas atmosphere if necessary to eliminate oxidation and corrosion effects.

The first step in LCF testing is preparation of the specimen for testing. The grips are removed from the load frame. A specimen is located, and is given a visual inspection. The diameter of the specimen is recorded, and shall be measured in at least two locations with a measurement device sensitive to 0.0125mm (0.0005in). The specimen is threaded into each end of the grips, and torqued to the proper value. The grips with the specimen attached are installed to the load frame.

The attachment bolts between the load cell and the grips are properly torqued. A gap will remain between the lower grip and the hydraulic ram. This gap is nearly always not equally distributed about the circumference. If the bolts between these components are tightened as-is, then a residual bending moment would result in the specimen, which would reduce the LCF life in the specimen, and skew the results.

The method for removing the bending moment is to shim the gap between the lower grip and the hydraulic ram with feeler gages. The gap between the components is measured, and shims are inserted to remove the gap. When the gap has been removed,

the bolts between the grips and hydraulic actuator are tightened to the proper torque. Thermocouple wires are wire tied to the specimen in three locations. The insulating canister is closed, and centered about the specimen.

A calibrated extensometer is mounted to the canister, and spring loaded against the specimen. The strain gage measures the longitudinal displacement of the specimen, and converts the displacements to a strain measurement using a Wheatstone bridge circuit. The extensometer used in elevated temperature testing has high temperature ceramic rods, which must be centered upon the gage section. The location of the extensometer is typically offset at cold build by a distance known as the stroke. The stroke is the offset required to correct for the thermal growth of the specimen during elevated temperature testing. Offsetting the specimen by the stroke at cold build allows the extensometer to be centered on the specimen during hot running conditions. Additional ceramic insulator felt is placed about the openings at the top and bottom of the insulating canister.

A test program is created in the TestStar software by choosing the test conditions, which often include temperature, strain amplitude, strain rate, and waveform. An initial estimate of the control gains (P, I, and D) must also be chosen. The test conditions which will stop testing are chosen to avoid damaging a specimen due to testing anomalies. These conditions are known as unit trip settings.

A modulus check is normally performed to determine if the system and specimen are operating as expected. The heaters are turned on, and set to the desired temperature of the test. It is important that the unit does not overshoot the desired temperature since this could affect the results. Sufficient time is allowed for the specimen to achieve

uniform steady-state temperatures after the thermocouples have stabilized to the set temperature prior to the beginning of testing.

The LCF test program begins, and the first few cycles are typically monitored to insure that the test is proceeding as expected. Most LCF tests run over a period of hours or days, and are often run unsupervised. The test conditions which will stop testing have already been established. Assuming the test runs as planned, the test is normally terminated either when the test specimen fails by rupture, or the limiting number of tests has been reached which is often called test run-out.

### 3.7. Test Post-Processing

After a test has been completed, the operator must post-process the data to determine if the test was valid. Often the initial and mid-life hysteresis loops, strain versus cycle, and stress versus cycle (stress history) plots are created for the test. The operator must consider whether any anomalies in the test have occurred that would invalidate the test. If so, the source of error is located, and the test is re-run.

Another aspect of post-processing is reduction of the data. If the data is considered valid, then the mid-life hysteresis loops are examined to determine the minimum and maximum stress, total strain range, and the inelastic strain range for the test. Design curves are generally based on the cycles to initiation ( $N_i$ ) of a crack, where the initiation is assumed when a certain percentage load drop has occurred during the test prior to failure. A 5% load drop was assumed for these tests. Often, some of the hysteresis loop data is stored for addressing questions that may arise regarding the data point. The data is then stored for use in the curve fitting procedure.

## 4. RESULTS

This section presents the results including the data and models developed in the course of this project. Data is both from the pre-existing data set and the additional data from high strain range tests gathered in this thesis. The models include the base linear regression process and the various models as explained in Chapter 3.

### 4.1. Base Data Set

The base data set includes 48 pre-existing data points for IN738 LC at  $R_\epsilon = -1$ .

The quantity of LCF data points in the base data set is shown by temperature and normalized strain range in Table 4.1.

**Table 4.1. Quantity, normalized strain range, and temperature of LCF data points in base data set for IN738 LC.**

24°C		400°C		750°C		850°C		900°C	
Norm. Strain Range ( $\Delta\epsilon/e$ )	Quantity	Norm. Strain Range ( $\Delta\epsilon/e$ )	Quantity	Norm. Strain Range ( $\Delta\epsilon/e$ )	Quantity	Norm. Strain Range ( $\Delta\epsilon/e$ )	Quantity	Norm. Strain Range ( $\Delta\epsilon/e$ )	Quantity
0.147	1	0.059	1	0.074	1	0.039	2	0.023	2
0.184	1	0.074	2	0.103	2	0.048	2	0.038	2
		0.089	7	0.148	3	0.058	2	0.053	2
		0.118	1			0.068	1	0.069	2
		0.148	5			0.077	1		
						0.097	8		
<b>TOTAL</b>	<b>2</b>		<b>16</b>		<b>6</b>		<b>16</b>		<b>8</b>

The base model is provided by linear regression of the data as described in Chapter 2 using the base methodology. Curve fit constants were calculated and graphed using MS Excel. The stress-strain models were obtained using the stress-strain equation (Eq. 2.9), and the strain-life was obtained by curve fitting the data using the Morrow-adjusted strain-life equation (Eq. 2.14).

The cyclic stress-strain curves plot the normalized stress amplitude ( $\sigma_a/\sigma_{ULT}$ ) versus the normalized strain amplitude ( $\epsilon_a/e$ ). The effect of data normalization must be considered when interpreting the plots. The effect of normalizing the stress amplitude by the ultimate strength should create stress-strain curve of similar slope. However, normalizing the strain amplitude by the elongation tends to shift the normalized strains at higher temperatures to lower values as shown in Figure 4.1a. The  $R^2$  error values show a relatively good fit for the cyclic stress-strain curve with a notable low at 900°C.

The effects of normalization must also be considered when interpreting the strain-life curve. The effect of normalizing the strain amplitudes by the elongation is a progressive decrease in normalized strain amplitude with an increase in temperature. Therefore, the expected trend that LCF life decreases with increased temperature is exaggerated as shown in Figure 4.1b. The effect of normalizing the cycles to initiation by a constant is an even shift of all data by a certain amount.

It is noted that the 400°C data is intermixed with the 750°C data between 200 and 1,000 normalized cycles, and has a low  $R^2$  value despite having a relative high number of data points as shown in Table 4.2. It is noted that the  $R^2$  values are low at 24°C and 750°C, but these may be explained by the lower number of data points. The 900°C model shows a large unexpected slope change relative to other model temperatures at cyclic lives less than 1,000 cycles.

**Table 4.2. Values of  $R^2$  from regression analysis using base data set.**

	Temperature					
Method	24°C	400°C	750°C	850°C	900°C	Average
Quantity of Data Points	2	16	6	16	8	9.6
Stress-strain	0.973	0.952	0.975	0.954	0.906	0.952
Strain-life	0.939	0.904	0.911	0.955	0.982	0.938

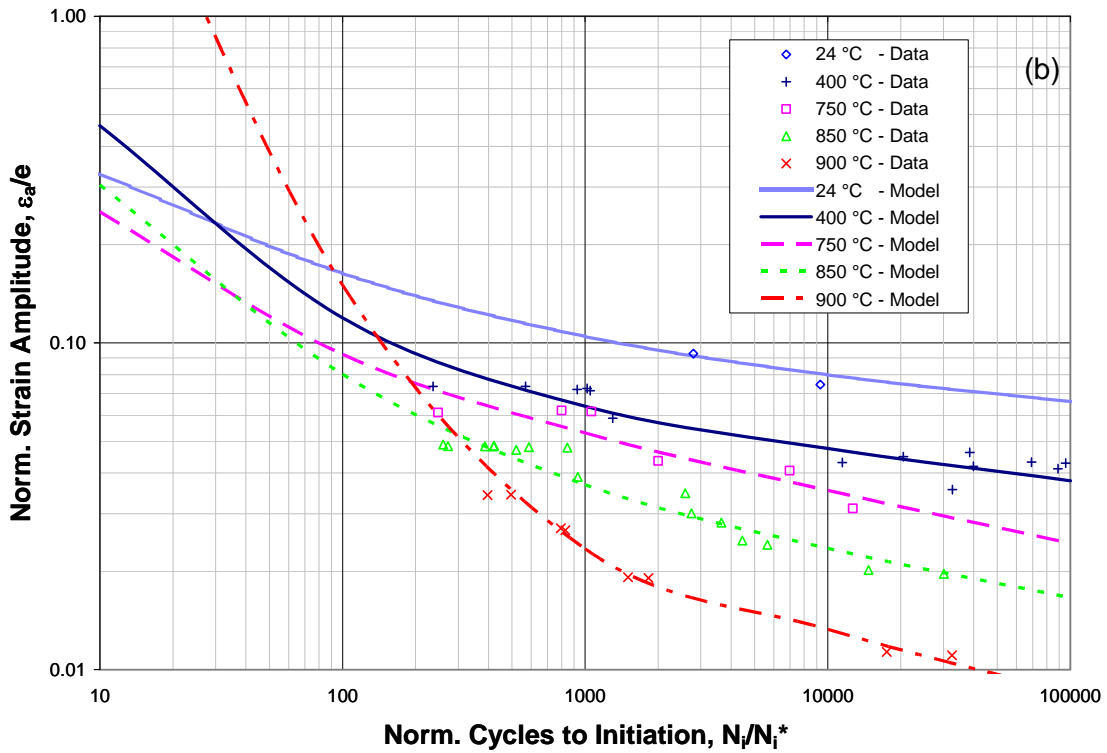
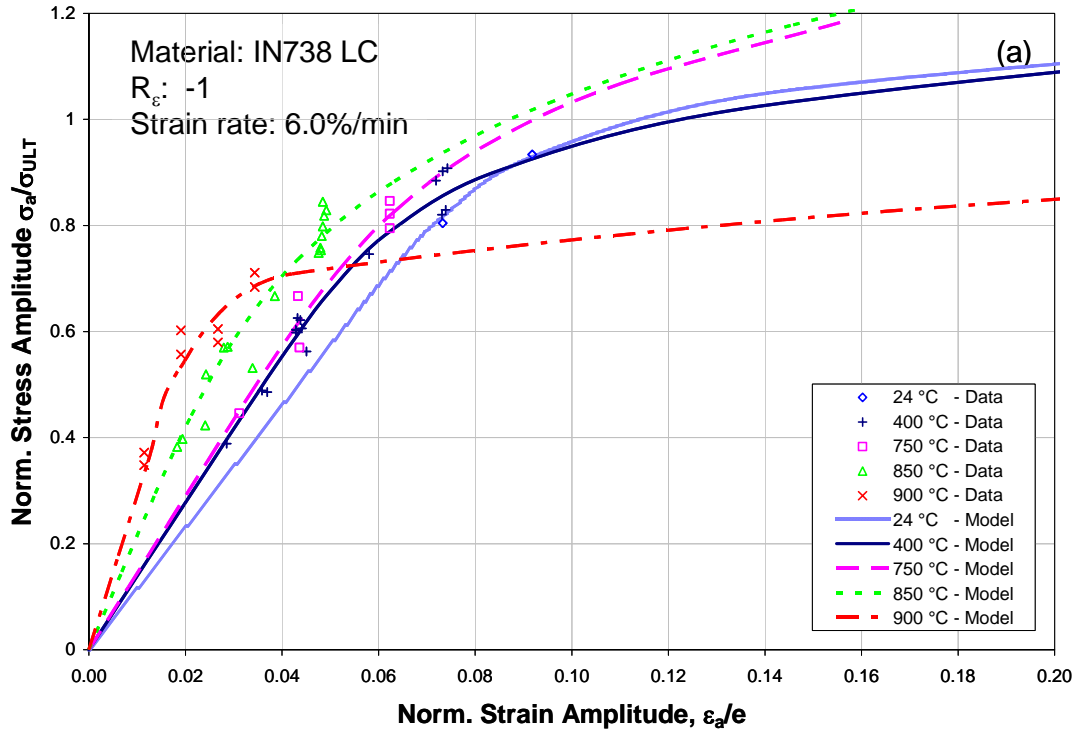


Figure 4.1. Experimental and modeled cyclic stress-strain and strain life behavior of IN738 LC using base data set.

#### 4.2. Fatigue Test Results

A total of 20 specimens were available for testing, and a strain rate of 6%/minute was used for testing. The test operator was very experienced with LCF testing, and engineering input was provided. The operator stated that previous attempts at the higher than typical strain ranges using similar Ni-base alloys have experienced difficulty. The problem has reportedly been the unit “tripping” during testing due to violation of a test requirement during testing prior to specimen failure.

Testing began at the lowest temperature of 400°C, and the 0.222 normalized strain range per the preliminary test matrix shown in Table 3.1. The first test (specimen D912-1) revealed unexpected behavior which included seemingly random jumps in the load and inability to achieve the desired strain control history. The stress versus time plot shows several spikes in the stress history plot at 65 and 92 normalized cycles as shown in Figure 4.2a. An inability to achieve strain control is also shown by the strain versus cycle plot in Figure 4.2b.

The test conditions were repeated using specimen D912-2. Again, an inability to achieve strain control was noted, when a large spike in strain occurred at 8 normalized cycles, and the specimen failed shortly thereafter at 19 normalized cycles.

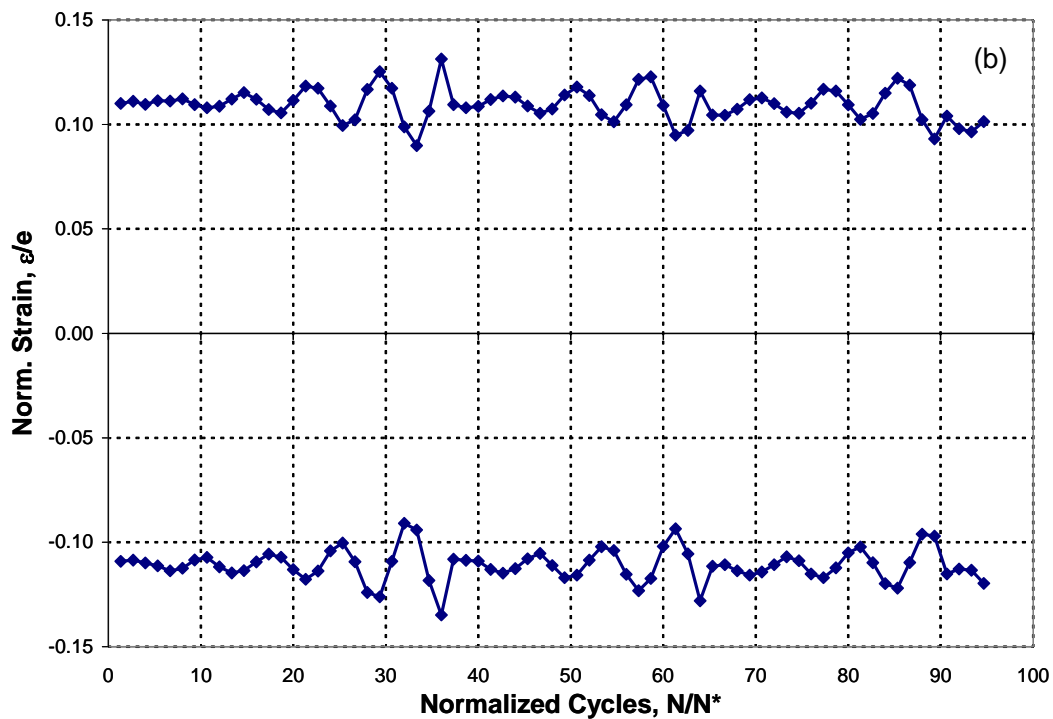
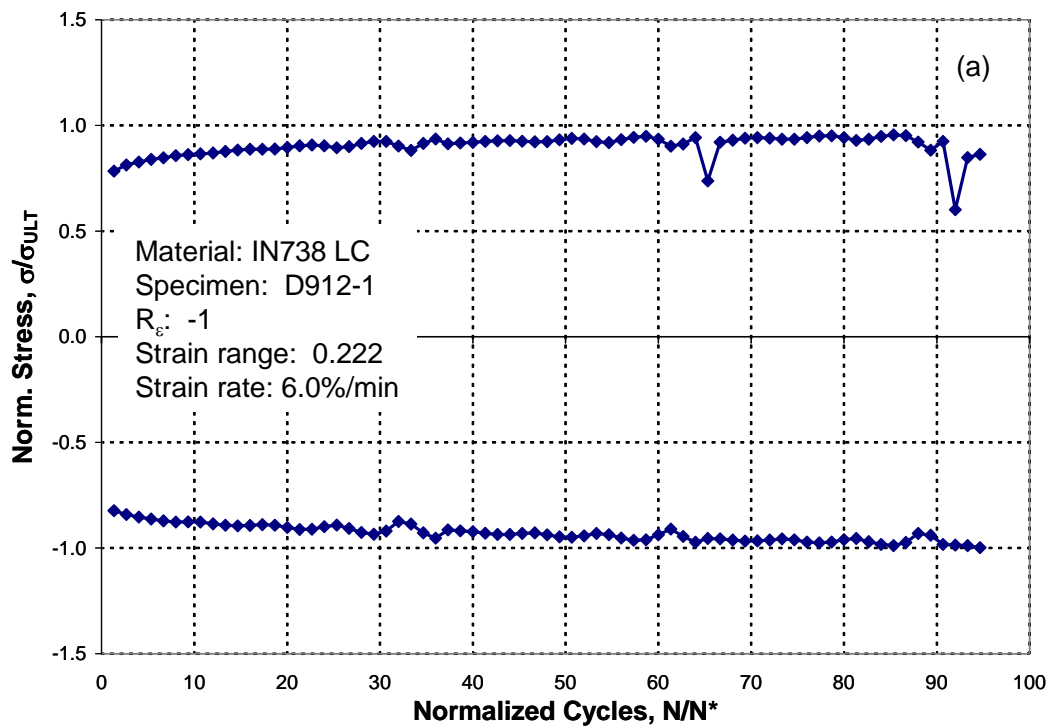


Figure 4.2. Cyclic (a) stress and (b) strain history for test D912-1 for IN738 LC at 400°C.

This behavior was identified as potentially indicative of serrated yielding, which is also known as discontinuous yielding or jerky flow. These effects have been explained by interstitial atoms pinning dislocations. The phenomenon occurs at strain rates where interstitial atoms can diffuse to the dislocation cores quickly enough to re-pin the dislocations after initial yielding. This is observed as repeated serrations throughout the stress-strain curve [21].

Serrated yielding is of interest because it has been known to interfere with reliable tensile tests and causes strain overshoots during strain-controlled LCF testing. It is known to occur with certain alloys, temperatures, and strain rates. Huron [21] does specify that it has been observed in superalloys such as IN600, IN718, or Waspalloy at temperatures in the range of 400°C.

Another noted issue in Figure 4.2b is the inability to maintain strain-control. Typical tests often show acceptable strain control with the default adjustment of the control settings. However, the high strain range tests will require an improved tuning technique, where the control settings were tuned for each specimen prior to testing after the specimen reaches a steady-state test temperature.

Several aspects of the test plan and matrix were modified. Testing at 400°C would be avoided to alleviate the potential for serrated yielding. However, this would only leave data at 750°C and 850°C, and it was desired to have data over a wider temperature range to test the extrapolation methods. Therefore, a room temperature data set was provided as a third temperature for application of the extrapolation methods. Five data points were gathered at 24°C, which allowed for 2 to be used to establish a base data set, and 3 additional high strain data points to establish the augmented data set as

shown in Table 4.3. The strain rate will remain at 6%/minute, and the strain ratio is  $R_\epsilon = -1$ .

**Table 4.3. Modified test matrix.**

Test Temp (°C)	Norm. Stress Amplitude ( $\sigma_a/\sigma_{ULT}$ )	Norm. Strain Range ( $\Delta\epsilon/e$ )	Test Quantity
24	0.804	0.147	1
24	0.903	0.184	1
24	0.970	0.220	1
24	1.017	0.257	1
24	1.054	0.294	1
750	0.909	0.150	1
750	0.977	0.174	1
750	1.030	0.199	1
850	0.851	0.116	1
850	0.908	0.136	1
850	0.957	0.155	1
TOTAL			11

The high strain range test results are shown in Table 4.4, and 11 tests were provided. All requirements were met for the tests to be valid per the ASTM standard, except that tests D912-8, D912-15, and D912-11 had significant excursions from maintaining strain control of upto 25%. This was despite the efforts to tune the controls for each specimen prior to testing. The deviation from strain control was calculated as a maximum deviation for any one cycle from the applied strain range in percent. All of other tests were within acceptable limits of 3%.

It was noted that significant strain hardening or softening occurred in this alloy, which was calculated by comparing the initial stress range to the stable mid-life stress range. It is interesting that more strain hardening occurred at 750°C than 24°C, but strain softening occurred at 850°C. A stress history and stress-strain mid-life hysteresis loop

plot for each test is shown in the Appendix. The notable exception is test D912-17 because data was inadvertently erased. A photograph of each failed specimen used for accepted test results and the three at 400°C which are indicative of serrated yielding are shown in the Appendix, Fig. A.12 to A.25.

**Table 4.4. High strain range test results.**

Specimen ID	Test Temperature (°C)	Norm. Strain Range ( $\Delta\varepsilon/e$ )	Max Deviation From Strain Range (%)	Mid-life Norm. Stress Amplitude ( $\sigma_a/\sigma_{ULT}$ )	Strain Hardening or Softening (+ / - %)	Norm. Mid-life Modulus ( $E/\sigma_{ULT}$ )	Normalized Cycles to Initiation ( $N_f/N_f^*$ )	Figure in Appendix
LCF-D912-35	24	0.147	2.7%	0.804	2.6%	209	9333	A.2
LCF-912-17	24	0.184	2.0%	0.934	7.7%	222	2795	-
LCF-912-20	24	0.220	1.9%	0.992	10.1%	224	680	A.3
LCF-D912-19	24	0.257	1.9%	1.029	9.4%	238	107	A.4
LCF-D912-25	24	0.294	1.5%	1.022	11.8%	216	196	A.5
LCF-D912-6	750	0.150	2.9%	0.929	5.6%	149	245	A.6
LCF-D912-14	750	0.174	0.7%	1.028	16.8%	214	160	A.7
LCF-D912-8	750	0.199	19.5%	1.013	24.7%	188	100	A.8
LCF-D912-16	850	0.116	1.2%	0.891	-6.9%	238	209	A.9
LCF-D912-15	850	0.136	13.2%	0.867	-4.9%	196	184	A.10
LCF-D912-11	850	0.155	24.5%	0.997	-1.7%	226	96	A.11

The following shows a sample of the outputs from various tests that were performed. The outputs from a typical strain-controlled test include stress versus time, stress versus cycles (stress history), and strain versus cycle, and stress versus strain (hysteresis loop) plots. This information is used in post-processing and assessing whether a test is valid.

The output of a stress versus time plot reveals whether there is plasticity occurring at the high strain amplitudes of these tests. Several features are revealed by comparing the stress versus time plot for specimens D912-19, D912-14, and D912-15 at temperatures of 24°C, 750°C, and 850°C respectively as shown in Figure 4.3. There is more plasticity occurring for each cycle at lower temperatures. Also, strain hardening is seen at 24°C and 750°C, but strain softening is occurring at 850°C.

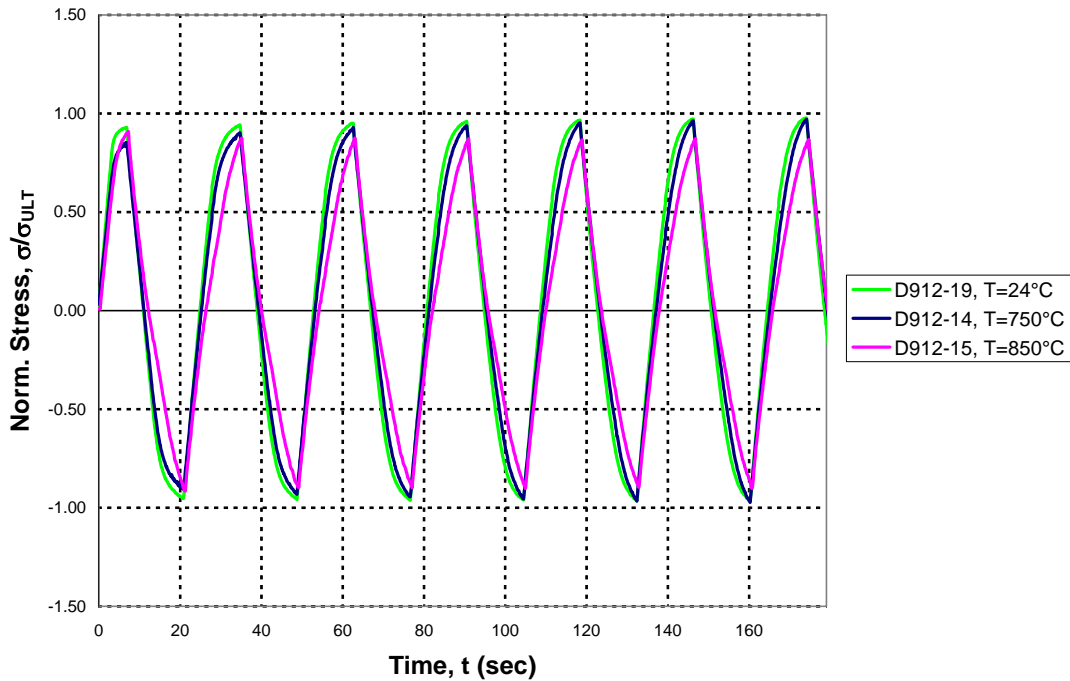


**Figure 4.3. Stress versus time output for 1.4% strain range at 24°C, 750°C, and 850°C.**

The strain versus cycle plot reveals any deviation from strain-control that has occurred during testing, which should be constant over the duration of the test. Some issues were found with keeping the strain constant during testing. Most of these issues were resolved by using a special tuning method to optimize the control settings prior to testing. An example of the deviation is shown in Figure 4.4 which allows comparison of two tests at 750°C: the 0.174 normalized strain range test, which had only 0.7% strain control deviation, and the 0.199 normalized strain range test, which had 19.5% deviation from strain control. It is seen that the 0.199 strain range test actually experienced a few cycles up to about 0.236 normalized strain range, and few cycles down to 0.160. Several efforts were made to tune the system to minimize these excursions, but they could not be

completely eliminated. The expected effect of excursions above the set strain range is reduction in the measured cyclic life from a true constant strain range test.

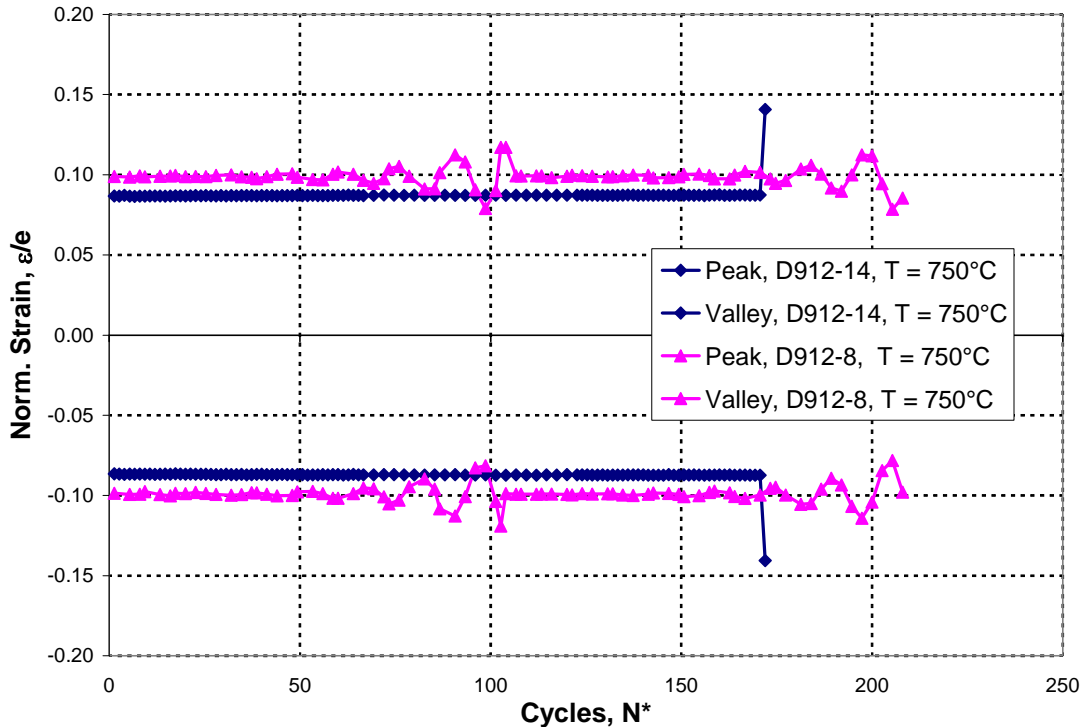


**Figure 4.4. Strain versus cycle plot comparison at 750°C.**

A hysteresis loop is a plot of the strain versus stress, and a loop is mapped out for each cycle during a test. The hysteresis loop for the 0.174 normalized strain range at 750°C is shown in Figure 4.5a. Strain hardening occurs in the first twenty loops. The twentieth loop is nearly the same as the mid-life loop, which indicates that strain hardening behavior has saturated. The mid-life loop is the median life hysteresis loop, and this hysteresis loop used for determining the amount of plastic strain.

The stress versus cycle plot or stress history diagram is used to show the drop in stress and load which indicates that a crack has formed in the specimen prior to failure.

This plot also shows whether strain hardening has occurred. Figure 4.5b shows the stress history plot for D912-14 test at 750C and 0.174 normalized strain range. Note that the majority of the strain hardening has occurred by normalized cycle 40. The stress range starts to drop at about normalized cycle 145 indicating a crack has formed in the specimen until final failure occurs at normalized cycle 170.

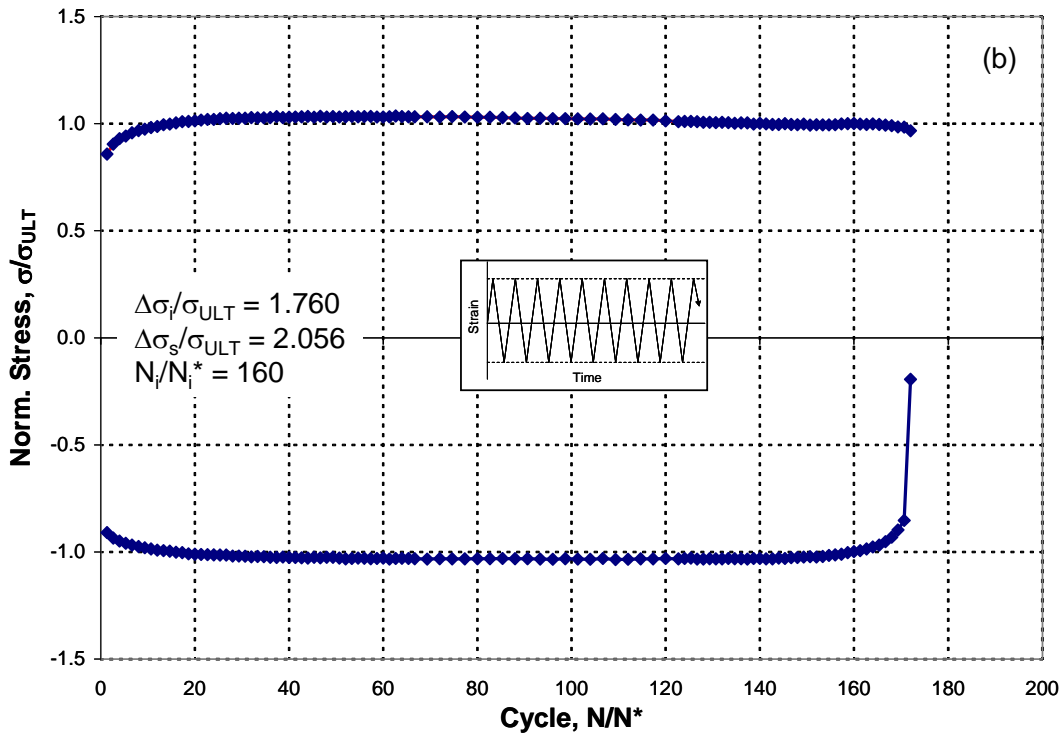
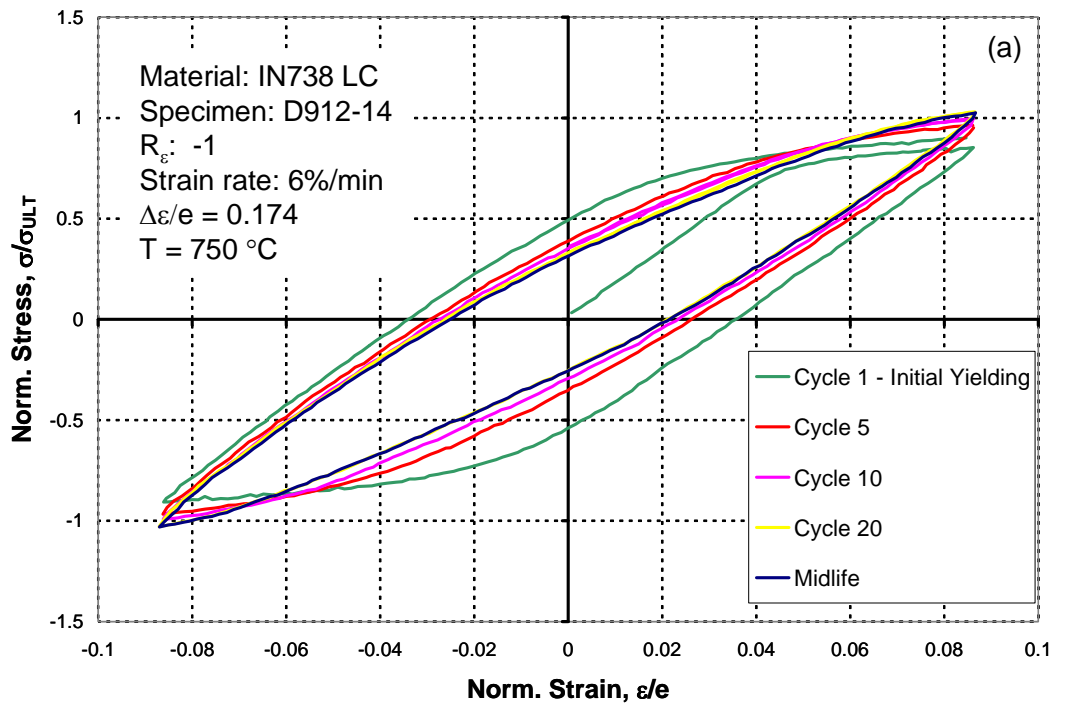
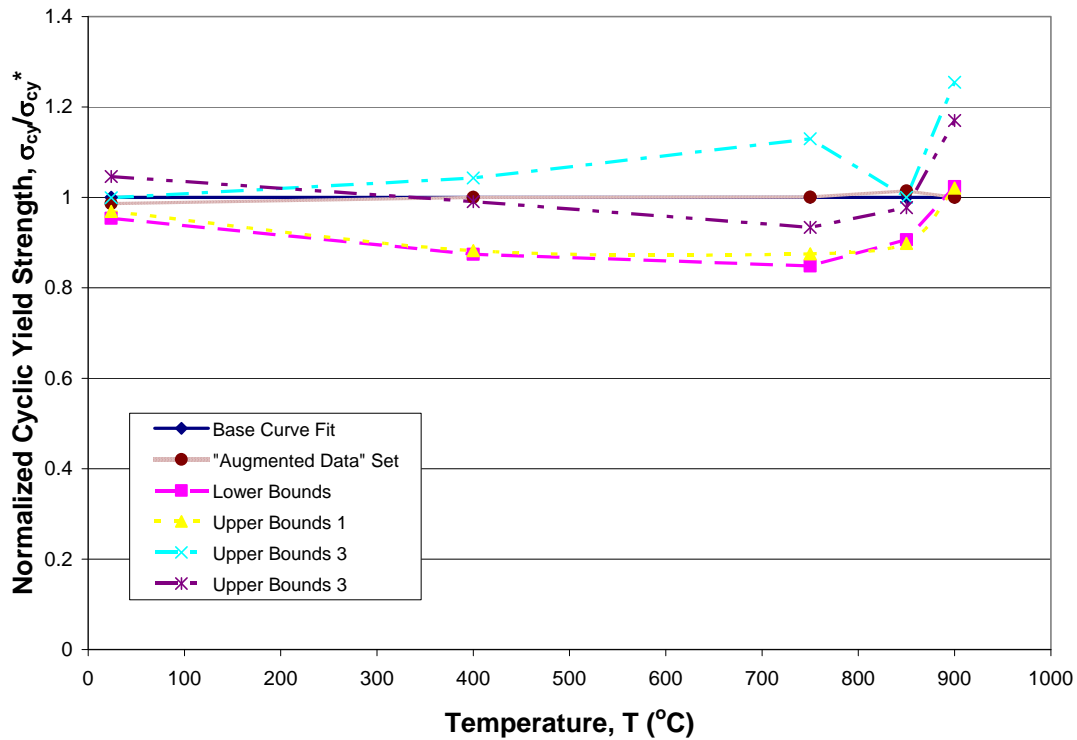


Figure 4.5. (a) Hysteresis loop and (b) stress history plot for specimen D912-14 at 1.4% strain range and 750°C.

### 4.3. Comparison

In the following section, a comparison is made between the various models generated during this project. The base model is compared to the extrapolation methods including: lower bounds (LB), upper bounds 1 (UB1), upper bounds 2 (UB2), and upper bounds 3 (UB3). The base model is provided by a standard linear regression using the base data set. Likewise, the “augmented model” is provided by a linear regression including both the base data set and the additional high strain data gathered in this project. It is expected that the augmented data set model will provide the best model for predicting the actual high strain behavior of the material. What remains to be determined is which model will provide the best approximation using data from the base data set: the base curve fit, LB, UB1, UB2, or UB3.

As an introduction to direct comparison of the stress-strain and strain-life curves, it is first informative to compare the cyclic yield strengths. The values of the cyclic yield have been normalized by the values from the base model. The base model and augmented models show nearly identical values, which is expected since the yield strength is already defined by the base data set. There is significant variation in the cyclic yield between the extrapolation models as shown in Figure 4.6. In comparison to the base model, UB2 is generally higher for the entire temperature range. Alternately, the LB and UB1 consistently show a lower cyclic yield than the base curve fit except at 900°C where they are equal. The UB3 shows much variation compared to base model, where it matches at 24°C and 850°C, is lower at 400°C and 750°C, and higher at 900°C.



**Figure 4.6. Comparison of calculated cyclic yield strengths using various methods.**

The main goal of this project was to find the best extrapolation method using a base data set to predict the high strain range behavior. This is evaluated by calculating  $R^2$  by comparing the strains from the extrapolation methods to the actual strains from the additional high strain tests. Since each method provides both a cyclic stress-strain and strain-life curve, the average  $R^2$  from the two curves is considered the best description of the ability to extrapolate. Therefore, this can only be evaluated where high strain data has been collected at 24°C, 750°C, and 850°C. This  $R^2$  value is termed “Extrapolated.”

A secondary objective is to determine if the resulting form of the extrapolation method will negatively impact the overall fit of the cyclic stress-strain or strain-life equation considering all of the available test data at each test temperature. This may be

evaluated at all temperatures regardless of whether high strain data has been generated. This  $R^2$  value is termed “Overall.”

There are 5 data points from the room temperature (24°C) data. Two data points were generated with normalized strain ranges of 0.184 and below are considered base strain range data, and the data points with normalized strain ranges of 0.220 and above are considered high strain range. It is not clear which method provides the best model considering the stress-strain curve as shown in Figure 4.7a. Both LB and UB1 appear well below the higher strain range test data.

The few data points provided in the strain-life curve show little scatter as shown in Figure 4.7b. It is not qualitatively apparent which approximation is the best in the strain-life plots. It appears that UB3 shows the most variation from the test data. All approximations match well at low strain ranges, but at high strain ranges there is more scatter in the data.

The highest  $R^2$  for extrapolation or overall fit is provided by the augmented model as expected as shown in Table 4.5. The  $R^2$  calculations show that the best extrapolation method is provided equally well by the base model or UB2 model with an average  $R^2$  of 0.961. The extrapolation method which provides the best overall fit with all the test data is also provided equally well by the base model or the UB2 model with an average  $R^2$  of 0.956.

**Table 4.5. Values of  $R^2$  from various extrapolation methods at 24°C.**

Purpose	Extrapolation			Overall Fit		
	Stress-strain	Strain-life	Average	Stress-strain	Strain-life	Average
Augmented Data Model	0.978	0.953	0.965	0.977	0.950	0.964
Base Data Model	0.980	0.942	0.961	0.973	0.939	0.956
Lower Bounds Model	0.902	0.942	0.922	0.661	0.937	0.799
Upper Bounds 1 Model	0.966	0.949	0.958	0.940	0.943	0.942
Upper Bounds 2 Model	0.980	0.941	0.961	0.974	0.938	0.956
Upper Bounds 3 Model	0.981	0.910	0.946	0.956	0.894	0.925

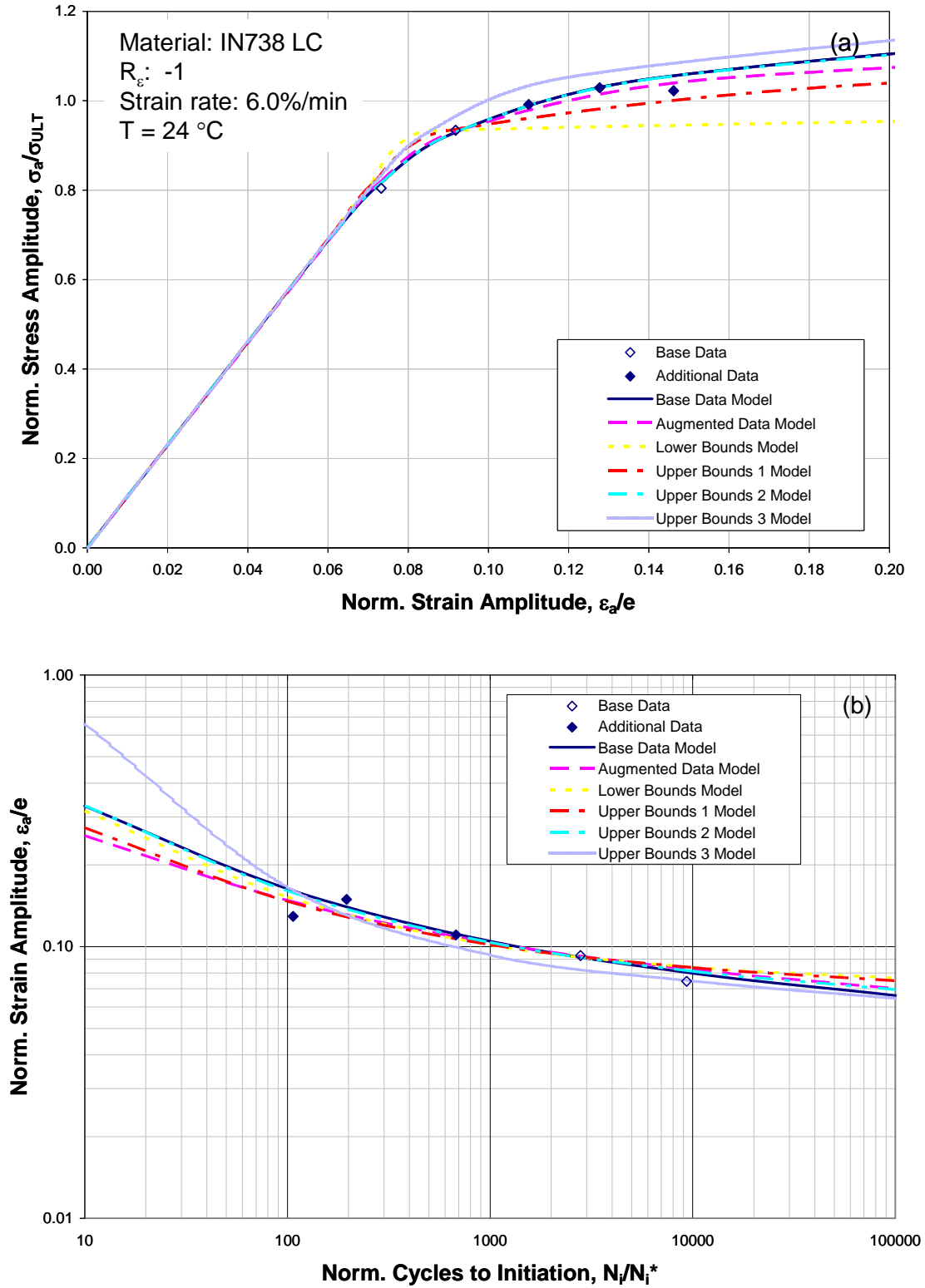


Figure 4.7. Comparison of (a) cyclic stress-strain models and (b) strain-life models for IN738 LC at 24°C.

No additional data was generated at 400°C, and all of the data was consider in the base strain range. It is still worthwhile to consider which method will provide a best overall fit to the available base data set. A total of 16 base data points were available at this temperature for curve fitting. The data on the cyclic stress-strain curve matches that of the base curve fit, UB2 or UB3. Both the LB and UB1 are well below the other curves as shown in Figure 4.8a.

The strain-life data at 400°C contains many low strain amplitude data points at high cycles, which are well above the normal maximum of 10,000 cycles. Only data points that were continued to failure were included in the curve fit as shown in Figure 4.8b. There is much scatter in the curve fits at high strain amplitudes, and it is not clear which curve fit is the best match to test data.

The 400°C data set does not include any high strain data points. The results are used to calculate an  $R^2$  value for the best overall fit with all available test data. The best overall fit is provided by the UB3 extrapolation method with an average  $R^2$  value of 0.947 as shown in Table 4.6.

**Table 4.6. Values of  $R^2$  for various methods at 400°C.**

Purpose	Overall Fit		
	Stress-strain	Strain-life	Average
Base Data Model	0.952	0.904	0.928
Lower Bounds Model	0.687	0.907	0.797
Upper Bounds 1 Model	0.710	0.906	0.808
Upper Bounds 2 Model	0.965	0.921	0.943
Upper Bounds 3 Model	0.947	0.947	0.947

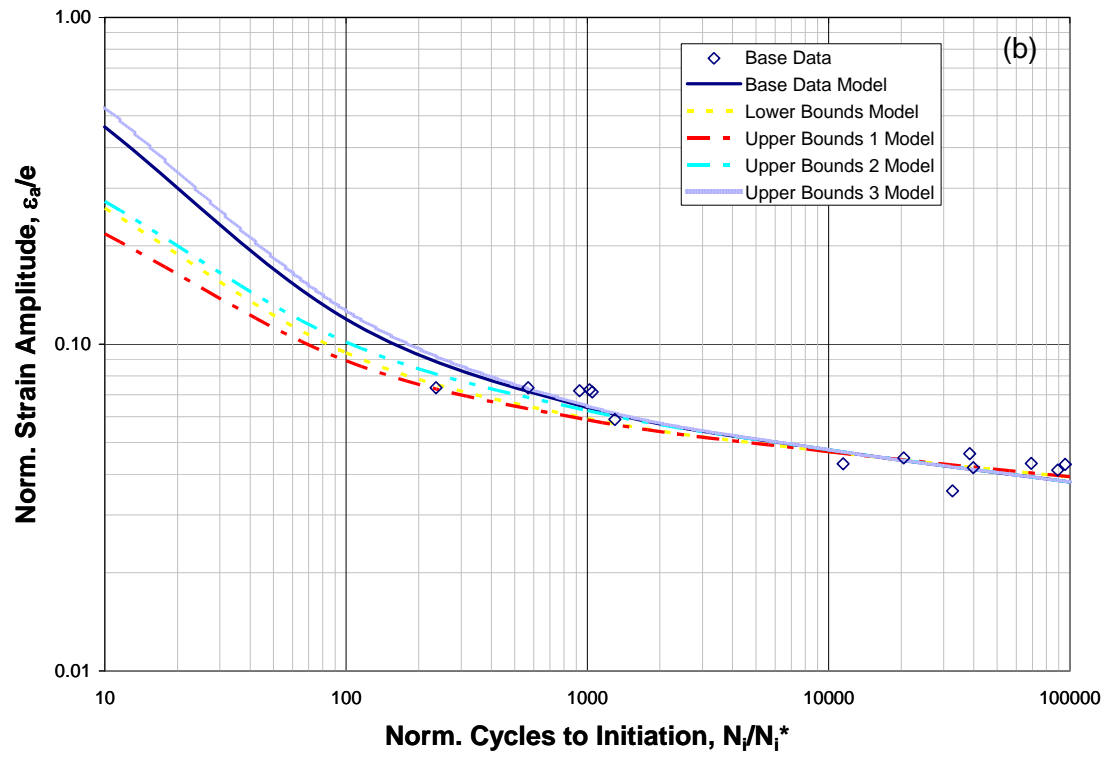
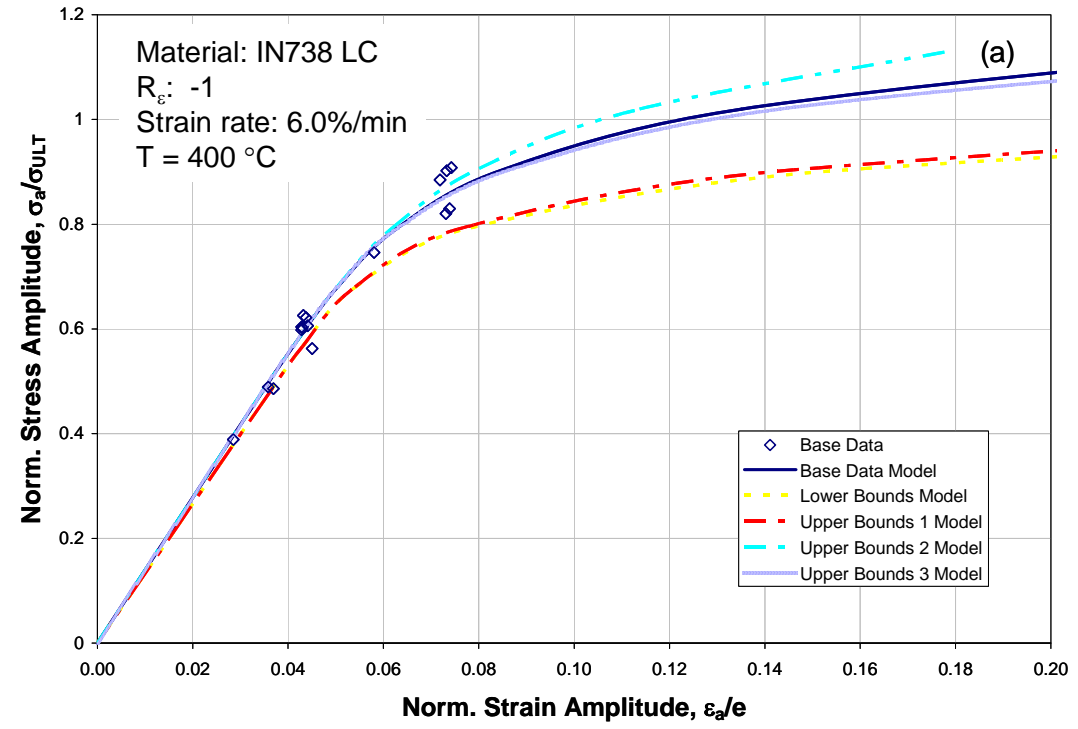


Figure 4.8. Comparison of (a) cyclic stress-strain models and (b) strain-life models for IN738 LC at 400°C.

The next temperature for comparison is 750°C. A total of six data points existed in the base data set, which were supplemented by three additional high strain range tests. The stress-strain curves are shown for comparison in Figure 4.9a. It is not visually apparent which approximation provides the best fit, but the base model and UB2 appear likely. Both LB1 and UB1 appear well below the high strain range test data.

The test data show moderate scatter in the strain-life plot at 750°C. Both the base curve fit and the UB2 have very little deviation from the augmented data curve fit as shown in Figure 4.9b. The LB1 and UB2 models show much deviation from the test data, but it is noted that these curves provide the only conservative estimate of behavior at the high strain range data points.

As expected, the augmented data model provides the highest  $R^2$  value of any method. The method providing the highest  $R^2$  for extrapolation and overall fit is provided by the base data model as shown in Table 4.7. The UB2 method is the 2<sup>nd</sup> best extrapolation method based on  $R^2$  for extrapolation and overall fit.

**Table 4.7. Values of  $R^2$  for various methods at 750°C.**

Purpose	Extrapolation			Overall Fit		
	Stress-strain	Strain-life	Average	Stress-strain	Strain-life	Average
Augmented Data Model	0.978	0.999	0.989	0.974	0.958	0.966
Base Data Model	0.978	0.998	0.988	0.975	0.957	0.966
Lower Bounds Model	0.874	0.988	0.931	0.771	0.897	0.834
Upper Bounds 1 Model	0.923	0.985	0.954	0.854	0.890	0.872
Upper Bounds 2 Model	0.977	0.996	0.987	0.971	0.954	0.962
Upper Bounds 3 Model	0.974	0.998	0.986	0.971	0.947	0.959

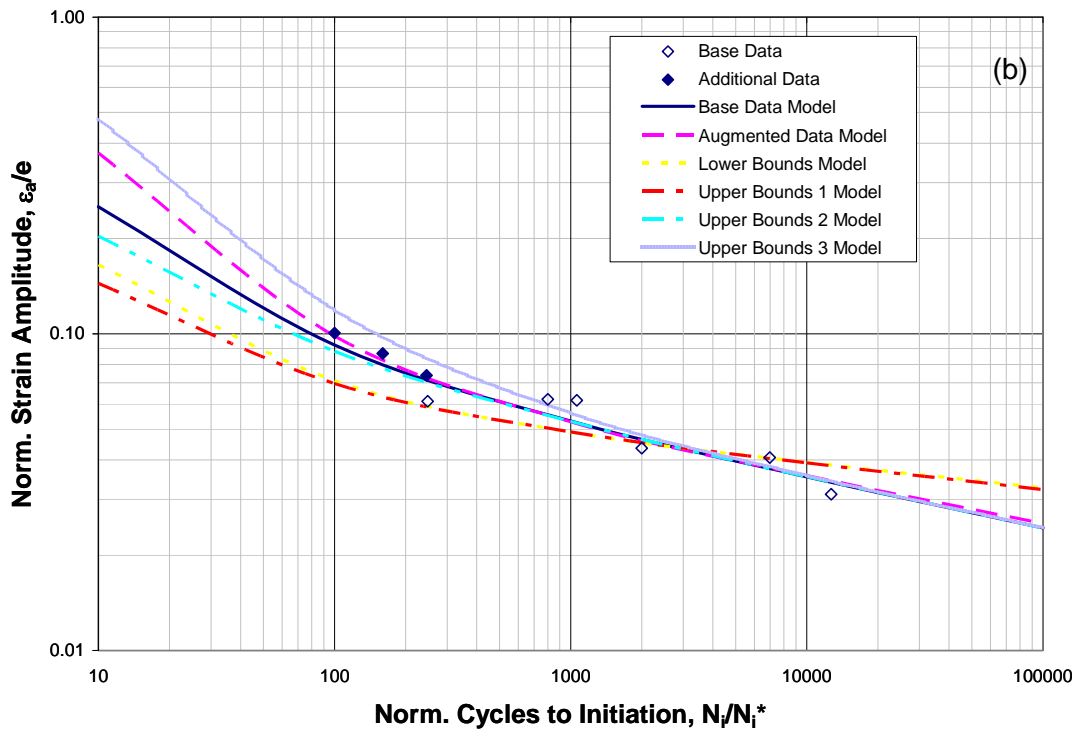
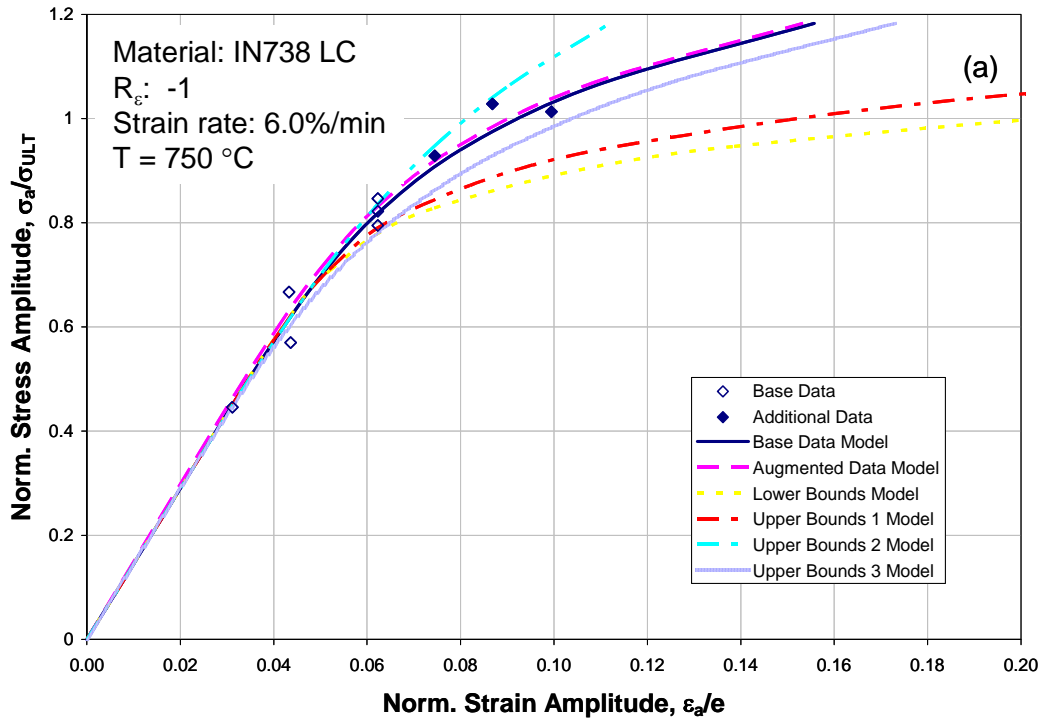


Figure 4.9. Comparison of (a) cyclic stress-strain models and (b) strain-life models for IN738 LC at  $750\text{ }^{\circ}\text{C}$ .

The temperature with the most test data is 850°C including 16 base data points, which were supplemented by 3 high strain amplitude data points. The resulting stress-strain curves at 850°C are shown in Figure 4.10a. The data does correlate well with the base curve fit, UB2 and UB3. The LB1 and UB1 curve fits are well below the other methods.

Limited scatter is seen in the strain-life curve data points. As a result most of the extrapolation methods are in good agreement over the full range of the test data, as shown in Figure 4.10b. It is noted that all of the high strain data points are above the LB1 and UB1 curve fits.

Another notable trend is seen in the  $R^2$  calculations at 850°C. The UB2 model does as well as the augmented data model for extrapolation with an average  $R^2$  of 0.981 as well as the overall fit with an average  $R^2$  value of 0.958. The  $R^2$  calculations are shown in Table 4.8.

**Table 4.8. Values of  $R^2$  for various methods at 850°C.**

Purpose	Extrapolation			Overall Fit		
Method	Stress-strain	Strain-life	Average	Stress-strain	Strain-life	Average
Augmented Data Model	0.972	0.990	0.981	0.958	0.959	0.958
Base Data Model	0.968	0.988	0.978	0.954	0.955	0.955
Lower Bounds Model	0.887	0.993	0.940	0.868	0.953	0.911
Upper Bounds 1 Model	0.870	0.993	0.932	0.850	0.952	0.901
Upper Bounds 2 Model	0.968	0.993	0.981	0.954	0.962	0.958
Upper Bounds 3 Model	0.927	0.986	0.957	0.916	0.951	0.934

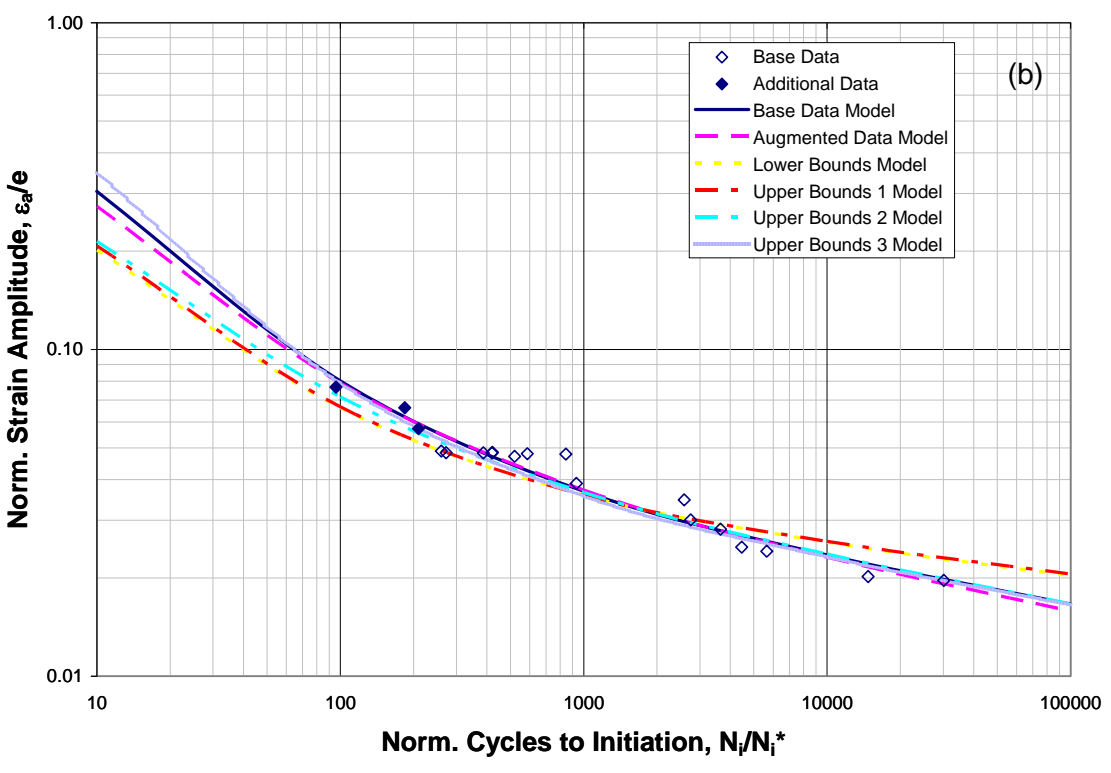
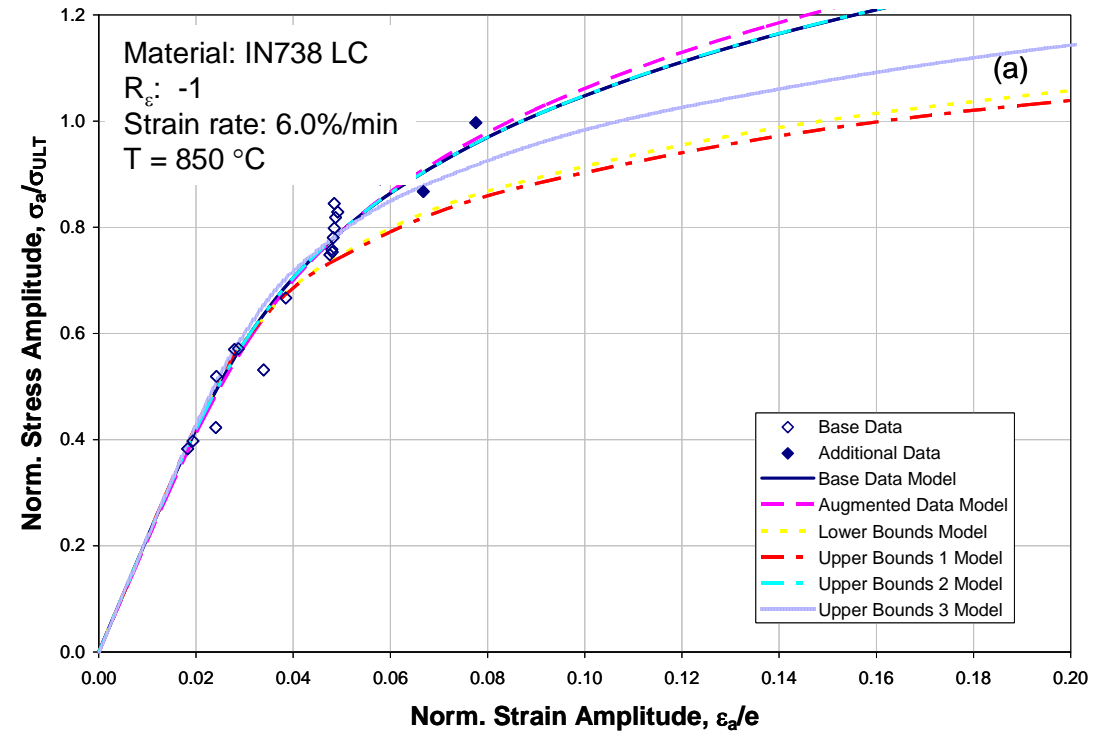


Figure 4.10. Comparison of (a) cyclic stress-strain models and (b) strain-life models for IN738 LC at 850°C.

The 900°C data include 8 data points all of which are considered low strain range, and in the base data set. The data set is being evaluated to find which method provides the best overall fit to the test data. An unusual trend is observed in the cyclic stress-strain response since the LB1 and UB1 trend well with the test data, but the UB2 and UB3 tend to over-estimate the behavior as shown in Figure 4.11a.

The strain-life data at 900°C shows a marked increase in life at high strain ranges. These results place the curve fit strain life curve well above all extrapolation method predictions as shown in Figure 4.11b. The R-squared calculations show that the best overall fit is provided by the UB3 extrapolation method as shown in Table 4.9.

**Table 4.9. Values of R<sup>2</sup> for various methods at 900°C.**

Purpose	Overall Fit		
	Stress-strain	Strain-life	Average
Base Data Model	0.906	0.982	0.944
Lower Bounds Model	0.929	0.932	0.931
Upper Bounds 1 Model	0.927	0.931	0.929
Upper Bounds 2 Model	0.924	0.972	0.948
Upper Bounds 3 Model	0.932	0.980	0.956

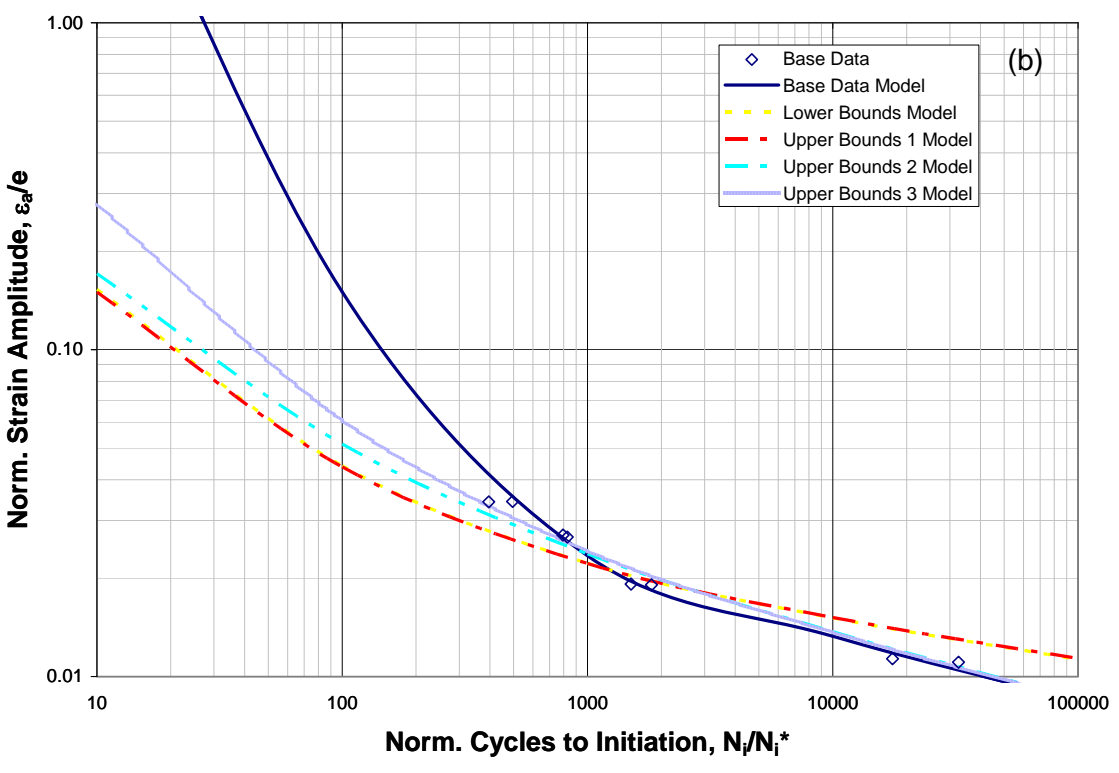
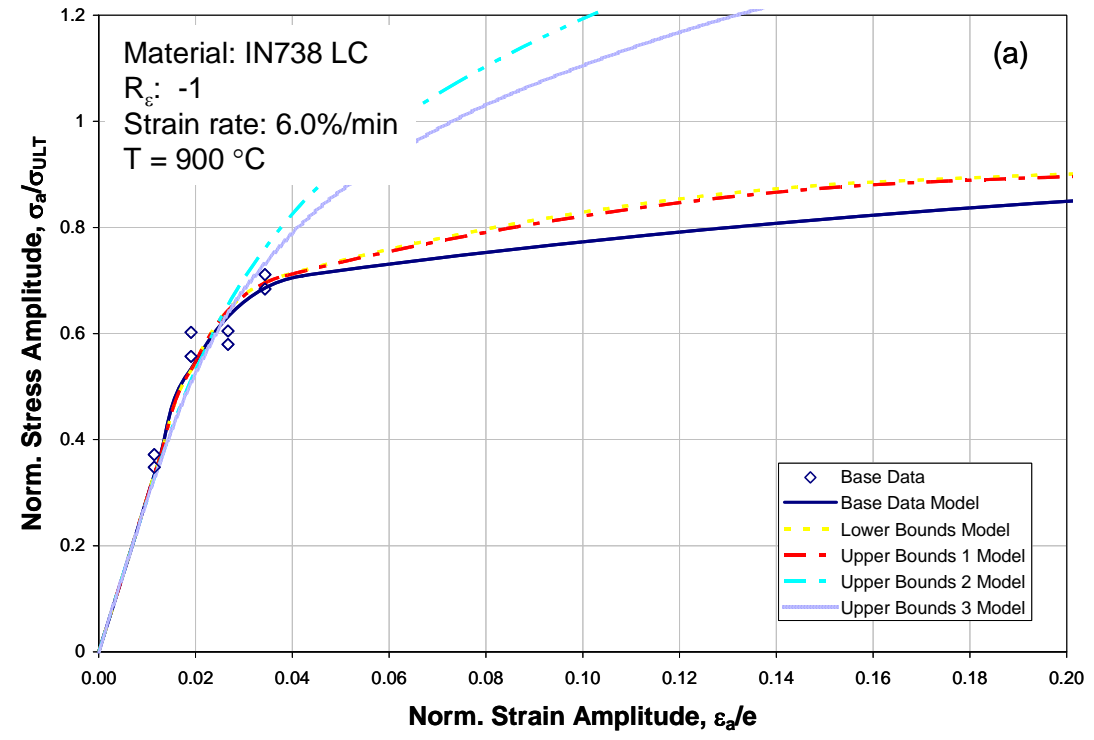


Figure 4.11. Comparison of (a) cyclic stress-strain models and (b) strain-life models for IN738 LC at 900°C.

The primary objective of this research is to develop a method for providing extrapolation of LCF data to high stress amplitudes using an existing strain range data set. Data was available to test the extrapolation methods at 24°C, 750°C, and 850°C. The average  $R^2$  reveals the expected result that the augmented data set is the best approximation method as shown in Table 4.10. Both the base data model and UB2 model share as the best approximation method with an average  $R^2$  value of 0.976. The  $R^2$  of LB1, UB1, and UB3 are lower than the base data model, which indicates that these methods are in fact less desirable than a standard regression curve fit for extrapolation of an existing LCF data set to high strain ranges.

**Table 4.10. Temperature average values of  $R^2$  for extrapolation methods.**

Method	Temperature °C			Average
	24	750	850	
Augmented Data Model	0.965	0.989	0.981	0.978
Base Data Model	0.961	0.988	0.978	0.976
Lower Bounds Model	0.922	0.931	0.940	0.931
Upper Bounds 1 Model	0.958	0.954	0.932	0.948
Upper Bounds 2 Model	0.961	0.987	0.981	0.976
Upper Bounds 3 Model	0.946	0.986	0.957	0.963

A secondary objective of this research was to insure that the approximation method does not negatively affect the match of curve fit to test data over the entire data range. This effect has again been evaluated by calculating a temperature averaged  $R^2$  value based on the overall best fit of 1) the base data model, 2) augmented data model, and 3) and the approximation methods as shown in Table 4.11. The resulting calculations intuitively indicate that the best fit is provided obtained by the augmented data model. This shows that there is no better substitute than actual experimental data.

Of the approximation approaches, however, the best methodology is provided by the UB2 with an  $R^2$  value of 0.954. UB2 has an advantage over the base linear regression process or base data model with an  $R^2$  of 0.950. This suggests that the small improvement in fit offered by UB2 is more significant over the entire data range than at the high strain data points. It is noted that the UB3 approximation was the highest at both 400°C and 900°C. The other approximation methods (LB and UB1) consistently showed lower  $R^2$  values than the base curve, which indicates that these methods are less desirable than a standard curve fit over the full data range.

**Table 4.11. Temperature average values of R-squared error for best fit over all test data.**

Method	Temperature °C					Average
	24	400	750	850	900	
Augmented Data Model	0.964	N/A	0.966	0.958	N/A	0.963
Base Data Model	0.956	0.928	0.966	0.955	0.944	0.950
Lower Bounds Model	0.799	0.797	0.834	0.911	0.931	0.854
Upper Bounds 1 Model	0.942	0.808	0.872	0.901	0.929	0.890
Upper Bounds 2 Model	0.956	0.943	0.962	0.958	0.948	0.954
Upper Bounds 3 Model	0.925	0.947	0.959	0.934	0.956	0.944

## 5. DISCUSSION

The following section provides a discussion of the results considering each method individually. Also, the rationale for the performance of each method is explained.

### 5.1. Augmented Data Model

The augmented data set method applied the standard regression procedure to the augmented data set. Recall that the augmented data set includes both the base data set along with the additional high strain data points conducted as part of this research. The cyclic stress-strain curves are shown in Figure 5.1a. Intuitively, this method provides the best option for characterizing the high strain data points. Likewise, this method provided the best method for an overall match to test data. These were demonstrated by  $R^2$  being higher than any approximation method for “extrapolation” or “overall” as shown in Table 4.10, and Table 4.11.

The resulting augmented data set models include data over the entire range defined as low-cycle fatigue from 100 to 10,000 normalized cycles, as shown in Figure 5.1b. Recall that at high mechanical strain amplitudes, the plastic strain component dominates the measured cyclic lives as described per the Coffin-Manson equation (Eq. 2.11). It is noted that the strain-life model does show an increase in slope with temperature at high strain amplitudes when high strain data is included in the data set.

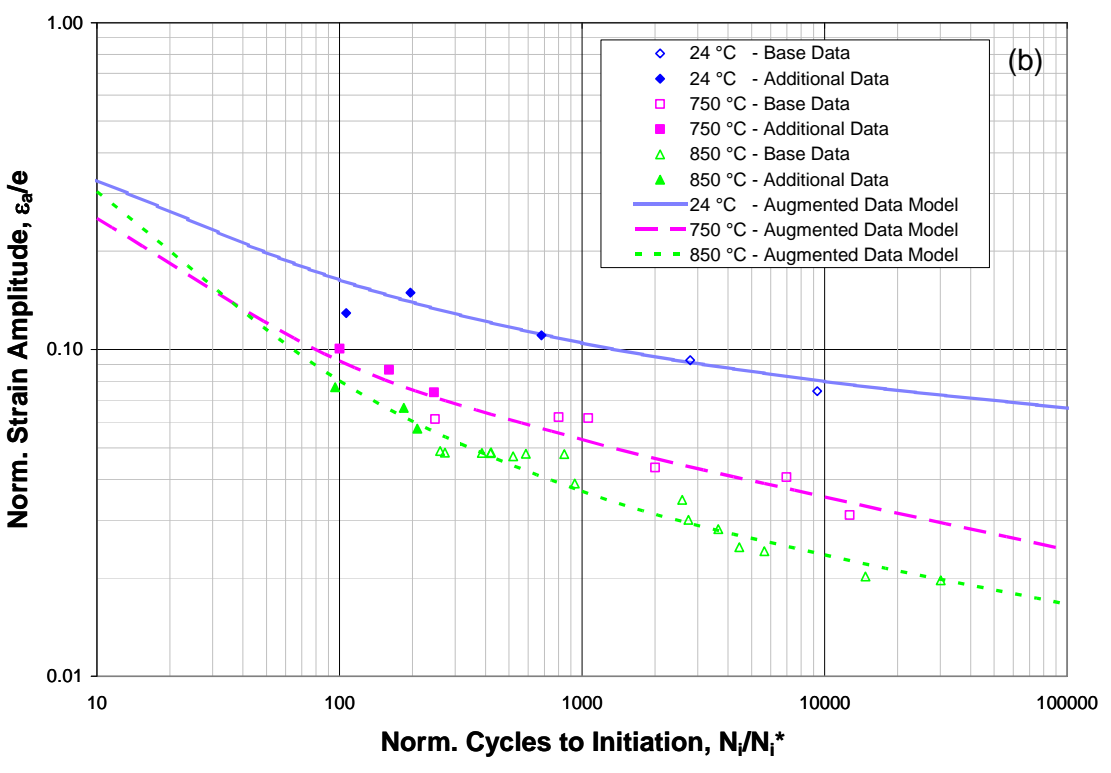
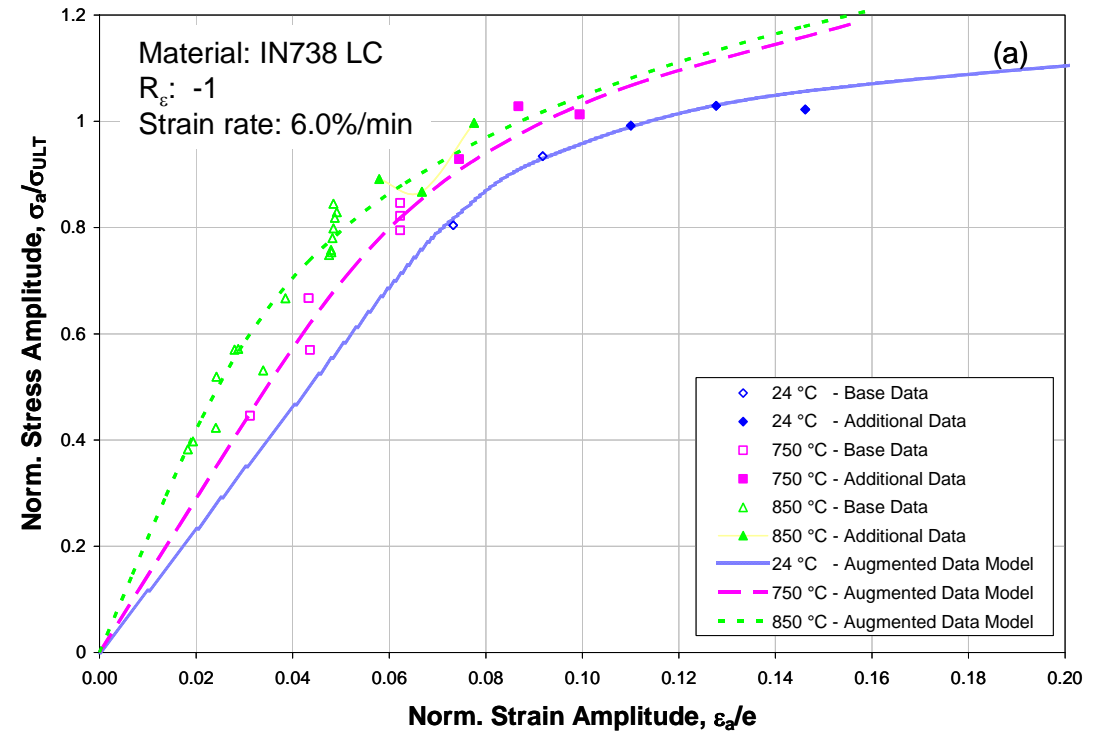


Figure 5.1. Comparison of (a) cyclic stress-strain curve and (b) strain-life curves using the augmented data model and data for IN738 LC at various temperatures.

## 5.2. Base Data Model

The base data model provides the baseline for predicting the stress-strain and strain-life curves at high strain ranges. The base model applied standard linear regression using the base data set as described in the reference methods. A plot of the stress-strain curve using the base model is shown in Figure 5.2a. Note that only the base data are included in the regression analysis to provide this model. The results show that the base model correlates well with the additional high strain data points.

The strain-life curves provided by the base model using the base data set worked very well at predicting the high strain range behavior of the material at 24°C, 750°C, and 850°C as shown in Figure 5.2b. The model shows more questionable results at 400°C and 900°C, but unfortunately high strain data was not able to be collected at these temperatures.

It is somewhat difficult to compare the strain-life models at 400°C and 750°C due to the method of normalization. However, it is noted that the strain-life data at 400°C intersects the data at 750°C between 400 and 1,000 normalized cycles. This is unexpected since LCF life is expected to decrease with temperature. One possible explanation is that serrated yielding may be causing reduced life and / or high scatter in the data at this temperature. This hypothesis is supported by the testing experience in this project, and is also shown by the low  $R^2$  value using the existing strain-life data at 400°C despite the relatively large number of data points (16) in the data set.

At 900°C there is another potential anomaly since a very sharp slope increase is found in the strain-life curve at less than 1,000 normalized cycles. One explanation is a lack of test data. Since only 8 data points are in this data set, it is possible that some

outlying data points are causing the apparent deviation. Another possibility is that the test environment could be affecting the results. It is noted that these tests were done in air, and a fair amount of oxidation may be occurring at this temperature. This could be causing low measured cyclic lives, which are affecting the fit of the model. Marchionni [22] has published a paper about the influence of testing IN738 LC at elevated temperatures in air versus inert atmosphere. Re-running these tests in an inert atmosphere may reduce this effect.

There is little evidence provided in this work to suggest that the standard curve fitting procedure is flawed. Despite all of the efforts to find a better method for estimating the high strain behavior of this material, simply extrapolating from the base data model provided identical  $R^2$  values as using the best approximation method (UB2).

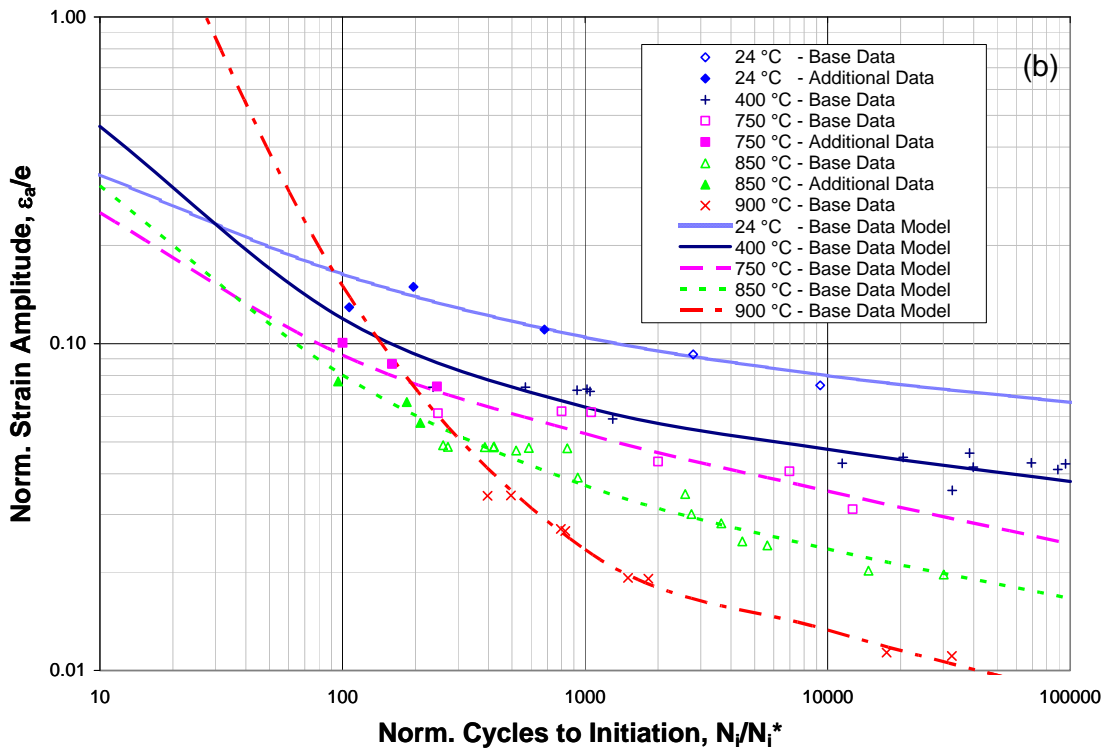
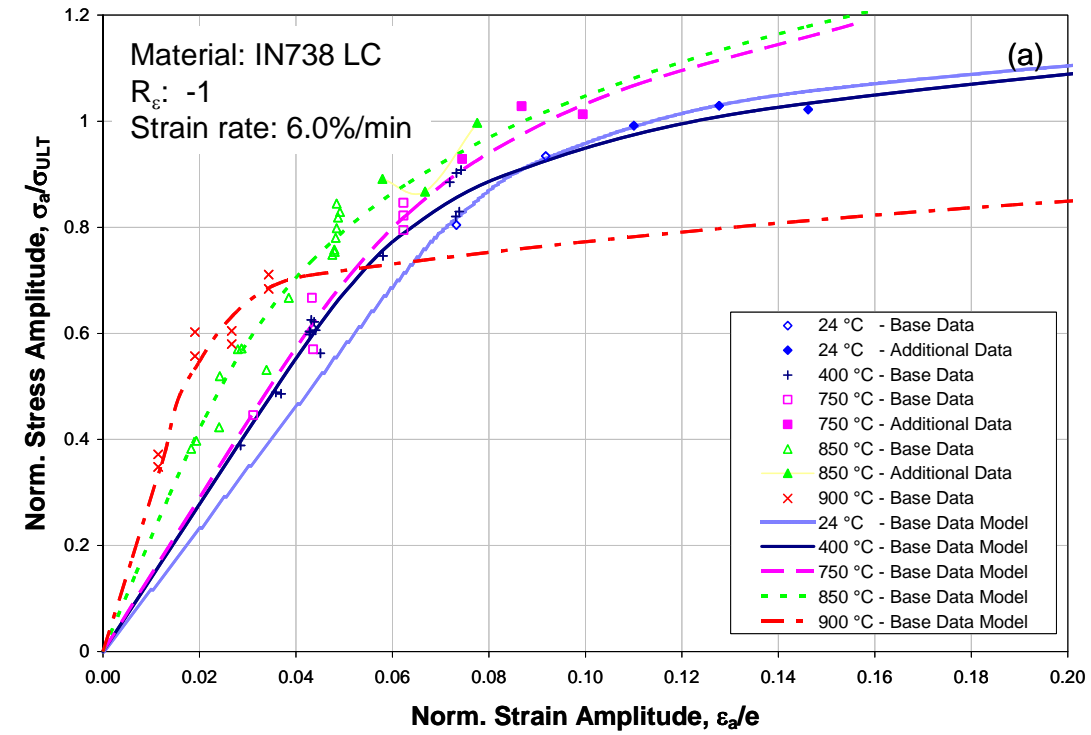


Figure 5.2. Comparison of (a) cyclic stress-strain curve and (b) strain-life curves using the base model and base data for IN738 LC at various temperatures.

### 5.3. Lower Bound Model

The LB model was thought to be a good estimate for the lower bounds of the material. Recall that the LB model includes an anchor point in the LCF data during the regression process.

One goal of the project was to acquire very strain range data to determine if the cyclic stress amplitude merges with the monotonic stress amplitudes as suggested by the data from Morrow and Tuler [6]. Their data suggested that this would occur at about 3.0% strain range with IN713 LC at room temperature. It was not possible to achieve such high strain ranges with the series of tests provided in this project. However, it is noted that the data at 24°C did show a maximum normalized stress amplitude of 1.029 at a normalized strain range of 0.257, which dropped to a normalized stress amplitude of 1.022 at a normalized strain range of 0.294. Likewise, the 0.174 normalized strain range at 750°C showed a higher normalized stress amplitude of 1.028 than the 0.199 normalized strain range value of 1.013 as shown in Figure 5.3a. This appears to correlate with the data from Morrow and Tuler by showing that there is a strain range which maximizes the strain hardening effect, above which the strain hardening effect diminishes. Higher strain range tests would be needed for further confirmation.

It is noted that 850°C does not show the same trend, since the stress amplitude continued to increase at the highest normalized strain amplitude tested. This was not unexpected since strain softening should show the opposite trend to strain hardening, where the stress range increases with strain amplitude at high strain amplitudes, eventually merging with the monotonic ultimate strength curve as the effect of strain softening diminishes.

However, it was unexpected to see that the LB model 850°C remains below the data at 850°C. It was anticipated that the LB model would over-predict stress for a given strain due to strain-softening, which is not the case considering the cyclic stress-strain curve. Additionally, since there is minimal strain softening occurring at 850C it was hypothesized that the LB model would provide accurate cyclic stress-strain curve, which is also not the case. Therefore, the LB method did not perform as anticipated in accuracy or in trends when minimal strain-softening occurs.

The LB strain-life curve did in general provide a lower bounds for the strain-life curve as shown in Figure 5.3b. This is an acceptable result considering that this method was not meant to accurately predict behavior, but was intended to provide a lower bounds of material behavior.

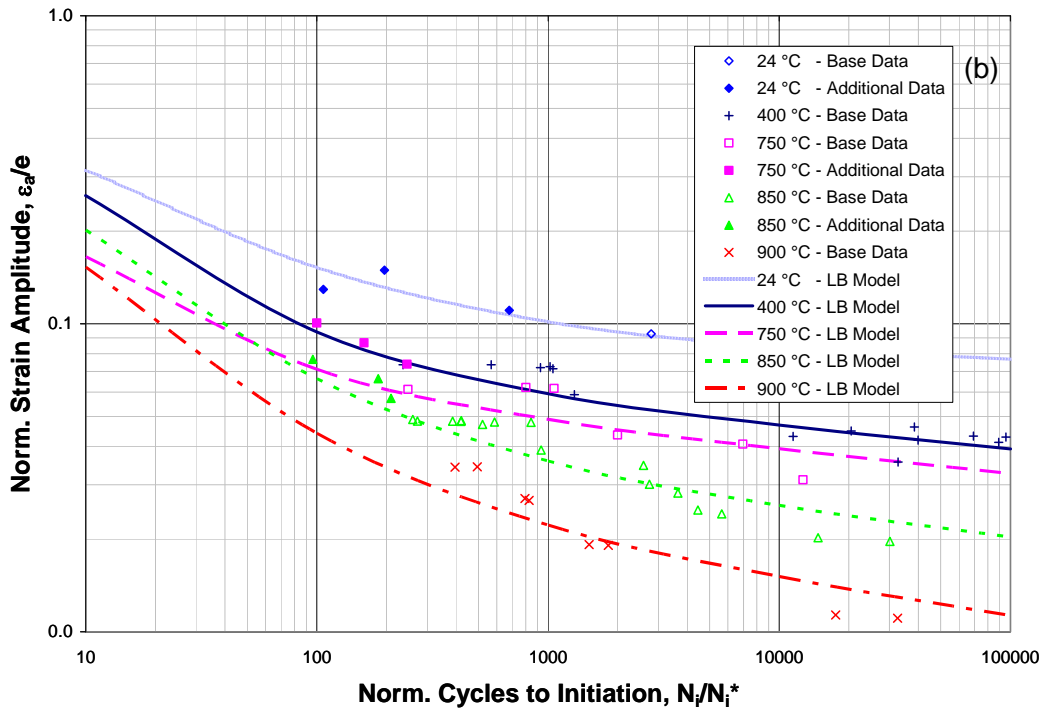
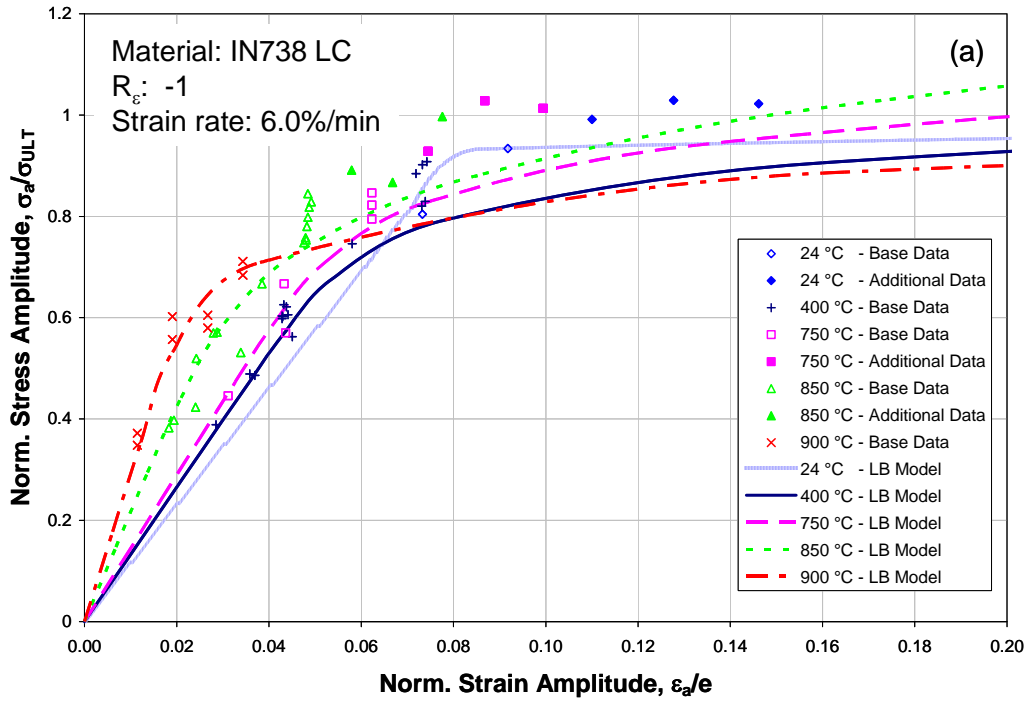


Figure 5.3. Comparison of (a) cyclic stress-strain curve and (b) strain-life curves using the LB model and base data for IN738 LC at various temperatures.

#### 5.4. Upper Bounds 1 Model

The UB1 model did not perform as expected, and in general performed much like the LB model rather than an accurate prediction of material behavior. This method adjusted the standard anchor point used in the LB model by using the shape change in the hysteresis loops between the initial and mid-life cycles. The stress-strain curves produced by this method are often conservative, and show a lower stress for a given strain compared to actual test data as shown in Figure 5.4a. The resulting strain-life curves are often overly conservative as well, when compared to the test data as shown in Figure 5.4b.

Recall that this method assumed a linear relationship between the initial plastic and mid-life plastic strain as well as between the initial stress range and mid-life stress range as shown in Figure 3.3a, and Figure 3.3b. Initially, regression was performed using only the base data set.

To further investigate the applicability of this method, linear regression was again performed using the augmented data set (base plus additional high strain data). This resulted in a limited change in the scaling constants as shown in Table 5.1 of less than 13%. Applying the revised scaling factors did not significantly change the outcome of the UB1 method, and had a negligible change on the  $R^2$  values for this method.

**Table 5.1. Comparison of Constants  $C_1$  and  $C_2$  from linear regression with base data set and augmented data set.**

Temperature (°C)	C1 - Base Data Model	C1 - Augmented Data Model	Change (%)	C2 - Base Data Model	C2 - Augmented Data Model	Change (%)
24	1.090	1.099	-0.8	0.694	0.770	-9.8
400	1.437	-	-	0.543	-	-
750	1.049	1.181	-11.2	0.632	0.690	-8.4
850	0.876	0.908	-3.5	1.105	0.980	12.8

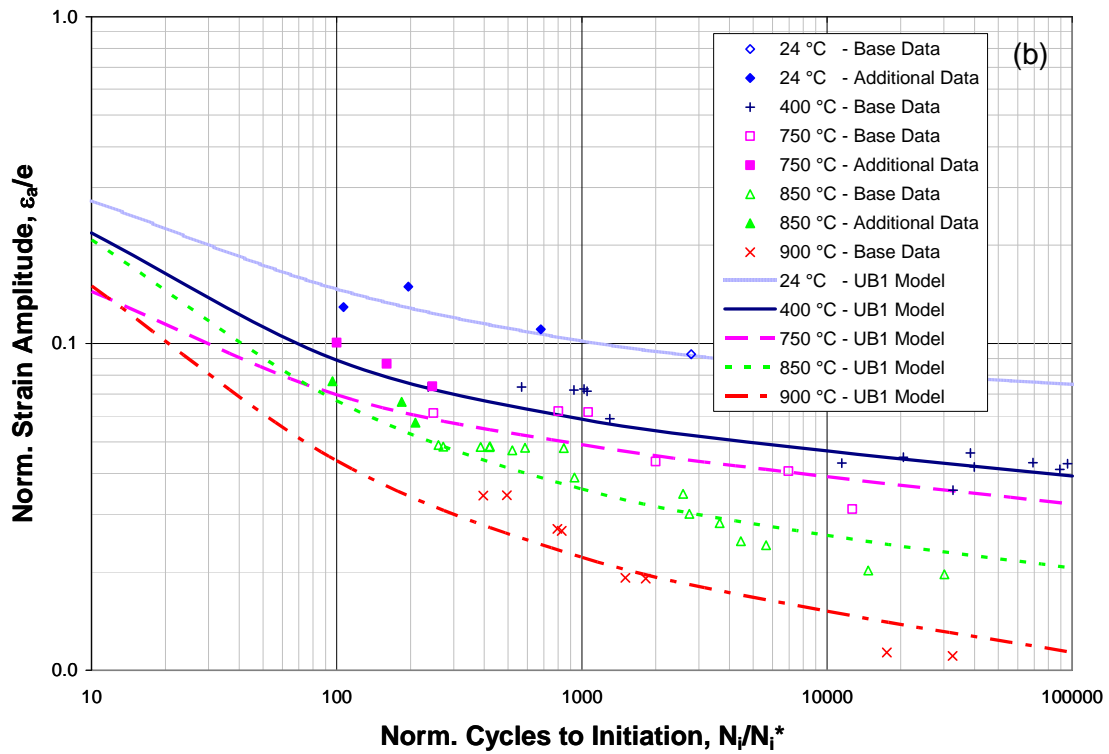
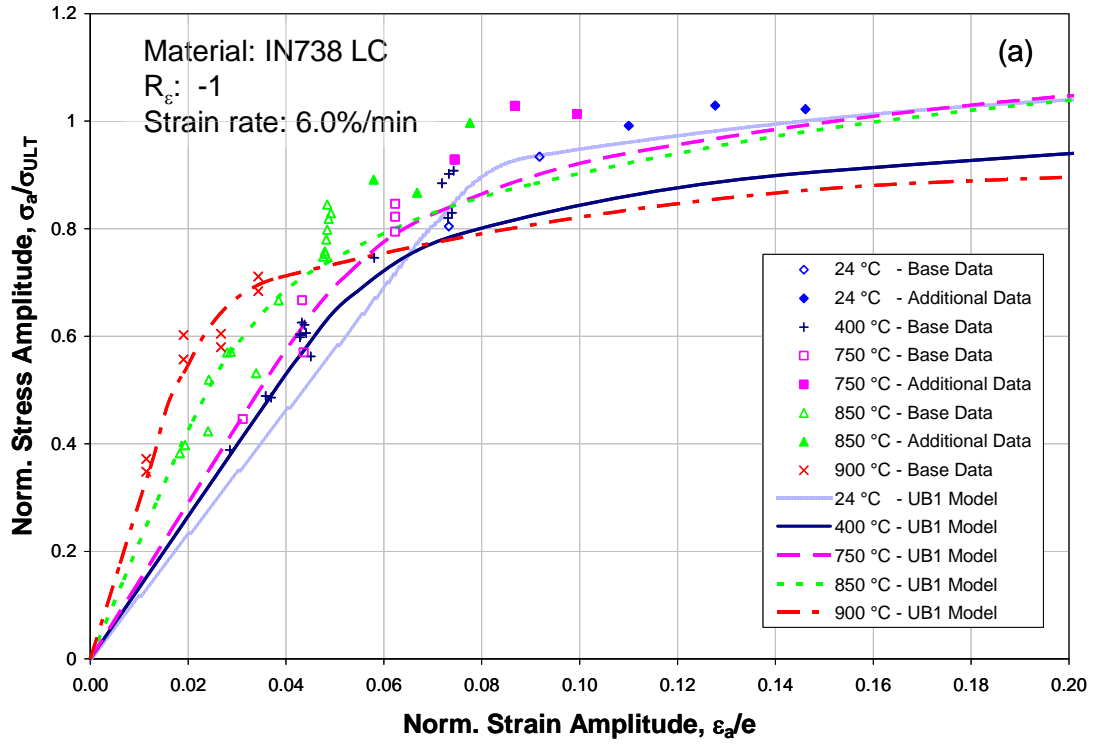


Figure 5.4. Comparison of (a) cyclic stress-strain curve and (b) strain-life curves using the UB1 model and base data for IN738 LC at various temperatures.

## 5.5. Upper Bounds 2 Model

It was demonstrated that the UB2 method is equally valid as the base method at predicting the high strain behavior of the extrapolated behavior of IN738 LC at high strain amplitudes outside of the existing test data. Recall that this method used strain compatibility to estimate the failure stress, which would occur at  $\frac{1}{2}$  cycle. It also assumed a failure strain equal to the failure elongation of a tensile test. This method is unique amongst the other methods since the failure stress is actually determined utilizing the existing LCF data set, and an assumption of behavior at  $\frac{1}{2}$  cycle.

The UB2 method provides the best overall fit through data points (including the high strain data points) of all the approximation methods. However, the margin of improvement was small over the base model. This method showed very similar behavior in predicting the stress-strain curve behavior of the base curve fit as shown in Figure 5.5a.

The UB2 method does provide more consistent looking stress-strain and strain-life curves. The stress-strain and strain-life curves trend well with temperature as shown in Figure 5.5 as apposed to the base model (Figure 5.2b), which showed a steep slope change especially at 900°C. The stain-life is especially improved since the regressions fit the anticipated behavior, which is that decreasing temperatures leads to increasing the cycles to crack initiation for constant strain amplitude.

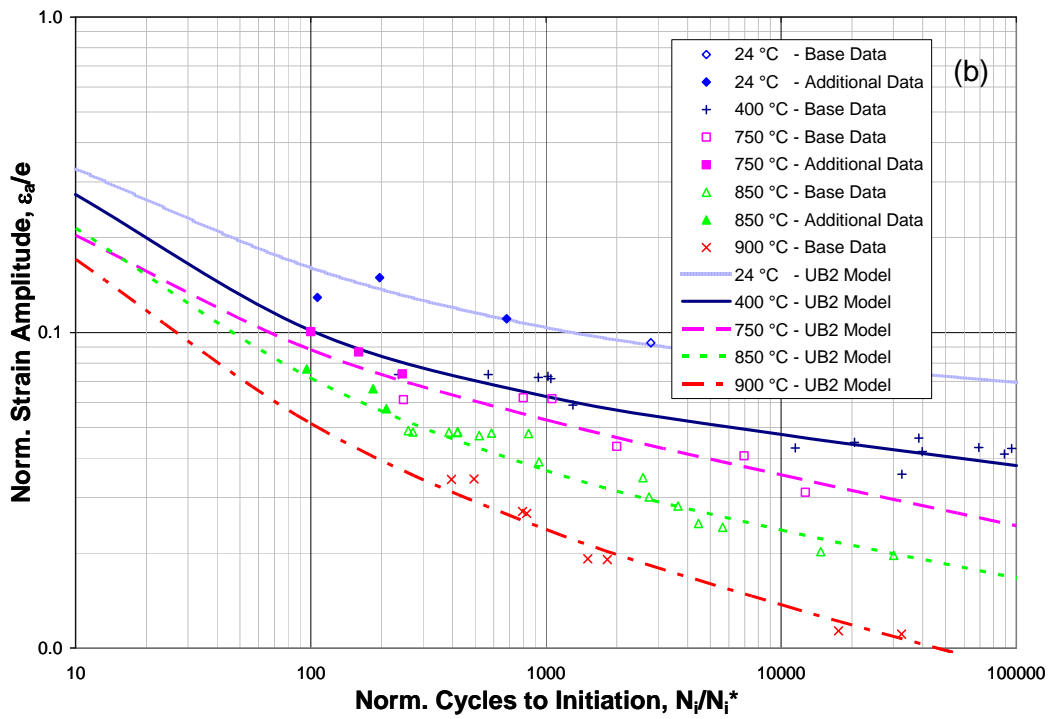
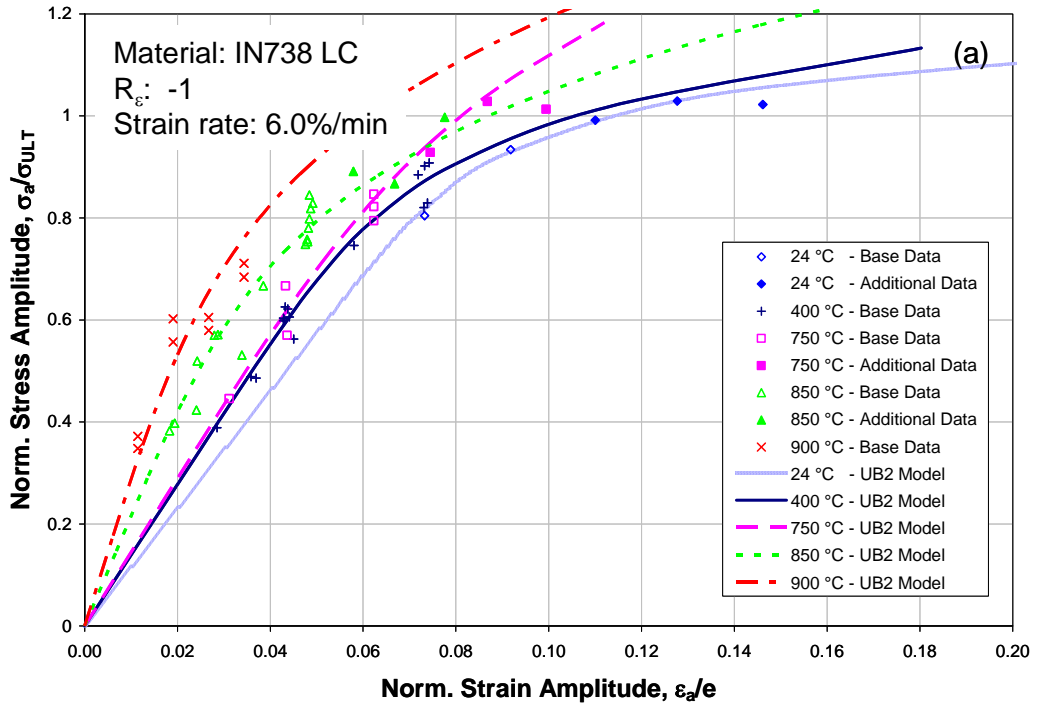


Figure 5.5. Comparison of (a) cyclic stress-strain curve and (b) strain-life curves using the UB2 model and base data for IN738 LC at various temperatures.

## 5.6. Upper Bounds 3 Model

The UB3 method was more accurate than other methods when significant scatter or potential anomalies exist in the data set at a certain temperature. Recall that this procedure grouped all temperatures of the plastic strain data together to find both constants describing the Coffin-Manson equation ( $\epsilon'_f, c$ ). The assumption was that the error induced by assuming a temperature independent Coffin-Manson equation would be offset by a significant reduction in the scatter in the plastic strain-life data.

The resulting stress-strain curves show a reasonable fit with the test data. As expected, the high strain portions of all the strain-life equations are reaching an asymptote due to using the same Coffin-Manson constants. However, the asymptotic slope is higher than is found in the base models (Figure 5.2b). This is likely due to that fact that most of the plastic strain data is at 850°C, which has a steeper slope with respect to temperature. This apparently has skewed the curve towards the high temperature data slope, and negatively affected the quality of the strain-life model.

It is noted that this method worked best when there were questionable trends observed in the data. For example, at 400°C and 900°C the UB3 method provided the overall fit to test data. Both of these temperatures may have experienced testing problems (serrated yielding at 400°C, and oxidation at 900°C). Therefore, it is possible that an indicator of outside testing issues is provided when this method has the highest  $R^2$  relative to other methods.

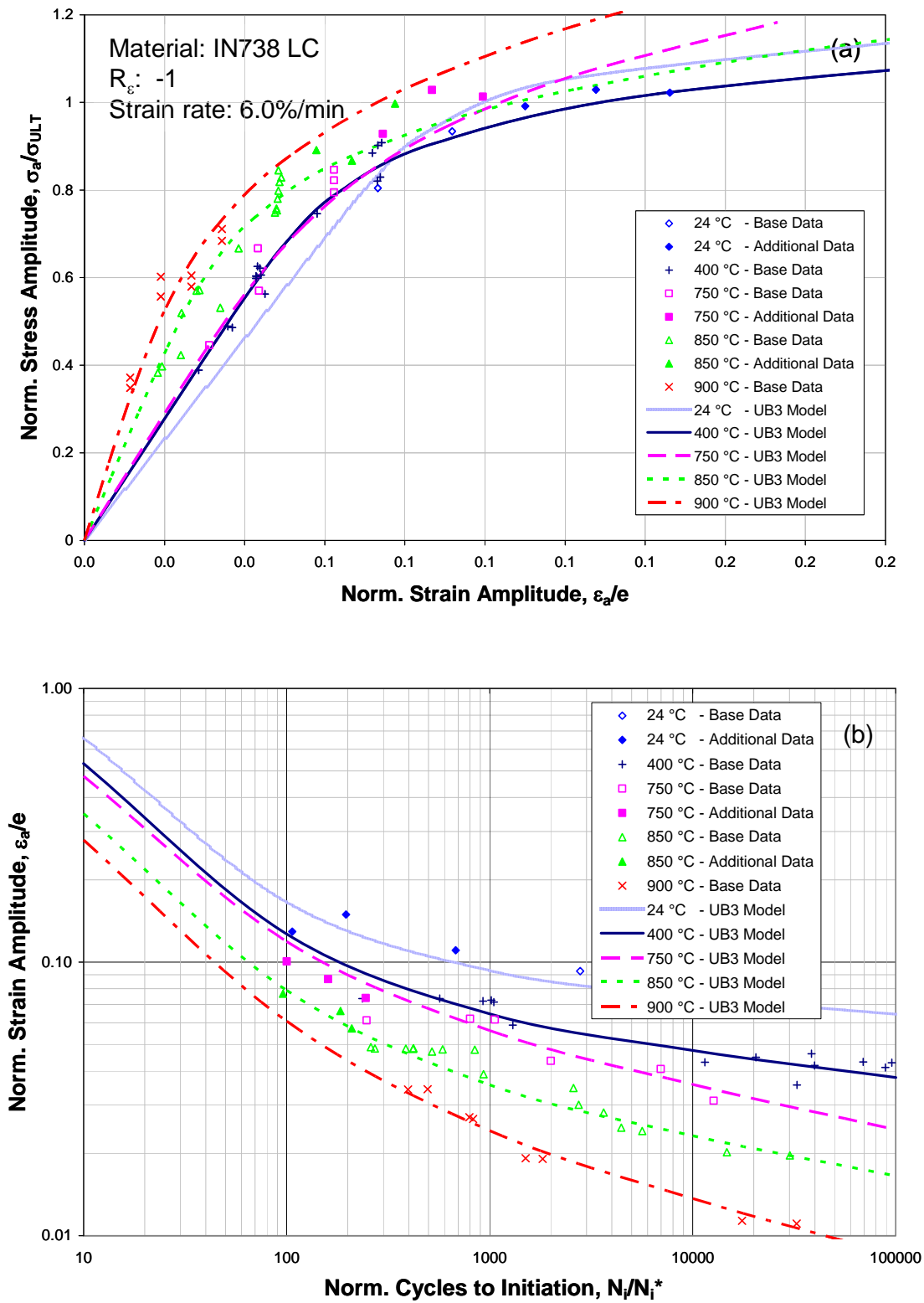


Figure 5.6. Comparison of (a) cyclic stress-strain curve and (b) strain-life curves using the UB3 model and base data for IN738 LC at various temperatures.

In the following, a simple ranking is applied to the  $R^2$  values presented in Table 4.10 and Table 4.11 to look for additional trends from the data. The overall evaluation of the extrapolation methods shows that the augmented data model is the most valid predictor of extrapolated high strain range behavior. The base model and UB2 approximation models are equally useful for prediction of the high strain range behavior at any of the test temperatures used as shown in Table 5.2. The UB1 was the poorest performer since it was meant to be a valid predictor of behavior.

**Table 5.2. Temperature average values of  $R^2$  for extrapolation methods.**

Method	Temperature °C			Average
	24	750	850	
Augmented Data Model	1	1	1	1.0
Base Data Model	2	2	2	2.0
Lower Bounds Model	5	6	4	5.0
Upper Bounds 1 Model	3	5	5	4.3
Upper Bounds 2 Model	2	3	1	2.0
Upper Bounds 3 Model	4	4	3	3.7

Likewise, a simple ranking was applied to the overall fit through all data at each temperature. These results show that the augmented data set is the best option, closely followed by the UB2 model, and then by the base data model as shown in Table 5.3. It is notable that the UB3 model does perform well at 400°C and 900°C. A correlation was noted between high  $R^2$  values of UB3 relative to other methods, and identification of potential outside testing issues. The UB1 is again a disappointment since this was meant to offer an improvement over the current methodology.

**Table 5.3. Temperature average values of  $R^2$  error for best over all test data.**

Method	Temperature °C					Average
	24	400	750	850	900	
Augmented Data Model	1		1	1		1.0
Base Data Model	2	3	1	2	3	2.2
Lower Bounds Model	5	5	4	4	4	4.4
Upper Bounds 1 Model	3	4	5	5	5	4.4
Upper Bounds 2 Model	2	2	2	1	2	1.8
Upper Bounds 3 Model	4	1	3	3	1	2.4

The original intention of this work was to develop a method for extrapolating from an existing LCF data set into high strain ranges outside of the data set. It is again reiterated that the best method for doing this is actually acquiring the high strain data points. In lieu of this, the best overall method is to apply UB2 or use of the base model curve fit. Use of the UB2 method also had the unexpected result of improving the overall fit with all available test data. Where high amount of variation or questionable trends are found in the test data, the UB3 method proved useful.

Another option for use of these methods is extrapolation in the early stages of setting up a test matrix for the material. If tensile test data and HCF data is available, the UB2 methodology could be used to estimate the LCF behavior of the material. This information could be used for planning a matrix for acquiring LCF test data.

It may be tempting to use these methodologies in an effort to provide an additional test data point in an existing test matrix with sparse data points. A note of caution is added that any extrapolation methods presented in this work will not improve the quality level of the database. These methods are not meant as a substitute for a characterization of a material by a sufficient quantity of valid test data.

## 6. CONCLUSIONS

The best most accurate method for improving the understanding of high strain LCF properties of IN738 LC is by including high strain range tests in the test matrix. It was demonstrated that more difficulty in achieving strain control may occur during high strain range tests. These difficulties may be addressed in part by making tuning adjustments for each specimen prior to testing.

It was demonstrated that the best method for extrapolating from an existing set of IN738 LC data set to high stress amplitudes was shared between the UB2 method (strain compatibility / anchor point combination) and the base model. Test data was used at 24°C, 750°C, and 850°C to demonstrate these effects. The UB2 method had the unexpected result of providing an overall better match with test data than the base linear regression method, which was demonstrated using data at 24°C, 400°C, 750°C, 850°C, and 900°C.

Testing anomalies which occurred at 400°C indicate a potential cause of unexpected trends may be due to testing issues specific to these temperatures rather than a fundamental problem with the base data set linear regression modeling technique. Additional evidence is provided by the observation that the 900°C tests occurred in air at a temperature where significant oxidation may be affecting the measured cyclic lives. The current modeling technique using linear regression curve fitting does not provide an indicator of the occurrence of outside testing issues.

The LB option (conventional anchor point) provided the expected affect of over-predicted the stress-strain behavior at moderate strain range levels at 24°C and 750°C. However, when strain-softening occurred at 850°C, the stress-strain curve was over-

predicted rather than under-predicted as expected. It was not possible verify whether the upper bounds option merged with the lower bounds options at very high strains since these tests were not achieved.

The UB1 method (hysteresis loop adjusted anchor point) proved poor at describing an upper bounds of the cyclic stress-strain and strain-life equation. Linearly extrapolating from stress range and strain range changes between the initial and stable mid-life cycle to scale a conventional anchor point had only a minor affect on the base anchor point.

The UB3 option (temperature independence of the Coffin-Manson equation) did not general perform well at providing an upper bounds of material behavior. A correlation was noted between UB3 having the highest  $R^2$  value, and high scatter in material data at 400°C. The UB3 option also had the highest  $R^2$  value at 900°C where possible influence due to oxidation may have influenced the measured cyclic lives. This indicates that the UB3 may be best used when large scatter or questionable results are present in the data set, or an indicator of outside testing issues.

A strain range at which the stabilized stress range was maximized appeared to occur at 24°C and 750°C. The 850°C did not show such a peak, but since strain softening was observed at this temperature, a peak would in fact not be expected. Additional testing would be required at higher strain ranges at 24°C and 750°C to confirm.

## 7. RECOMMENDATIONS

As an outcome of this investigation, several options exist for improving the results from this study. One option is to provide additional high strain tests at the missing temperatures of 400°C and 900°C. Options that may alleviate the issues of testing at 400°C may include changing the strain rate of the test, and additional fine tuning of the control settings. It would be beneficial to determine if there is questionable data at 900°C. Additional tests could be provided in air at 900°C at high strain ranges. Also, it is worth comparing tests in an inert environment at 900°C especially at low strain ranges, and high lives to determine if oxidation is affecting the high cyclic lives.

Acquiring these results would provide more evidence supporting UB2 as an anchor point or show that the standard linear regression model is the preferred method for extrapolation for an existing data set. These results may also show whether the UB3 method is in fact a good indicator of questionable data in a data set.

If true, valid high strain range test data could be provided to observe failure in a few cycles, then a more appropriate approximation method could be devised. This would most likely require tests above 2.0% strain range, and ASTM suggests an hourglass specimen for these tests. It is also noteworthy to consider that both the data from Morrow and Tuler [6], and the data from Marchionni [22] provided test data above 2.0% strain range. Both of these sources used tubular specimens as typically used for induction heating, and it is possible that a tubular specimen design allows for greater testing ease at high strain ranges. It would be advisable to conduct these tests at room temperature to reduce cost and expense during the learning period. The room temperature tests also

required the least adjustment of the control settings to achieve constant strain. After methods are developed at room temperature, the high temperature tests could follow.

APPENDIX A – EXPERIMENTAL HYSTERESIS LOOPS AND STRESS HISTORIES

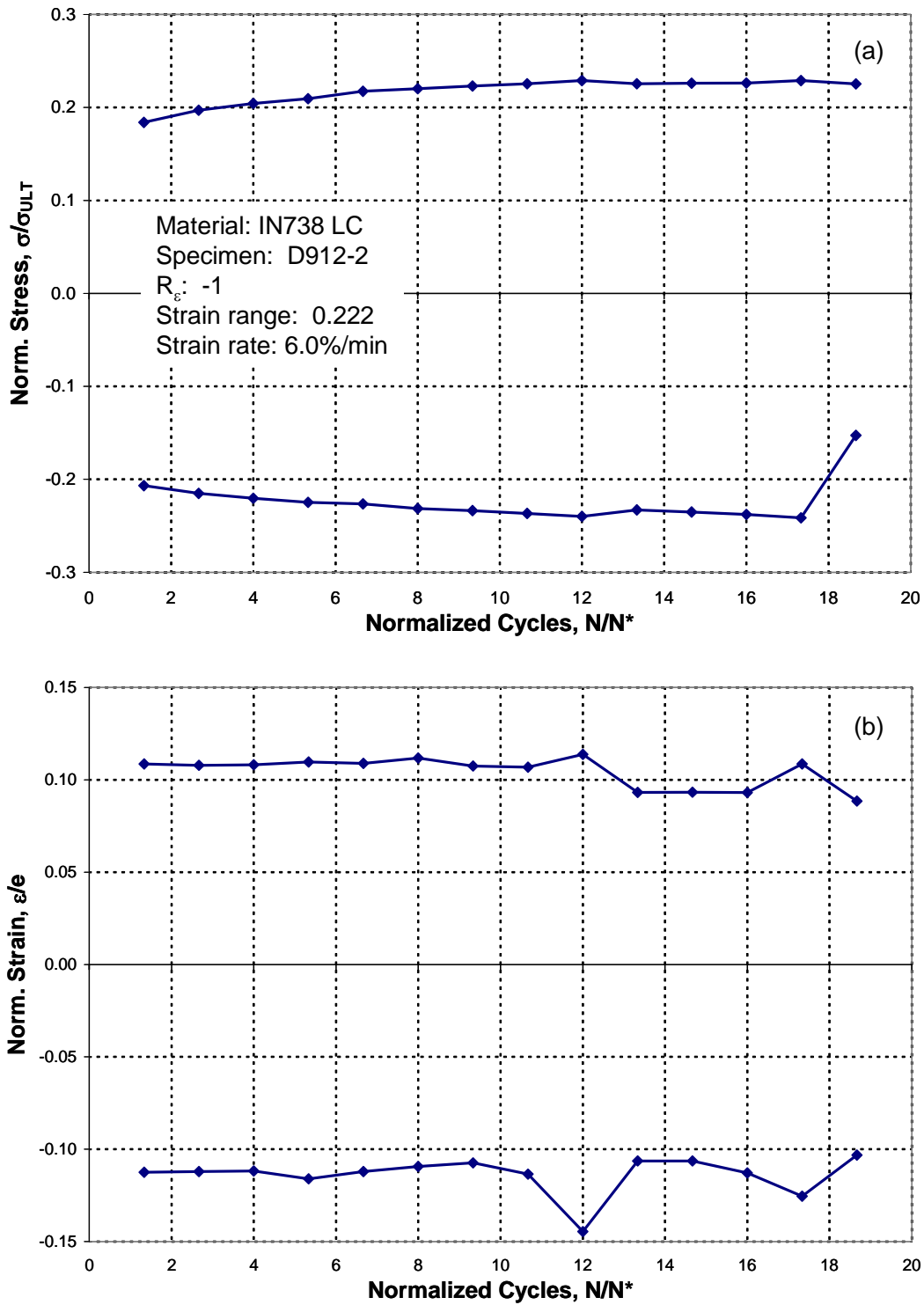


Figure A.1. Cyclic (a) stress and (b) strain histories for test specimen D912-2 at 400°C.

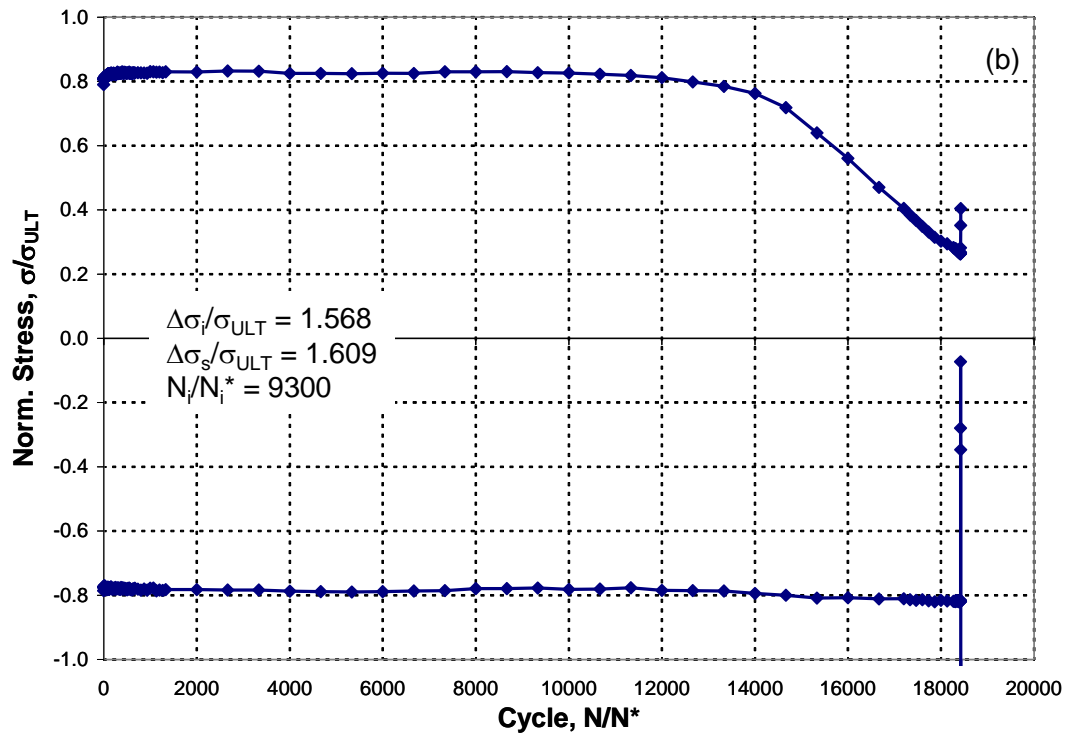
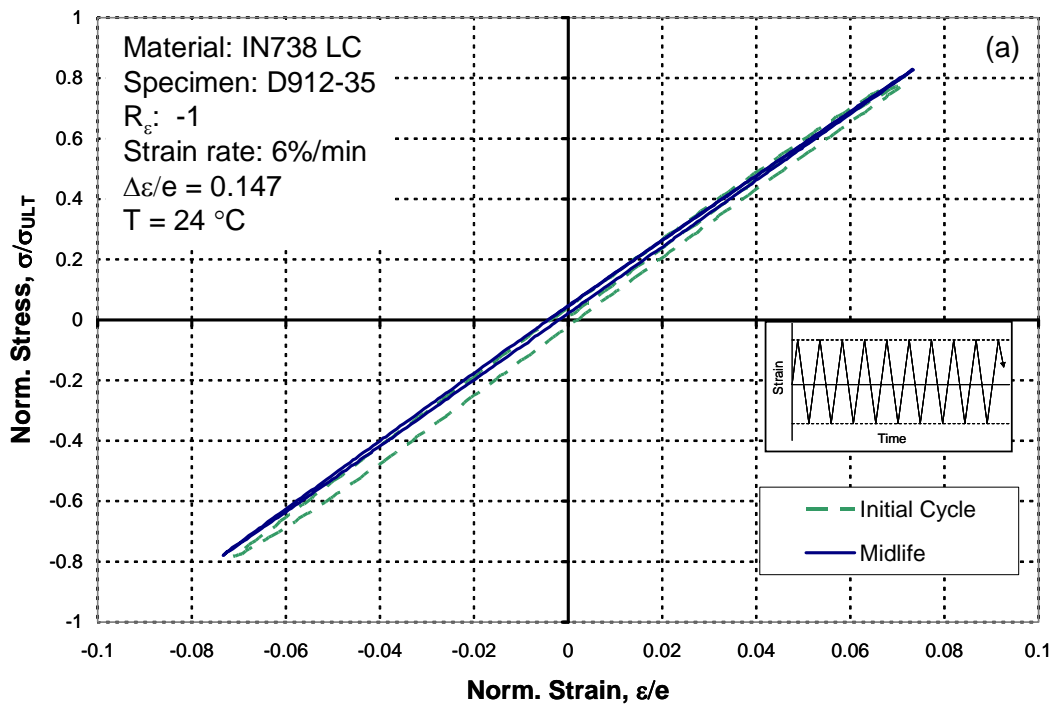


Figure A.2. (a) Hysteresis loops and (b) stress cycle plots for LCF test specimen D912-35 at 24°C.

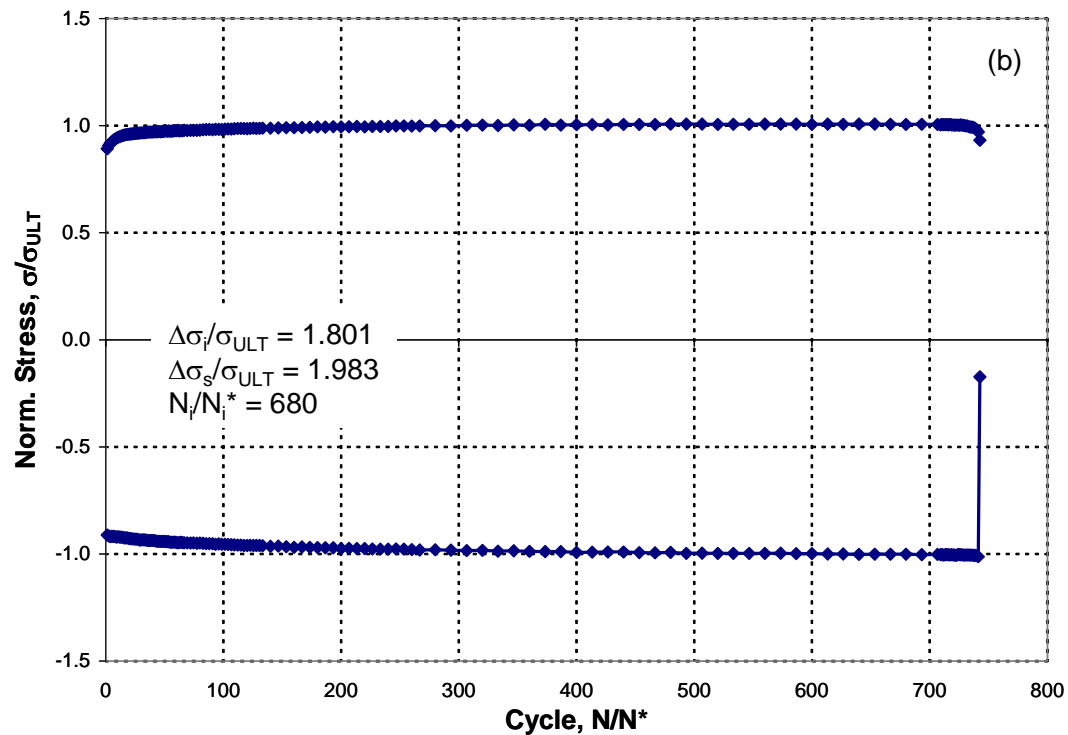
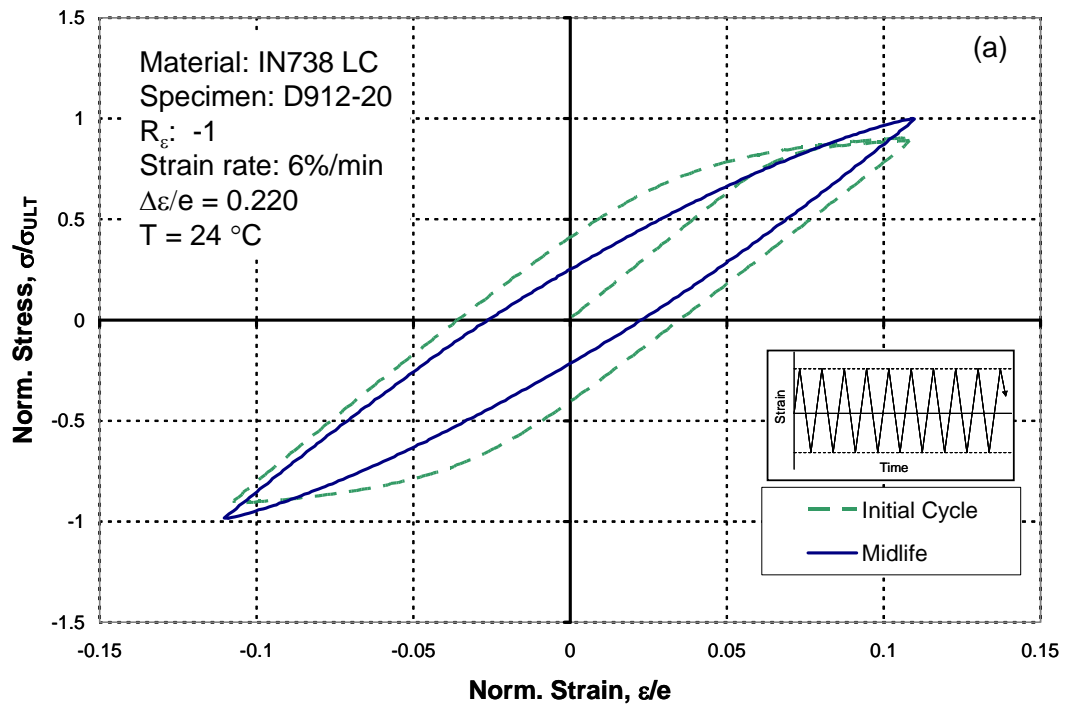


Figure A.3. (a) Hysteresis loops and (b) stress cycle plots for LCF test specimen D912-20 at 24°C.

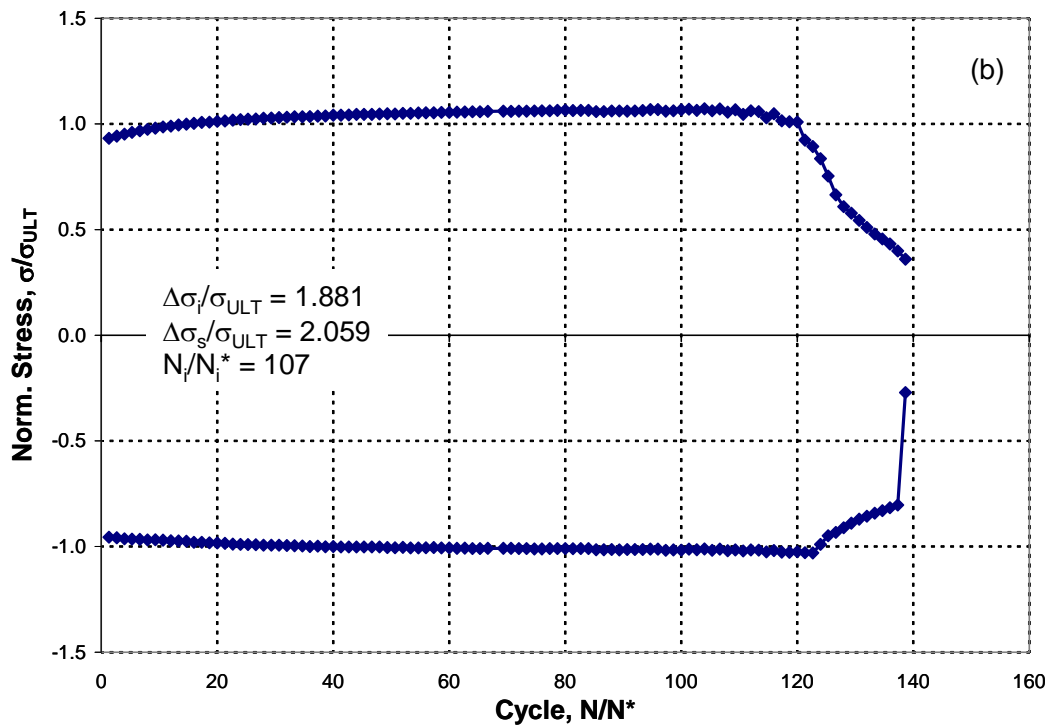
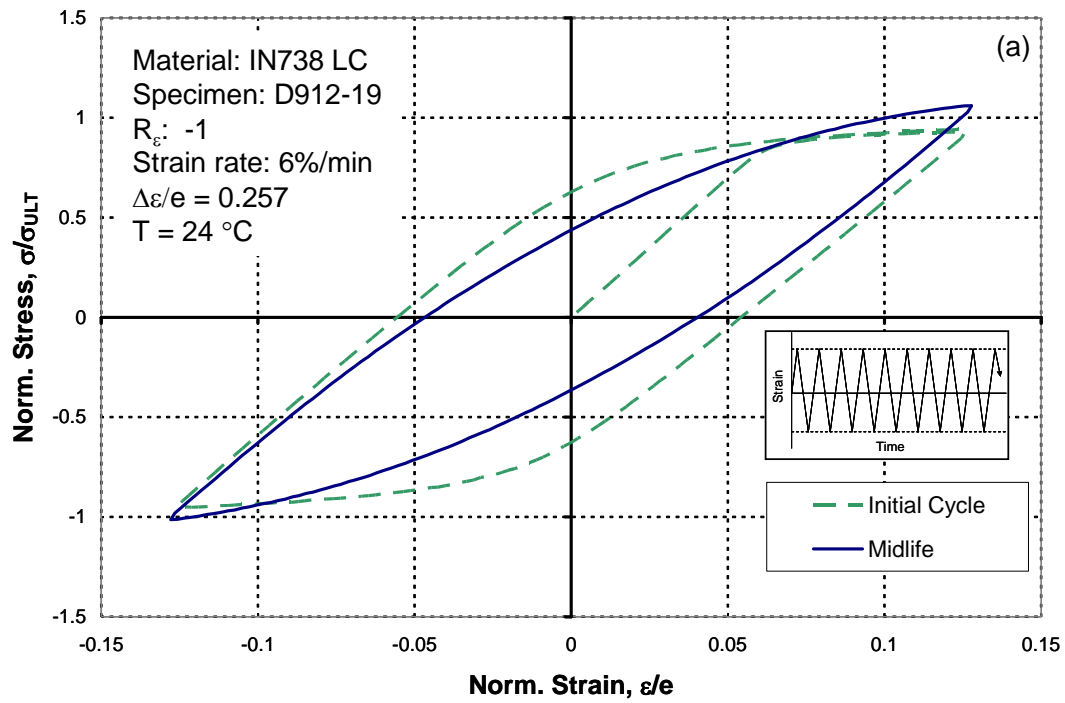


Figure A.4. (a) Hysteresis loops and (b) stress cycle plots for LCF test specimen D912-19 at 24°C.

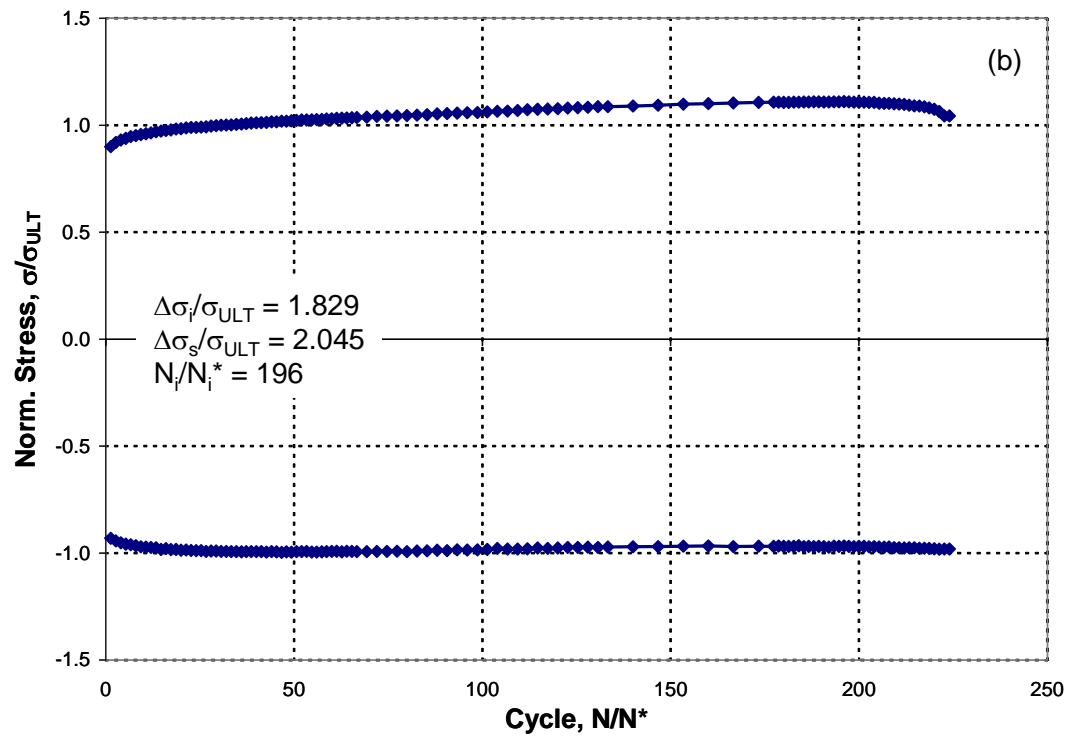
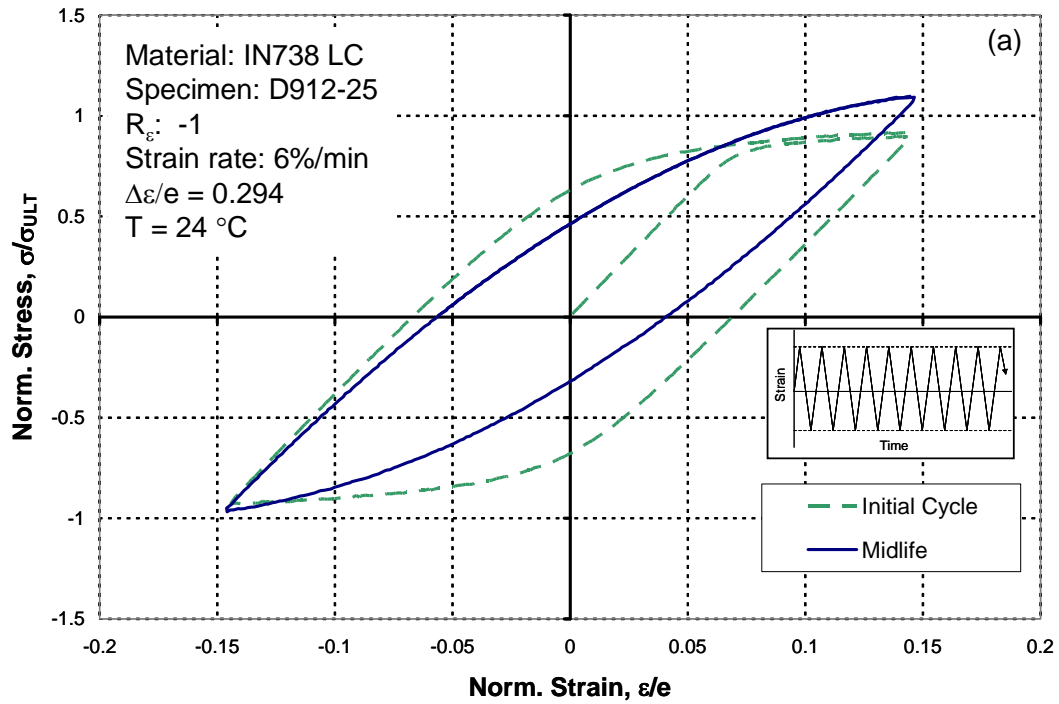


Figure A.5. (a) Hysteresis loops and (b) stress cycle plots for LCF test specimen D912-25 at 24°C.

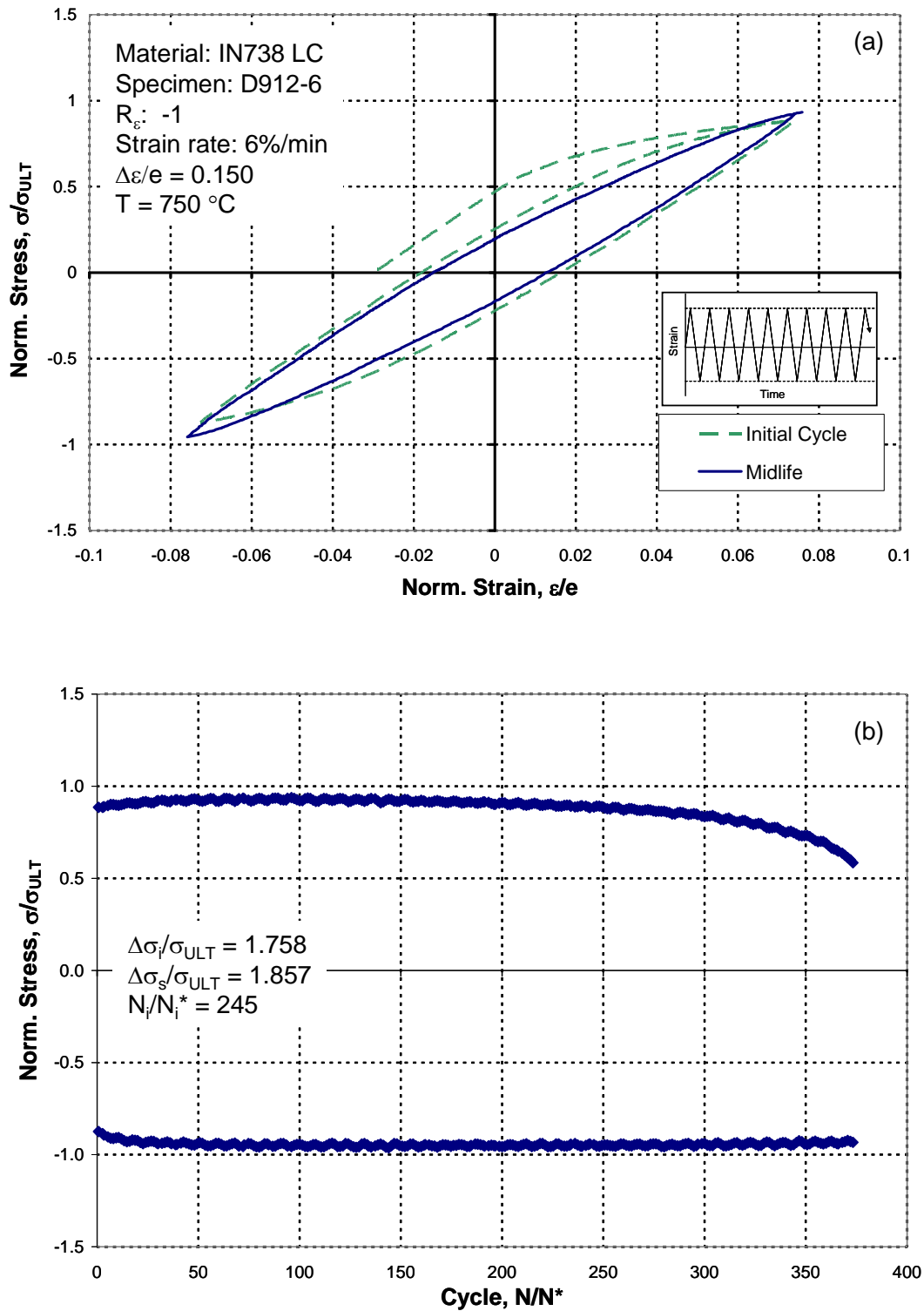


Figure A.6. (a) Hysteresis loops and (b) stress cycle plots for LCF test specimen D912-6 at 750°C.

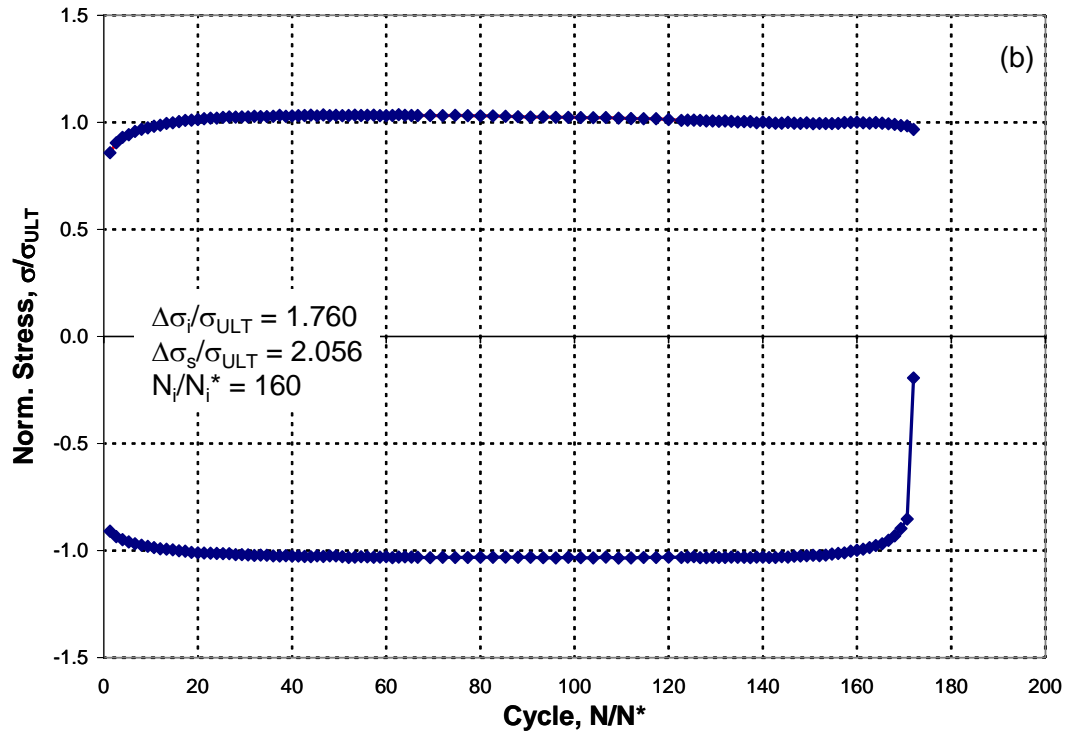
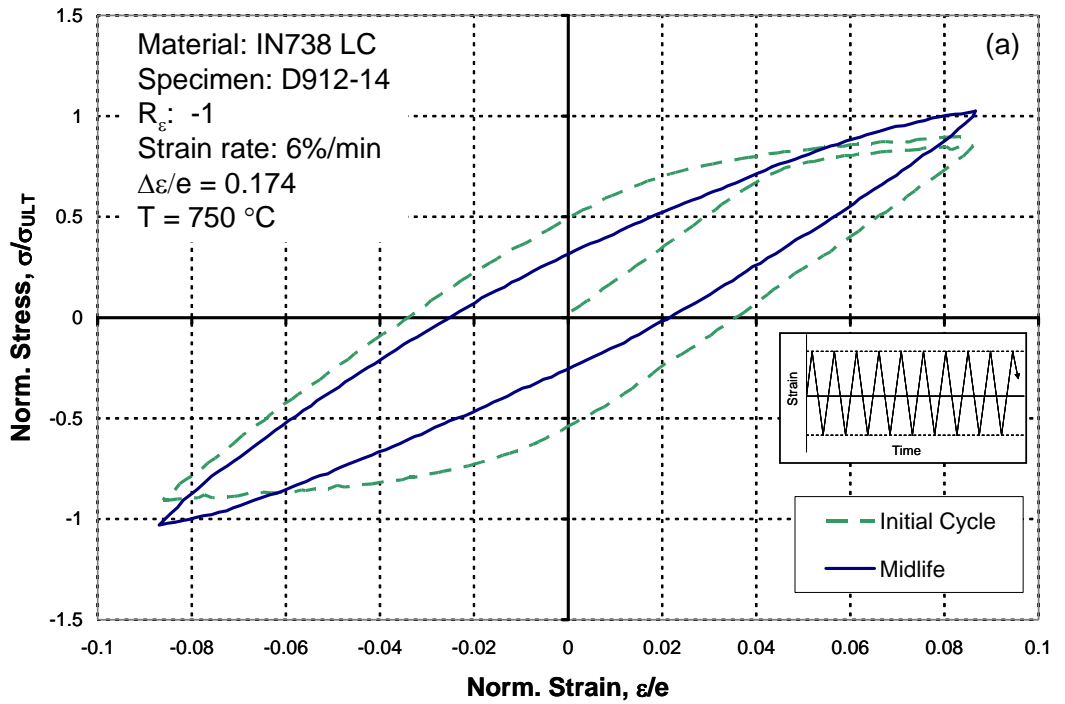


Figure A.7. (a) Hysteresis loops and (b) stress cycle plots for LCF test specimen D912-14 at 750°C.

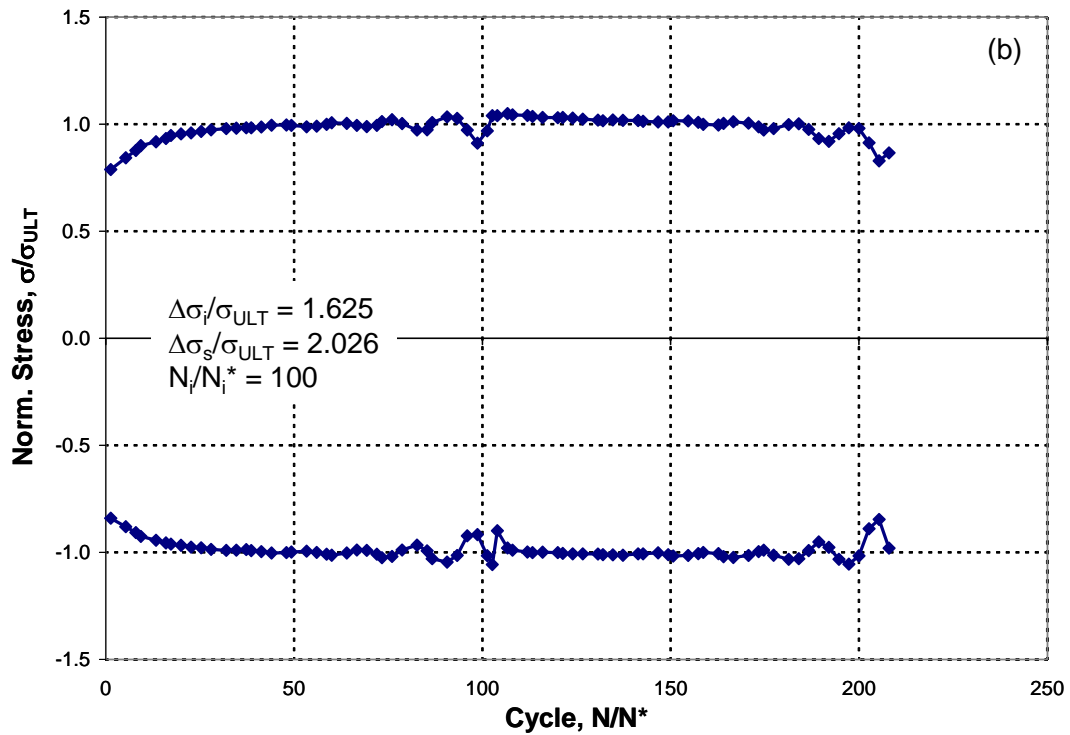
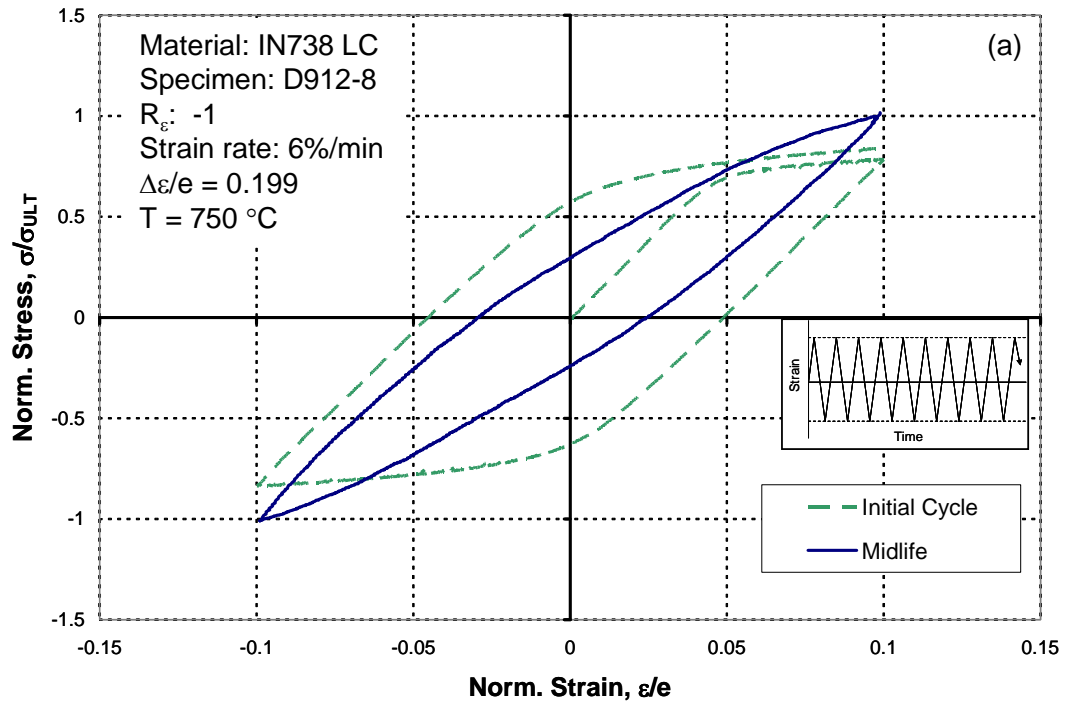


Figure A.8. (a) Hysteresis loops and (b) stress cycle plots for LCF test specimen D912-8 at 750°C.

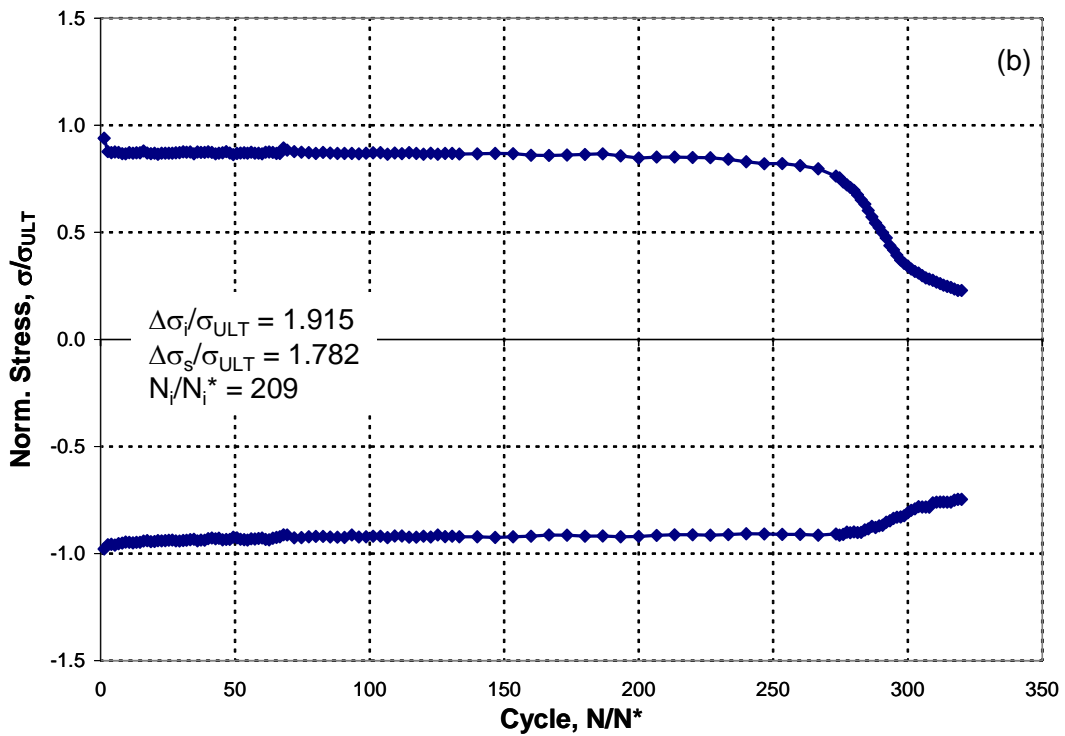
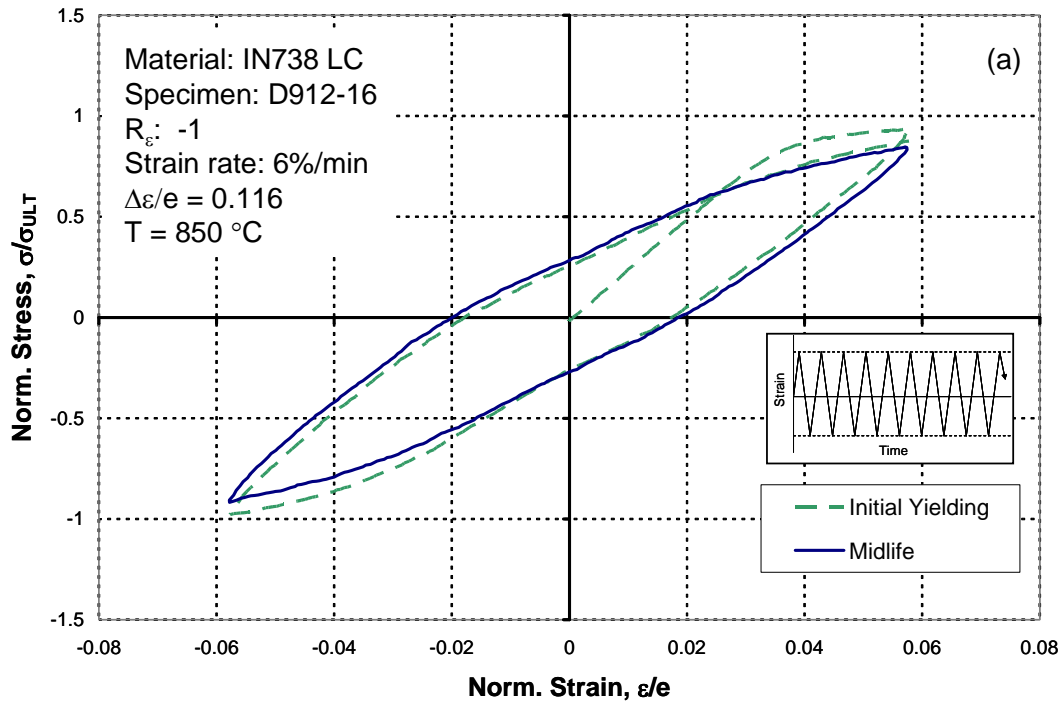


Figure A.9. (a) Hysteresis loops and (b) stress cycle plots for LCF test specimen D912-16 at 850°C.

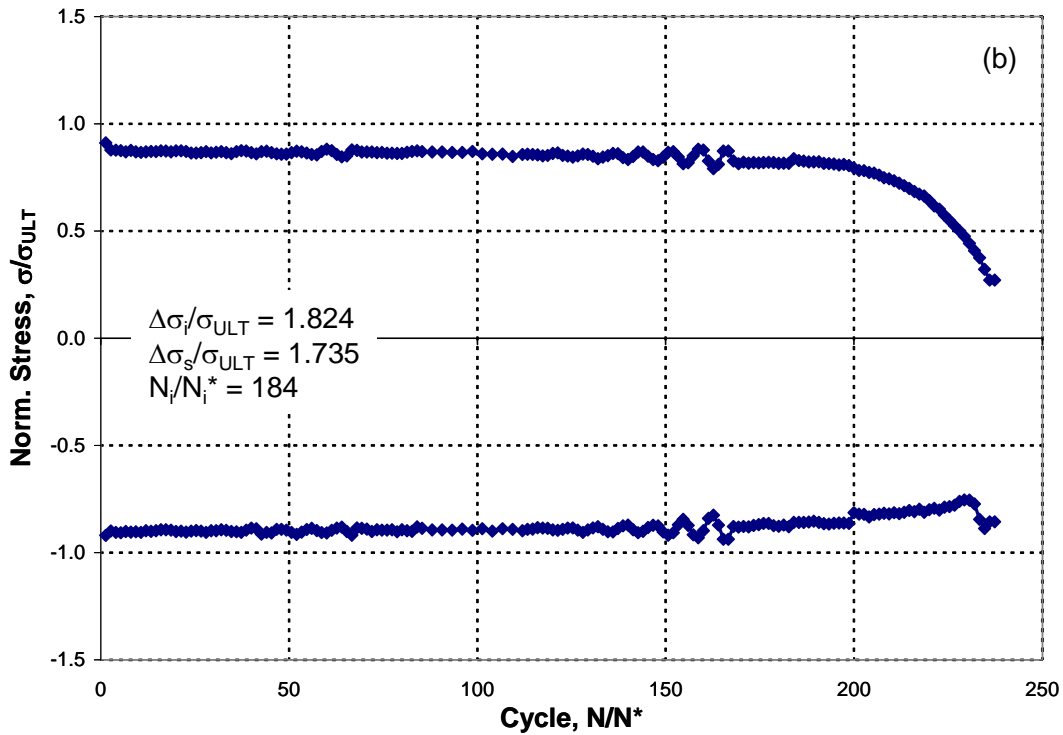
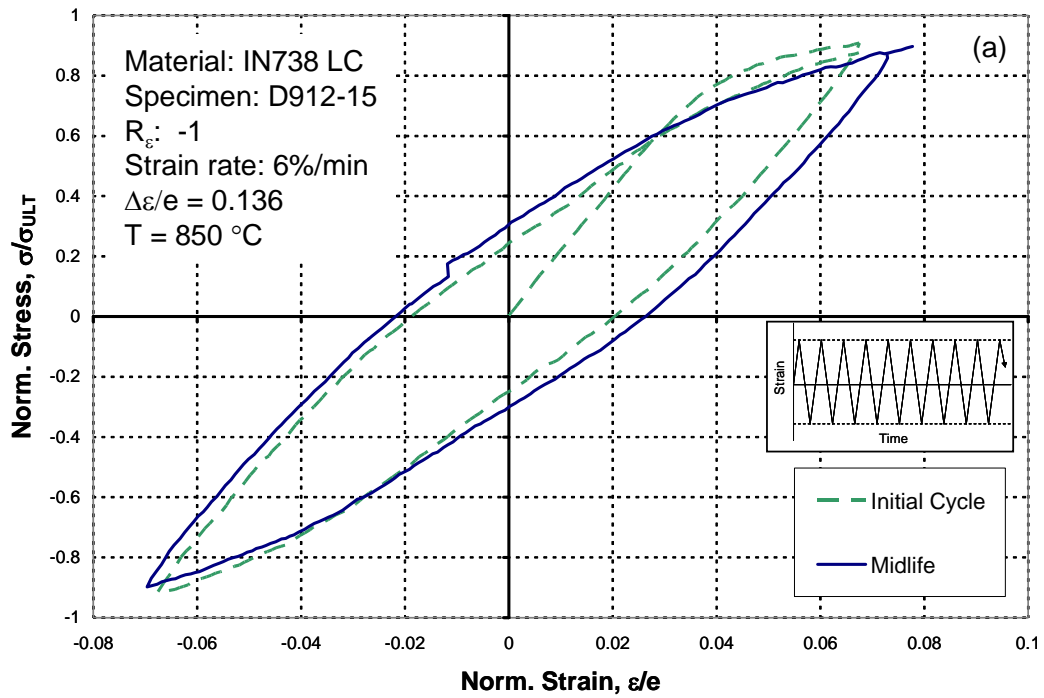


Figure A.10. (a) Hysteresis loops and (b) stress cycle plots for LCF test specimen D912-15 at 850°C.

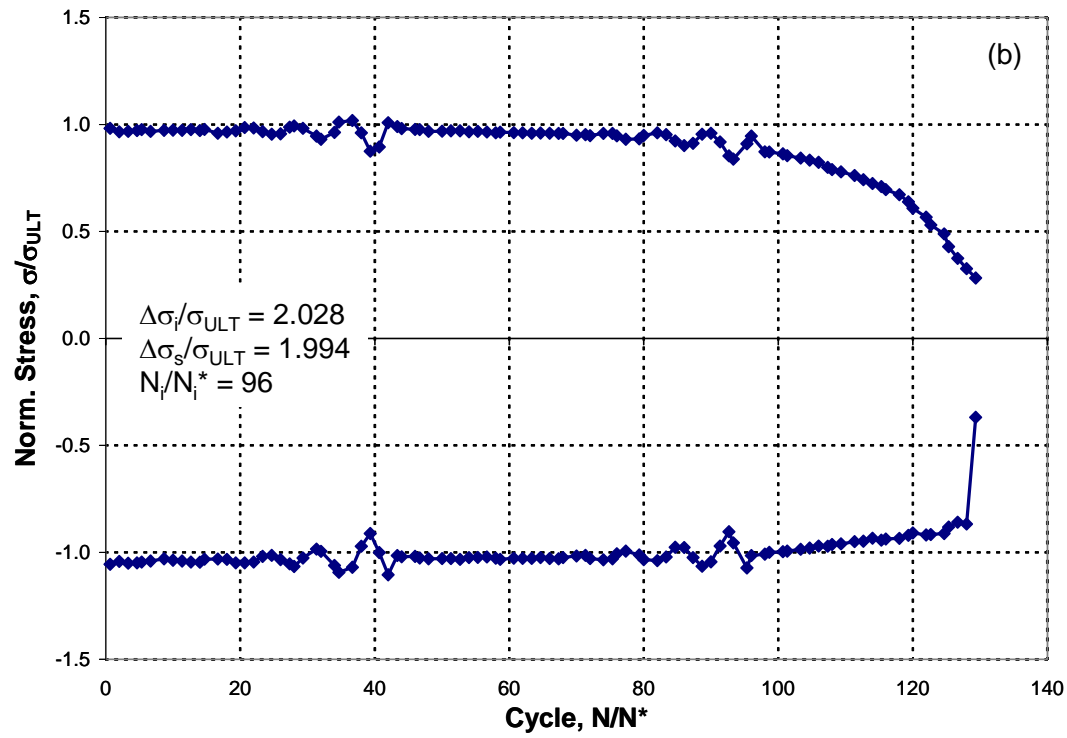
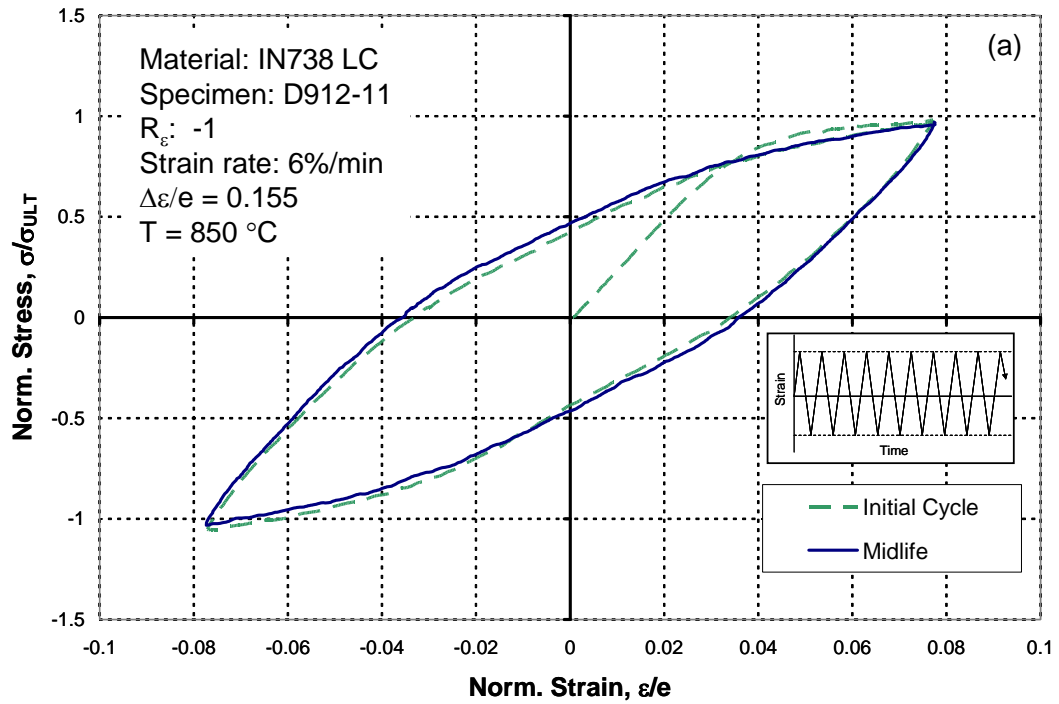


Figure A.11. (a) Hysteresis loops and (b) stress cycle plots for LCF test specimen D912-11 at 850°C.

APPENDIX B – SPECIMEN PHOTOGRAPHS



**Figure A.12. Photograph of fractured specimen D912-35, 24°C test temp and 0.8% strain range.**



**Figure A.13. Photograph of fractured specimen D912-17, 24°C test temp and 1.0% strain range.**



**Figure A.14. Photograph of fractured specimen D912-20, 24°C test temp and 1.2% strain range.**



**Figure A.15. Photograph of fractured specimen D912-19, 24°C test temp and 1.4% strain range.**



**Figure A.16. Photograph of fractured specimen D912-25, 24°C test temp and 1.6% strain range.**



**Figure A.17. Photograph of fractured specimen D912-33, 400°C test temp and 1.2% strain range.**



**Figure A.18. Photograph of fractured specimen D912-1, 400°C test temp and 1.5% strain range.**



**Figure A.19. Photograph of fractured specimen D912-2, 400°C test temp and 1.5% strain range.**



**Figure A.20. Photograph of fractured specimen D912-6, 750°C test temp and 1.2% strain range.**



**Figure A.21. Photograph of fractured specimen D912-14, 750°C test temp and 1.4% strain range.**



**Figure A.22. Photograph of fractured specimen D912-8, 750°C test temp and 1.6% strain range.**



**Figure A.23. Photograph of fractured specimen D912-16, 850°C test temp and 1.2% strain range.**



**Figure A.24. Photograph of fractured specimen D912-15, 850°C test temp and 1.4% strain range.**



**Figure A.25. Photograph of fractured specimen D912-11, 850°C test temp and 1.6% strain range.**

## REFERENCES

- 1 EPRI Report. "Reducing Life Cycle Costs for Gas Turbine Hot Section Components". Product ID: 1014679. November 2006.
- 2 Viswanathan, R., "Damage Mechanisms and Life Assessment of High-Temperature Components," ASM International, Metals Park, Ohio.
- 3 Dowling, N.E., "Mechanical Behavior of Materials," 2<sup>nd</sup> Ed. Prentice Hall, New Jersey, 1999.
- 4 Lemaître, J., Dufailly J., "Modeling Very Low Cycle Fatigue," International Journal of Damage Mechanics, Vol. 4 – April 1995, p. 153-170.
- 5 Bannantine, J.A., Comer, J.J., Handrock, J.L., "Fundamentals of Metal Fatigue Analysis," Prentice-Hall, New Jersey, 1990.
- 6 Morrow, JoDean, Tuler F.R., "Low Cycle Fatigue Evaluation of Inconel 713C and Waspaloy," Transactions of the ASME, Journal of Basic Engineering, Volume 87, Series D, June 1965, p 275-289.
- 7 Balikci, Ercan, "Microstructure Evolution and Its Influence on Thermal Expansion and Tensile Properties of the Superalloy IN738LC at High Temperatures," Ph.D. Thesis, Louisiana State University., 1998.
- 8 Burke, M.A., Beck, C.G., "The High Temperature Low Cycle Fatigue Behavior of the Nickel Base Alloy IN-617," Metallurgical Transactions A, V 15A, April 1984 -661.
- 9 ASTM International, "Standard Practice for Statistical Analysis of Linear of Linearized Stress-Life (S-N) and Strain-Life ( $\epsilon$ -N) Fatigue Data." E739-91, 2004.

- 10 Manson, S.S., "Fatigue – Complex subject – Some simple approximations,"  
Experimental Mechanics, v5, n7, July 1965, p193-226.
- 11 Kim, K.S., Chen X., Han, C., Lee, H.W., "Estimation methods for fatigue properties  
of steels under axial and torsional loading," International Journal of Fatigue, 24  
(2002) p. 783-793.
- 12 Park, Jun-Hyub, Song, Ji-Ho, "Detailed evaluation of methods for estimation of  
fatigue properties," International Journal of Fatigue, vol. 17, No 5, 1995, p. 365-373.
- 13 Ong, J.H., "An improved technique for the prediction of axial fatigue life from tensile  
data," International Journal of Fatigue, vol. 15, No 3, 1993, p. 213-219.
- 14 Meggiolaro, M.A., Castro J.T.P., "Statistical evaluation of strain-life fatigue crack  
initiation predictions," International Journal of Fatigue, vol. 26, 2004, p. 463-476.
- 15 Coffin, L.F. Jr., "Introduction to high-temperature low-cycle fatigue." Experimental  
Mechanics, v8, n5, May 1968, p218-224.
- 16 Stephens, R.I., Fatemi, A., Stephens, R. R., Fuchs, H.O., "Metal Fatigue in  
Engineering," 2<sup>nd</sup> Ed, John Wiley & Sons, New York.
- 17 Brown, W.F. Jr, Hill L.R., "Aerospace Structural Metals Handbook, 37<sup>th</sup> Ed. Code  
4217. CINDAS/USAF CRDA Handbooks Operation, Purdue University, West  
Lafayette, IN. 2001.
- 18 Yandt, Scott A., "Development of a Thermal-Mechanical Fatigue Testing Facility,"  
M.S. Thesis, 2000, Carleton University, Canada.
- 19 ASTM International, "Standard Practice for Strain-Controlled Fatigue Testing," E  
606 -04. 2004.

- 20 Neter, Wasserman, Kutner, "Applied Linear Statistical Models," 3<sup>rd</sup> Ed., Irwin, Burr Ridge Illinois. 1990.
- 21 Huron, E.S., "Serrated Yielding in a Nickel-Base Superalloy," Superalloys 1992. The Minerals, Metals, & Materials Society 1992.
- 22 Marchionni, M., Ranucci, D., Picco, E., "High-Temperature Low-Cycle Fatigue Behavior of IN738LC Alloy in Air and In Vacuum," High temperature alloys for gas turbines conference proceedings, 1982, p 791-804.
- 23 Xia, J., Kovac, J., McQuiggan, G., Wolfe, B., "SGT6-5000F (W501F) Engine Enhancements to Improve Operation Flexibility." POWER-GEN International 2005 – Las Vegas, Nevada, 2005.
- 24 ASTM International, "Standard Terminology Relating to Fatigue and Fracture Testing," E1823-96. 2002.
- 25 Danzer, R., Bressers, J., "The Application of Stress Rupture Data for the Prediction of the High Temperature Low Cycle Fatigue Lives of Two Nickel-Base Alloys," Proceedings of a Conference Held in Lie'ge, Belgium. 1996.